Mechanisms of Membrane Targeting and Activation of Phosphatidylinositol-4-Phosphate 5-Kinases (PIP5Ks)

by

Benjamin Rhys Duewell

A dissertation accepted and approved in partial fulfillment of the

requirements for the degree of

Doctor of Philosophy

in Chemistry

Dissertation Committee:

Brad Nolen, Ph.D., Chair

Scott Hansen, Ph.D., Advisor

Kenneth Prehoda, Ph.D., Core Member

Parisa Hosseinzadeh, Institutional Representative

University of Oregon

Summer 2024

DISSERTATION ABSTRACT

Benjamin R. Duewell

Doctor of Philosophy in Chemistry

Title: Mechanisms of Membrane Targeting and Activation of Phosphatidylinositol-4-Phosphate 5-Kinases (PIP5Ks)

The ability for cells to localize and activate peripheral membrane binding proteins is critical for signal transduction. Ubiquitously important in these signaling processes are phosphatidylinositol phosphate (PIP) lipids, which are dynamically phosphorylated by PIP lipid kinases on intracellular membranes. Functioning primarily at the plasma membrane, phosphatidylinositol-4-phosphate 5-kinases (PIP5K) catalyzes the phosphorylation of PI(4)P to generate most of the PI(4,5)P_2 lipids found in eukaryotic plasma membrane. Recently, we determined that PIP5K displays a positive feedback loop based on membrane-mediated dimerization and cooperative binding to its product, PI(4,5)P_2. In Chapter II of this dissertation, we examine how two motifs contribute to PI(4,5)P_2 recognition to control membrane association and catalysis of PIP5K. Using a combination of single molecule TIRF microscopy and kinetic analysis of PI(4)P lipid phosphorylation, we map the sequence of steps that allow PIP5K to cooperatively engage PI(4,5)P_2. We find that the specificity loop regulates the rate of PIP5K membrane association and helps orient the kinase to more effectively bind PI(4,5)P_2 lipids. After correctly orienting on the membrane, PIP5K transitions to binding PI(4,5)P_2 lipids near the active site through a motif previously referred to as the substrate or PIP binding motif (PIPBM). Our data reveals that the PIPBM has broad specificity for anionic lipids and serves a critical role in regulating membrane association in vitro and in vivo. The strength of the interaction between the PIPBM and various PIP lipids depends on both the membrane density and the extent

phosphorylation on the inositol head group. Overall, our data supports a two-step membrane binding model where the specificity loop and PIPBM act in concert to help PIP5K orient and productively engage anionic lipids to drive the positive feedback during PI(4,5)P_2 production. In Chapter III, we follow up on a recent study that showed PIP5K exist in a weak monomer-dimer equilibrium in solution but can shift to a dimeric state following membrane association. Dimerization potentiates PIP5K function, increasing lipid kinase activity 20-fold, providing a possible mechanism for the rapid PI(4,5)P2 generation seen during signaling events. In Chapter III we established a novel FÖrster Resonance Energy Transfer (FRET) biosensor to detect and quantify PIP5K dimerization on supported lipid bilayer technology using Total Internal Reflection Fluorescence Microscopy (TIRF-M). This FRET biosensor allows for the frequency and duration of PIP5K dimerization to be quantified with high resolution. We used this FRET biosensor to demonstrate that human PIP5K paralogs (α, β, and γ) are able to heterodimerize. Previous studies have shown that PIP4K enzymes inhibit PIP5K enzymes by an unknown mechanism. Here, we use the FRET biosensor to demonstrate the mechanism of inhibition is via blocking the dimer interface. The creation of this PIP5K dimerization FRET biosensor establishes a novel assay for examining how proteins and peptides modulate membrane-mediated dimerization of PIP5K, which will be critical for elucidating the mechanisms that control cellular PI(4,5)P_2 lipid homeostasis in the future.

This dissertation includes previously published, unpublished, and co-authored work.

CURRICULUM VITAE

NAME OF AUTHOR: Benjamin R. Duewell

GRADUATE AND UNDERGRADUATE SCHOOLS ATTENDED:

University of Oregon, Eugene

University of California, Irvine

DEGREES AWARDED:

Doctor of Philosophy, Biochemistry, 2024, University of Oregon

Bachelor of Science, Molecular Biology and Biochemistry, 2019, University of California, Irvine

AREAS OF SPECIAL INTEREST:

Protein Biochemistry

PROFESSIONAL EXPERIENCE:

Graduate Research Assistant, Hansen Lab, University of Oregon, Eugene, OR, 2019 – 2024

Graduate Teaching Assistant, Department of Chemistry and Biochemistry, University of Oregon, Eugene, OR, 2019 – 2020, 2023

Undergraduate Researcher, Goulding Lab, University of California Irvine, Irvine, CA, 2017-2019

Undergraduate Researcher, Loftus Lab, University of California Irvine, Irivne, CA, 2016 - 2018

Resident Advisor, University of California Irvine, Irvine, CA, 2016 – 2019

GRANTS, AWARDS, AND HONORS:

Cecil Curfman Scholarship	2015
Summer Undergraduate Research Program Fellowship	2018
National Institutes of Health Training Grant (T32)	2020-2022
Annual IMB Retreat Poster Presentation Award	2021
University of Oregon John Keana Fellowship	2023
Conference Travel Award- DiscoverBMB 2024	2024

PUBLICATIONS:

Duewell BR, Hansen SD. A novel FRET biosensor for visualizing membrane-mediated dimerization of PIP5K. (2024) ***Manuscript in preparation***

Duewell BR, Faris KA, Hansen SD, Molecular basis of product recognition during PIP5K-mediated production of PI(4,5)P2 with positive feedback, ***Journal of Biological Chemistry*** (2024), doi: https://doi.org/10.1016/j.jbc.2024.107631

Duewell BR*, Wilson NE*, Bailey GM, Peabody SE, Hansen SD. (2024). Molecular dissection of PI3Kβ synergistic activation by receptor tyrosine kinases, GβGγ, and Rho-family GTPases. ***eLife***. https://doi.org/10.7554/eLife.88991.3

Rathinaswamy MK, Jenkins ML, **Duewell BR**, Zhang X, Harris NJ, Evans JT, Stariha JT, Dalwadi U, Fleming KD, Ranga-Prasad H, Yip CK, Williams RL, Hansen SD, Burke JE. (2023). Molecular basis for differential activation of p101 and p84 complexes of PI3Kγ by Ras and GPCRs. ***Cell Reports.*** https://doi.org/10.1016/j.celrep.2023.112172

Hansen SD, Lee AA, **Duewell BR**, and Groves JT. (2022). Membrane-mediated dimerization potentiates PIP5K lipid kinase activity. ***eLife***. https://doi.org/10.7554/eLife.73747

ACKNOWLEDGMENTS

These acknowledgements must begin with my advisor, Professor Scott Hansen. He spent countless hours mentoring me, helping me make sense of data, and giving me patience and space to grow. In my years working with Dr. Hansen, I've had the pleasure of meeting many of his colleagues, past and current. I'm endlessly amazed by the positive words and sentiments I hear. The rigor he puts into his work is inspiring, and the time he's given to the department is more than admirable. I'm so proud of him for getting tenure, though to be honest, there was never any doubt in my mind that he would. Any and every department would be lucky to have member like him. Finally, I need to acknowledge his patience as a boss when I had medical issues this past year. I knew that he was okay with me prioritizing myself in those moments. Many people these days talk about student-first mentoring, but Dr. Hansen practiced it. I'm forever grateful for the opportunity to have worked with such a fine scientist and human.

Next, I need to give thanks to my family. From the hours spent in my father's human anatomy classroom playing with the fake skeletons and models, to reading his textbooks, endlessly collecting knowledge. If you're looking for where my passion for science began, look in Davis High school room 407. In that light, I need to take space to specifically acknowledge my father. He always encouraged my questions, always pushed me to be better than before. I'm sad that when I was young, I didn't appreciate the lessons he taught me. I'm sad because if I could go back and understand those lessons, let them sink in earlier, I wonder what kind of man I would be. Regardless, he must be thanked. Those lessons taught me to always find more of me to give in my work, my hobbies, my life. I strive to better myself because of his encouragement, and I thank him. I love him, and I know my work makes him proud. To my mom, thank you for showing me what a strong leader is. I see the time and effort you put into your work, and it amazes me. Thank you

for showing me what dedication to my work is. Thank you for your unending love. And, perhaps most of all, thank you for time over the last eight months. I don't know how I could have gotten through those scary times without your calls, without your calm, without your love. Finally, to my brother, thank you for showing me audiobooks. This sounds like an odd thanks, compared to the ones I gave above, but it guided me through the long hours performing experiments. I love books again, and it's because of him. Thank you, my family, I love you and wouldn't want any other.

A short thanks needs be given to my soccer teams at UO. Soccer has been a necessary outlet to the struggles and frustrations of my graduate studies. It gave me a space where I could be good at something and strive to get better. Soccer keeps me grounded in both calm and tumultuous times. Thanks to all of you for your hard work and being my teammates.

A thanks to my many friends, graduate students and not, who helped keep me sane. A most special thanks, though, to Grace Waddell. Being the first two graduate students in a lab can be tough, but we worked hard together. Her dedication to her work modeled a fiery work ethic in me. I couldn't have accomplished anything without her.

Most important to thank, though, is my partner, Gerryko. Gerr moved to Eugene with me, got his master's here with me, and he grew here with me. I'm running out of space and could write an entire dissertation on my love for him. But suffice to say, he is my world and I thank him for his patience in the face of long workdays, frustrated soccer days, and all the other ups and downs that accompany my personality. Thank you for loving me at my best and my worst. I love you and the family we've made with our cat Teddy.

TABLE OF CONTENTS

Chapter Page

LIST OF FIGURES

Figure Page

LIST OF TABLES

CHAPTER I

INTRODUCTION

Phosphatidylinositol phosphate lipids- a simple tool used by cells to solve complex biological problems

Cells are complicated environments composed of various macromolecules that interact to facilitate chemical reactions that make processes such as replication, movement, signal transduction, and division possible. These processes must be regulated both spatially and temporally to ensure successful function[1]. Failure to regulate these complex chemistries leads to disease phenotypes in organisms and often to cellular and organismal death[2–4]. Spatial regulation is often achieved in cells via compartmentalization. Many mechanisms exist to achieve spatial compartmentalization in cells, from the network of numerous low affinity interactions to facilitate a partition into another material state, to ribosomal RNA packaging tRNA and messenger RNA into a physically enclosed area to streamline translation[5]. In eukaryotes, however, the hallmark of spatial compartmentalization of chemical reactions is achieved via their complex and elaborate membrane system. Each membrane structure, called organelles, partitions the distinct signaling processes that take place within, from the nucleus regulating the housing of DNA and transcriptional processes, to the plasma membrane regulating the initial response to extracellular cues and internalization of foreign molecules. The chemistry performed by each organelle necessitates the recruitment of specific proteins to their subcellular locations[6–8]. The process of recruiting and localizing the correct proteins to their cognate compartments requires finely tuned regulation. While eukaryotic organisms have evolved many pathways to carry out specific localization to membrane compartments, the phosphatidylinositol phosphate (PIP) lipid class of

phospholipid is widely considered to be the key spatiotemporal cue that directs protein localization to the various intracellular membranes[9].

Phosphoinositides, like other phospholipids, are composed of a diacylglycerol backbone linked to their headgroup via a phosphodiester bond. The scaffolding power of the PIP lipid resides in the malleability of the inositol ring headgroup of the lipid. The *myo*-inositol ring headgroup is made up of six carbons, each with a reactive hydroxyl group. These reactive -OH groups can be modified in various ways depending on how the organism has evolved to use phosphoinositides. In *mycobacterium*, for example, the inositol ring of phosphatidylinositol lipid is mannosylized to create phosphatidylinositol mannoside, a sugar modification that regulates cell growth and viability[10]. Alternatively, eukaryotic organisms have evolved the ability to phosphorylate the inositol headgroup of phosphatidylinositol at the 3, 4, and 5 position of the PIP headgroup. The placement and number of phosphates distinguish the seven different forms of PIP lipids found in mammals (PI(3)P, PI(4)P, PI(5)P, PI(3,4)P_2, PI(3,5)P_2, PI(4,5)P_2, and PI(3,4,5)P_3) (**Figure 1.1A**). Despite the relative similarity of the net state and chemical structure shared between these seven PIP lipids, studies have routinely shown that each lipid has unique scaffolding abilities, regulating the localization of distinct classes of proteins that have different specificity [11–13]. The seven PIP lipid species are synthesized at distinct membrane organelles (**Figure 1.1B**), where they can recruit specific proteins to intracellular membrane. Studies that have depleted PIP lipids at different intracellular membranes show that organelle function is drastically disrupted when proteins fail to localize to distinct pools of PIP lipids[14–17]. Mutations in humans that disrupt PIP lipid synthesis or degradation are often either embryonic lethal or cause many degenerative disorders[2,3,18].

Figure 1.1

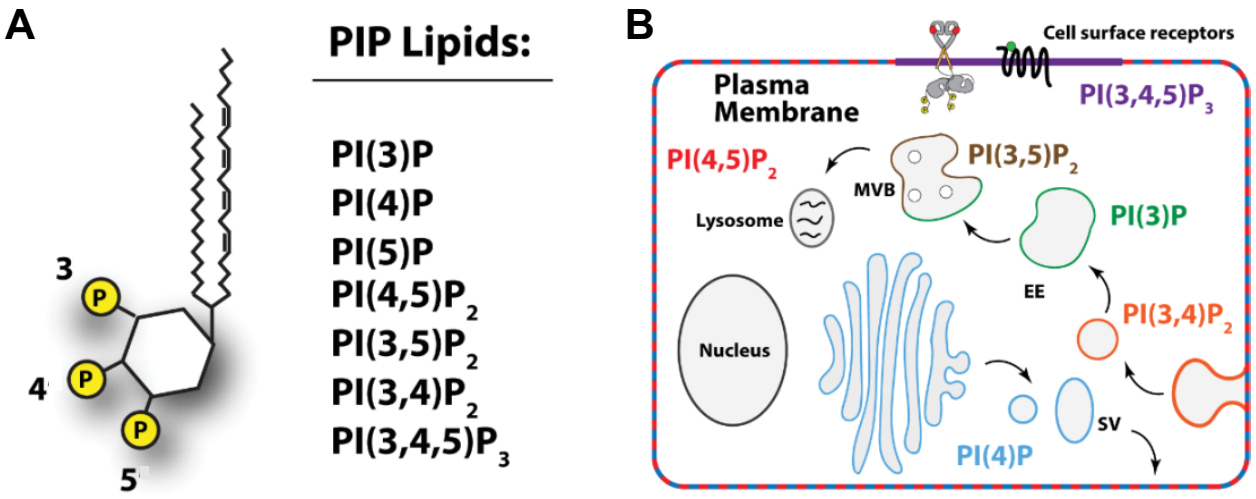

Figure 1.1
PIP lipid structure and their subcellular locations.
There are seven PIP lipid species that differ by the placement and number of phosphate groups on the inositol headgroup. PIP lipids serve as markers of different intracellular compartments and serve as docking sites for various protein effectors. Illustration designed by Grace Waddell, Ph.D.

The concentration and distribution of these lipids can change rapidly during cell signaling events[19]. PIP lipids can broadly be described as either constitutively present or as transiently produced second messengers. PI(4)P lipids, for example, are constantly being produced in the Golgi by the enzyme denoted PI4K, which phosphorylates the 4-position of phosphatidylinositol[20]. These lipids are critical for vesicular trafficking from the Golgi to the plasma membrane, and as such are required by the cells at all times and don't greatly fluctuate in their cellular concentrations[21]. Alternatively, are the rapidly synthesized phosphoinositides following receptor stimulation whose transient lifetime ends as they are quickly destroyed following downstream antagonist activation. These lipids include $PI(3,4,5)P_3$ and $PI(3,4)P_2$. $PI(3,4,5)P_3$ is created by PI3K, an autoinhibited enzyme that requires multiple inputs to stimulate activity[22]. This negative regulation is only relieved during cell signaling events, providing the

reason for its low abundance in resting cells. $PI(4,5)P_2$ is one phosphoinositide that exists in a dual capacity as both a constitutively present lipid that controls general cellular function, but can also be synthesized in rapid bursts to control important cell signaling events[23,24].

PI(4,5)P2, a lipid with a multifaceted nature in cell signaling

The most abundant PIP lipid in mammalian cells is $PI(4,5)P_2$, comprising approximately 2-5% of the total lipids in the plasma membrane's inner leaflet[25,26]. If each PIP lipid is associated with regulating the function of a different membrane compartment, $PI(4,5)P_2$ should be considered the regulator of the inner leaflet of the plasma membrane. In this section, we will discuss the three main roles of $PI(4,5)P_2$ lipids during cell signaling events: the role of $PI(4,5)P_2$ as a substrate for phospholipase C and PI3K pathways, its role in fundamental signaling pathways, and finally its rapid synthesis during signaling events such as phagocytosis and the Wnt signaling pathway.

$PI(4,5)P_2$ lipids were first discovered as metabolites that exhibited rapid turnover during some cell signaling events[27]. Further studies into calcium signaling demonstrated that $PI(4,5)P_2$ was the main substrate for the enzyme phospholipase C, which breaks the phosphodiester bond of $PI(4,5)P_2$ to generate inositol 1,4,5-triphosphate (IP3) and diacylglycerol, two potent signaling molecules that drive a variety of physiological events such as muscle contraction and vasodilation[28]. Often PLC activity is studied in reference to cardiac pumping, and studies have shown that depletion of $PI(4,5)P_2$ lipids at the membrane can halt successful cardiomyocyte contractile behavior[29]. This requires that $PI(4,5)P_2$ lipids are rapidly replenished following contraction, though little is known about the mechanisms that control this expedited replenishment[30]. In more recent years, $PI(4,5)P_2$ has been identified as the primary substrate for class one phosphatidylinositol 3-kinases (PI3K), which phosphorylate the 3-position of the inositol

ring to create $PI(3,4,5)P_3$[19,31]. This lipid stimulates many signaling pathways, including cell migration, polarization of neurons, apoptosis, and insulin transduction[19,31,32].

Beyond simply functioning as a precursor substrate, $PI(4,5)P_2$ has been shown to be critical for many other signaling processes. It functions as a necessary cofactor for the nucleation promoting factor N-WASP, for example. N-WASP requires binding to $PI(4,5)P_2$ lipids to relieve autoinhibition and then stimulate the activity of the Arp2/3 complex, leading to branched actin formation[33]. Indeed, $PI(4,5)P_2$ is a widespread regulator of actin nucleation and branched actin networks, binding to a wide variety of actin-associating proteins and regulating the initiation and inhibiting actin severing proteins like cofilin[34]. Similarly, cytoskeletal anchoring to the plasma membrane is also mediated by $PI(4,5)P_2$ lipids binding to ezrin, radixin, moesin (ERM) family proteins with high affinity to anchor the actin filaments to the membrane[35,36]. Processes that rely on actin to function, like endocytosis, have also been shown to require abundant $PI(4,5)P_2$ lipids to function. In the case of endocytosis, $PI(4,5)P_2$ facilitates both branched actin filament formation via interactions with N-WASP as described above, but also through recruiting both the Adaptor Protein Complex 2 (AP-2 complex) as well as dynamin to site of endocytosis[7]. Clearly, the lipid is essential for the accurate establishment of actin dynamics in eukaryotes.

Constitutive $PI(4,5)P_2$ lipid levels are necessary to stabilize conformational changes in many ion channel proteins as well. Selective permeability is a hallmark of all cells, but especially neurons and muscle tissue. $PI(4,5)P_2$-dependent ion channels require the ability to interchangeably shift from a closed conformation to open[37]. Many ion channels including voltage-gated potassium channels, calcium-activated chloride channels, and transient receptor channels (TRP) have been shown to function in a $PI(4,5)P_2$-dependent manner[38–40]. This role in ion channel gating makes $PI(4,5)P_2$ lipids critical mediators of function, m-current generation, and plasticity of synapses in

neurons[41]. Each of these examples highlight a cellular process that requires stable levels of $PI(4,5)P_2$. When this constant pool of $PI(4,5)P_2$ is depleted in resting cells, cytoskeletal anchoring falls apart, rate of endocytic event slows, and ion channels fail to function[37,42,43].

Often $PI(4,5)P_2$ lipids are considered to exist at a steady concentration at the plasma membrane, unlike $PI(3,4,5)P_3$ lipids which are transiently created in short bursts for following receptor activation[44]. However, there do exist signaling pathways that are able to rapidly stimulate synthesis of $PI(4,5)P_2$ lipids beyond the basal levels in resting cells. For example, activation of the Wnt signaling pathway causes up to a 4-fold increase in membrane $PI(4,5)P_2$ lipid concentration[45]. As discussed earlier, phospholipase C activation causes a dramatic decrease in $PI(4,5)P_2$ concentration at the plasma membrane, this decrease is quickly replenished through unknown synthesis mechanisms. Some studies have shown that macrophage phagocytosis stimulates the accumulation of $PI(4,5)P_2$ lipids rapidly at the site of invagination[46].

Overall, the research clearly shows that $PI(4,5)P_2$ lipids function as critical mediators of cellular processes. Interestingly, $PI(4,5)P_2$ functions as both a fundamental signaling PIP lipid, omnipresent at the plasma membrane, but simultaneously as a signaling lipid, formed rapidly in response to receptor activation. A natural question that arises from this dichotomy is: How is both transient and rapid $PI(4,5)P_2$ synthesis possible? This is one of the guiding questions that drove my thesis work. While I do not fully answer this question, I do provide some potential mechanisms that could explain this phenomenon.

PI(4,5)P2 synthesis: Three pathways, one answer.

If we wish to uncover the mechanisms that drive both transient and rapid $PI(4,5)P_2$ synthesis in cells, we must first understand what avenues mammalian cells have evolved to produce this signaling lipid. $PI(4,5)P_2$, as its name suggests, is a phosphoinositide phosphorylated

at the 4 and 5-position of the inositol ring. As such, there are three potential substrates able to be modified to create this lipid (**Figure 1.2**). First, we'll discuss the least likely pathway. Phosphatidylinositol-3,4,5-trisphosphate ($PI(3,4,5)P_3$) lipids, as their name suggest, contain phosphates at the 3, 4, and 5-position of the inositol ring and can be dephosphorylated by a 3-phosphatase to synthesize $PI(4,5)P_2$. Phosphatase and Tensin Homology (PTEN) phosphatase is the enzyme associated with this activity in mammalian cells. PTEN is classified as a tumor suppressor gene, and is one of the key regulators of the $PI(3,4,5)P_3$ signaling pathway[47,48]. During $PI(3,4,5)P_3$ synthesis, PTEN antagonizes the pathway by destroying these lipids. PTEN activity is often described as functioning as a spatial regulator of the signaling pathway, narrowing the regions of the membrane populated by $PI(3,4,5)P_3$ lipids. The scarcity of $PI(3,4,5)P_3$ lipids in resting cells, however, means that PTEN does not have abundant substrate to use to synthesize new $PI(4,5)P_2$ lipids in the absence of receptor activation. Indeed, the constant supply of $PI(4,5)P_2$ required at the plasma membrane of cells is not likely produced in any large quantity by PTEN. During some cell signaling pathways, phagocytosis is one key example, $PI(3,4,5)P_3$ is rapid produced in large quantities[49]. One might propose that PTEN activity could be, at least in part, responsible for the corresponding rise in $PI(4,5)P_2$ lipids seen during phagocytic events. However, seeing that $PI(3,4,5)P_3$ is solely synthesized during phagocytosis from $PI(4,5)P_2$ precursor lipids, it is then impossible for PTEN to synthesize $PI(4,5)P_2$ beyond the basal levels seen before cell signaling begins. With these arguments in mind, we can assuredly state that PTEN is not primarily responsible for either the stable $PI(4,5)P_2$ generation in resting cells, nor the rapid $PI(4,5)P_2$ seen following receptor activation.

Figure 1.2

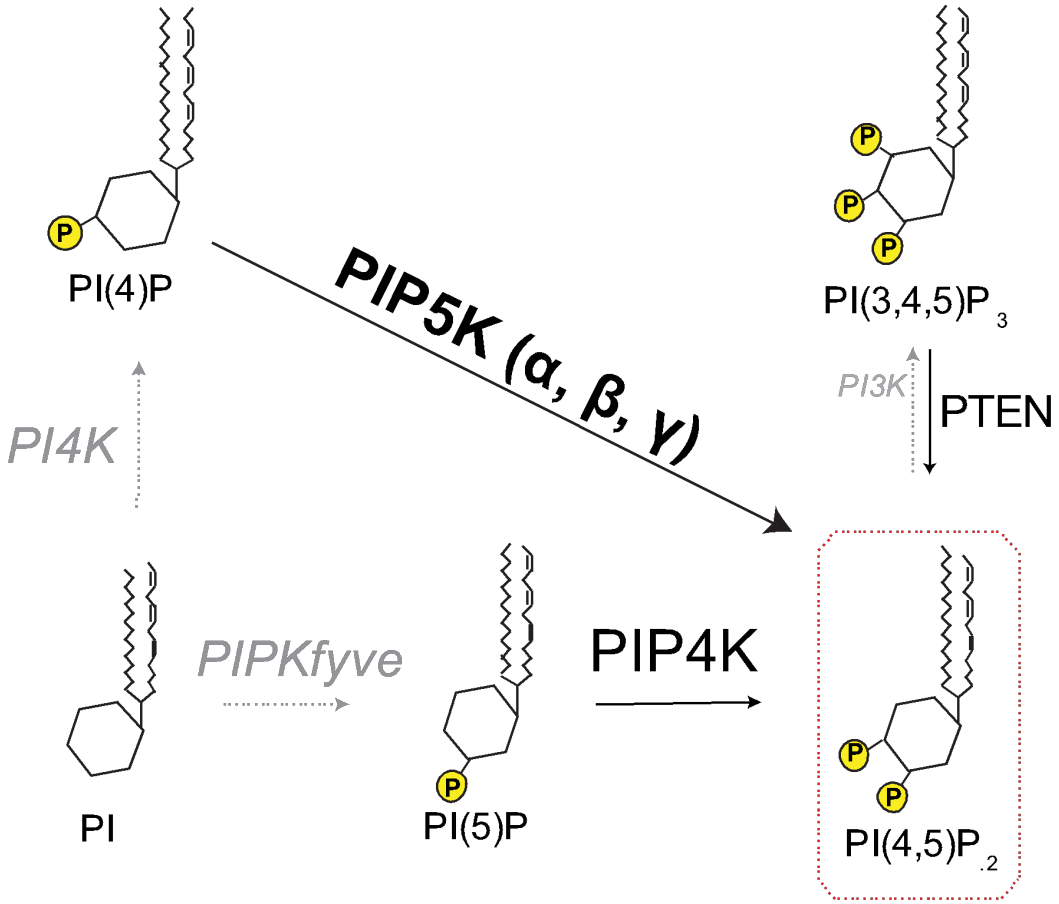

Figure 1.2
Possible PI(4,5)P_2 synthesis pathways
Illustration depicting the possible pathways to synthesizing PI(4,5)P_2. Synthesis begins with phosphatidylinositol (PI), which is phosphorylated by either PI4K to produce PI(4)P, or PIPKfyve to produce PI(5)P. PI(5)P can be phosphorylated by PIP4K to produce PI(4,5)P_2. Alternatively, PI(4)P can be phosphorylated PIP5K to create the lipid. The final pathway is taking the precursor lipid PI(3,4,5)P_3 and dephosphorylating the 3-position of the inositol ring, catalyzed by PTEN.

Another potential pathway mammalian cells have evolved to facilitate PI(4,5)P_2 generation is through phosphorylation of the precursor lipid phopshatidylinositol-5-phosphate (PI(5)P). Phosphatidylinositol-5-phosphate 4-kinase (PIP4K) enzymes are primarily responsible for catalyzing the phosphorylation of the 4-position on the PI(5)P inositol ring[50]. There exist three paralogs in the mammalian genome denoted as PIP4KIIA, PIP4KIIB, and PIP4KIIC. These three

proteins are a family of enzymes called type II phosphatidylinositol phosphate kinases (type II PIPKs). PIP4K enzymes have been shown to regulate cell growth, with higher cellular concentration being linked to decreased proliferation through a mostly unknown mechanism[51]. In *Drosophila*, PIP4K activity is essential for salivary gland development and, convergently from previous studies, cellular PIP4K concentrations are correlated with increased tissue size[52]. Despite these findings, it is known that PIP4K enzymes do not play an essential role in synthesizing $PI(4,5)P_2$. In fact, recent studies suggest that PIP4K enzymes actually antagonize $PI(4,5)P_2$ development through a mechanisms that we'll discuss later in this introduction[53,54]. If mammals have evolved three genes to facilitate $PI(4,5)P_2$ production via phosphorylation of the PI(5)P substrate, why would these proteins not produce a substantial amount of cellular $PI(4,5)P_2$? Similarly to PTEN, the reason is that PI(5)P lipids are scarce. PI(5)P is thought to make up only about 0.5% of total phosphoinositide lipids in the cell[55]. With such low abundance, the high specificity of PIP4K for the PI(5)P substrate, and recent studies that show knockouts of PIP4K enzymes increasing cellular $PI(4,5)P_2$, we can conclude that the PI(5)P route is not the dominant pathway used to produce either the stable $PI(4,5)P_2$ membrane pools nor the rapidly produced pools in response to receptor activation.

This leaves one pathway remaining, $PI(4,5)P_2$ generation through phosphorylation of phosphatidylinositol-4-phosophate (PI(4)P). PI(4)P lipids rival $PI(4,5)P_2$ for the title of most abundant PIP lipid in the cell. The two main membranes with enriched PI(4)P concentrations are the Golgi networks and inner leaflet of the plasma membrane. In congruence with the idea that PI(4)P is the critical pathway to production of inner leaflet $PI(4,5)P_2$ lipids, studies that inhibit PI(4)P production or destroying Golgi PI(4)P pools lead to a global reduction in $PI(4,5)P_2$ lipid concentrations[14,16]. If Golgi PI(4)P is depleted, cells can no longer recover $PI(4,5)_2$ lipids following

phospholipase C activation, suggesting that rapidly produced $PI(4,5)P_2$ utilizes PI(4)P as the primary substrate in this pathway[56]. PI(4)P is phosphorylated at the 5-position of the inositol ring by the type I PIPK family of enzymes called phosphatidylinositol-4-phosphate 5-kinase (PIP5K). Like PIP4K enzymes, there exist three PIP5K paralogs in the mammalian genome, encoding for PIP5KA, PIP5KB, and PIP5KC. The activity of PIP5K is closely linked with the same pathways that $PI(4,5)P_2$ regulates. Endocytic events rely on PIP5K activity to function, with studies that deplete PIP5K isoforms dramatically decrease in number of endocytic events occurring in cells[57]. Wnt signalosome formation has been recurrently shown to require PIP5K activity, with catalytically inactive mutant cell lines having vastly decreased responsiveness to stimulation with Wnt3A[45,58]. Studies that stimulate PIP5K activity increase the current of ion channels and modulate actin dynamics[59,60]. The findings from these studies overwhelmingly demonstrate the importance of PIP5K and the PI(4)P pathway for the synthesis of not just the stable pools of $PI(4,5)P_2$, but also those pools rapidly produced in response to external cues. How this one enzyme can function in both these distinct ways is not well understood. Though, recent advancements in the mechanistic biochemistry governing the regulation of PIP5K activity, pushed forward by the work in this thesis, may begin to paint the picture. For now, we turn to analyzing what the field does know about the regulation of PIP5K activity.

Mechanisms of PIP5K activity and regulation

As discussed earlier, PIP5K exists as three isoenzymes in the mammalian genome. These paralogs have tissue-specific expression patterns. PIP5KC is considered the neuronal-specific PIP5K, present at high concentrations in muscle and brain tissues[61]. PIP5KA and PIP5KB are more broadly expressed, with PIP5KA being present in all tissues except for most muscle tissues, and PIP5KB being the main PIP5K paralog present in the digestive tract[62]. Importantly, all three PIP5K

paralogs contain a central kinase region that is well conserved between the paralogs and their splice variants[63]. Most biochemistry studying PIP5K to date has focused under the assumption that the three kinases have redundant cellular functions. Therefore, our discussions of PIP5K regulation will not be broken down into paralog-specific findings in this dissertation. Instead, we will discuss the general knowledge the field has for how PIP5K localizes to the membrane and becomes active. In this section, these topics will be broken down into two pieces: intrinsic regulation of PIP5K activity, and cofactor-driven regulation of PIP5K activity.

PIP5K phosphorylates PI(4)P lipids at the 5-hydoxyl group on the inositol ring via ATP hydrolysis. Little was known about the structural mechanisms that governed achievement of ATP hydrolysis and the motif that bound PI(4)P lipids until the first seminar crystal structure papers that used the zebrafish homolog of PIP5KA[63,64]. In these two initial papers, researchers discovered the well-conserved PI(4)P lipid binding motif, or substrate binding motif, is the site of substrate binding. The 5-hydroxyl group is positioned in proximity to the gamma-phosphate of ATP. The substrate binding motif and ATP-binding pocket are unique motifs to PIPKs but exist in a conserved manner in both type I (PIP5K) and type II PIPKs (PIP4K). If the substrate binding motifs and ATP-binding pockets of both PIP5K and PIP4K enzymes are well conserved, why do they each phosphorylate different substrates? Kinases, along with their active sites and ATP binding pockets, often contain motifs called activation loops, which are alpha helices or disordered loops that protect the active site and regulate the specificity of the kinase. In PIP5K and PIP4K, the activation loop (also referred to as the specificity loop) have been shown to regulate the substrate preference for each family of kinase[63,65–67]. Studies that swapped the PIP4K specificity loop for PIP5Ks specificity loop demonstrated a swapping of substrate specificity[65]. More recently, however, it was shown that the PIP5K specificity loop doesn't just act as a specificity gate, but

also functions as an amphipathic helix that buries itself into the membrane[67]. NMR studies suggest that the specificity loop is disordered in solution but adopts a helical conformation upon binding to lipids. Mutations that disrupt the adoption of the helical conformation, but retain the important residues for PIP lipid association, drastically decreases the activity of PIP5K enzymes, suggesting that the helix conformational change critical for kinase function. The specificity loop is thought to be a driving factor of PIP5K's membrane localization and targeting. Studies that have tracked the localization of fluorescent PIP5K in a variety of cell types all show that PIP5K enzymes targets the inner leaflet of the plasma membrane[66,68]. Studies that mutated the specificity loop showed a marked decrease in membrane localization. Why PIP5K targets the plasma membrane specifically is not known. If we interpret the current state of our knowledge of how PIP5K is regulated, we would conclude that localization is based on associating with PI(4)P lipids. Indeed, there are pools of PI(4)P at the plasma membrane, though this doesn't seem like a plausible explanation, as PI(4)P also exists at higher molar concentrations in the Golgi membrane network[21]. If PI(4)P was the driving factor controlling PIP5K inner leaflet targeting, we would expect to see an equally high, if not higher, concentration of Golgi localized PIP5K. Recently, a potential answer to this question arose from research studying PIP lipid pattern formation. It was discovered that PIP5K exhibits positive feedback in the presence of its product, $PI(4,5)P_2$[69]. Positive feedback is based on an increased affinity for PIP5K to $PI(4,5)P_2$ lipids, driving localization as $PI(4,5)P_2$ is synthesized, leading to a greater density of PIP5K on the membrane. This higher affinity for PIP5K to bind $PI(4,5)P_2$ over PI(4)P could explain the localization patterns of inner leaflet targeting in cells. However, the structural motifs responsible for $PI(4,5)P_2$ binding remained unknown before my dissertation, and therefore it was unclear if PI(4,5)P2 lipid binding was the key driving factor controlling PIP5K membrane targeting in cells. Previously, it was predicted that PIP5K existed as

a constitutive dimer, similar to type II PIP4K[64,70]. This was recently disproven, and PIP5K was shown to undergo membrane-mediated dimerize[71]. Dimeric PIP5K has 20-fold higher activity when compared to monomeric. This dimerization is thought to be transient in nature, though we did not have a method for tracking dimerization in real-time before the work in this dissertation. Overall, the field has recently made great headway determining how structural features regulate PIP5K activity in vitro. However, several questions concerning PIP5K regulation remain unanswered. What motif(s) are used by PIP5K to sense $PI(4,5)P_2$ lipids? What localizes PIP5K to the inner leaflet of the plasma membrane? Can we develop a FRET assay to visualize membrane-mediated dimerize of PIP5K and study the regulation of this process by various peripheral membrane binding proteins?

PIP5K, like all other proteins, is not just regulated intrinsically, but also through protein-protein interactions. PIP5K has been shown with interact with a variety of small GTPases by co-immunoprecipitation[72–75]. These proteins are suggested to help recruit PIP5K to intracellular membranes, perhaps aiding in the stimulation of rapid $PI(4,5)P_2$ synthesis by enhancing PIP5K localization in distinct areas of the membrane that have high GTPase activity. Though, no studies to date have addressed the ability for small GTPases to change PIP5K activity using purified proteins. In addition, the molecular basis of the interaction between PIP5K and small GTPases has not been defined through structural biochemistry. These reported interactions extend beyond the scope of my dissertation, but are mentioned to provide context for some of the mechanisms that could drive rapid $PI(4,5)P_2$ synthesis in cells. One protein that we will focus research on in this thesis is the PIP4K family of enzymes. A study that knocked out all three genes encoding the PIP4K paralogs in mice detected elevated levels of $PI(4,5)P_2$ lipids, which altered cellular metabolism of insulin due to enhanced PI3K signaling[54]. Further biochemical analysis showed that

the reason for increased $PI(4,5)P_2$ lipid levels in cells was due to PIP4Ks ability to interact with an inhibit PIP5K lipid kinase activity[76]. The PIP4K-PIP5K interactions have been shown in the past, though until this thesis no mechanism was well understood to describe how PIP4K inhibit PIP5K activity.

A single molecule fluorescence approaches to study the mechanisms of PIP5K membrane localization and activation

My dissertation focused on deciphering the mechanisms of PIP5K's positive feedback mechanism and density-dependent dimerization. We primarily used reductionist biochemistry approaches, which included a combination of supported lipid bilayers (SLBs) and total internal reflection fluorescence (TIRF) microscopy to study how purified PIP lipid modifying enzymes associating with lipids. In chapter II, we use site directed mutagenesis to identify the structural motifs able to bind to $PI(4,5)P_2$ with high fidelity. We found that both the specificity loop and PIPBM can facilitate binding to $PI(4,5)P_2$ lipids. The specificity loop functioned to sense specific lipids, increasing the binding affinity for proteins to PI(4)P and $PI(4,5)P_2$ lipids, but not PI(5)P lipids. Alternatively, the PIPBM functioned as a broad anionic lipid sensor, being able to facilitate binding to a variety of PIP lipids as well as phosphatidylserine lipids, another anionic phospholipid with a unique lipid head group. The PIPBM preferentially binds to lipids with higher negative charge, having a lower affinity for singly phosphorylated PIP lipids (PI(4)P and PI(5)P), and with a much higher affinity for doubly and triply phosphorylated PIP lipids. Finally, we established the ideal separation of function mutant for in vivo studies to use by making mutations that disrupted metal ion coordination in the ATP binding pocket of PIP5K.

In chapter III, we describe a new Forster Resonance Energy Transfer (FRET) assay to visualize PIP5K homodimerization in real-time on supported lipid bilayers using single molecule

TIRF-M. Previous studies relied on changes in diffusivity and dwell time of membrane bound as proxies for the monomeric or dimeric states. Using rational design principles, we mutagenized PIP5KB to create a single surface exposed cysteine residue that could be fluorescently labeled via maleimide-C2 Alexa Fluor (AF) within the Forester radii of the selected dye pairs. We show that when PIP5K adopts a dimeric conformation, the dyed PIP5K's undergo FRET and we readout dimerization. Using this readout, we determined the lifetime of dimerization, diffusion characteristics of dimerized PIP5K, and frequency of dimerization. We used this assay to show that PIP5K paralogs can heterodimerize (i.e. PIP5KA-PIP5KB complex). Finally, we used Alphafold3 to predict how PIP5K enzymes interact with PIP4K. Alphafold predicted that the PIP5K:PIP4K interaction is mediated by the dimer interface of PIP5K, suggesting that PIP4K could inhibit PIP5K via blocking dimerization. We mutated PIP5K and showed that monomeric PIP5K is unable to recruit PIP4K enzymes to membranes. Further, we showed that monomeric PIP5K is not significantly inhibited by PIP4K enzymes unlike wild type. Finally, we used our FRET assay to show that PIP4K blocks PIP5K dimerization.

Overall, the work presented in this thesis greatly enhances our understanding of PIP5K regulation. It highlights the strength of a reductionist biochemistry approach for determining the molecular basis of protein-protein and protein-lipid interactions. This work also greatly enhances our understanding of PIP4K. We provide mechanistic insights for both PIP4K recruitment to $PI(4,5)P_2$ lipids, as well as the first description for how PIP4K can inhibit PIP5K enzymes, namely by blocking dimerization.

Chapter II of this dissertation contains previously published and co-authored material. Experiments were performed by me, Katie Faris, and Scott Hansen. Chapter III contains currently unpublished work and will be co-authored by myself and Scott Hansen.

CHAPTER II

Molecular basis of product recognition during PIP5K-mediated production of $PI(4,5)P_2$ with positive feedback

This chapter includes co-authored material. Experiments were performed by me, Katie Faris, and Scott Hansen.

INTRODUCTION

Phosphatidylinositol phosphate (PIP) lipids are important second messengers that function as molecular scaffolds for numerous membrane binding proteins. PIP lipids are dynamically interconverted between seven different species by specialized kinases and phosphatases [9]. Research has demonstrated that each PIP lipid species exists in spatially distinct subcellular membranes and function to recruit specific enzymes to their necessary location for proper signaling [77,78]. The most abundant PIP lipid that mediates signaling at plasma membrane is phosphatidylinositol-4,5-bisphosphate ($PI(4,5)P_2$), comprising between 2-5% of total plasma membrane lipids [79–81]. Unlike most PIP lipids, $PI(4,5)P_2$ is omnipresent at the plasma membrane and is critical for several constitutive cellular functions, including cytoskeletal assembly [82,83], ion channel gating [40,84], and endocytosis [85]. Without a constant and stable pool of $PI(4,5)P_2$, these cellular signaling events are hindered and cells adopt disease-like states [86].

Phosphatidylinositol-4-phosphate 5-kinase (PIP5K) family of enzymes are responsible for creating the bulk of $PI(4,5)P_2$ lipids in eukaryotic cells [87]. PIP5K enzymes function by binding their substrate, phosphatidylinositol-4-phosphate (PI(4)P), then catalyzing the phosphorylation of the 5-hydroxyl group on the inositol lipid head group in the presence of $Mg^{(+2)}$-ATP [88,89]. This

activity has been described as specific to the PI(4)P substrate, although PIP5K can also phosphorylate the 5-OH of other PIP lipid species with lower efficiency [65,66,90,91]. In mammals, PIP5K exists as three paralogs (i.e. α, β, and γ) that display tissue specific expression patterns [92–94]. Localization studies in macrophages have shown that PIP5K paralogs predominately localize to the plasma membrane [68]. PIP5K has been implicated in many cellular pathways, with specific regulatory importance in the Wnt pathway [45], phagocytosis [60,95], and focal adhesions [96,97]. More recently, medical studies have begun to target PIP5K with potential as a cancer therapeutic [2]. Studies that have knocked out PIP5K from both prostate and breast cancers models showed diminished tumorigenesis and metastatic properties [98]. The drugs designed to inhibit PIP5Kα activity show promise reducing tumor growth and proliferation, however, these drugs have low specificity for PIP5K [18]. As our understanding of PIP5K's role in tumor proliferation evolves, it is important that we continue to decipher the molecular mechanisms that regulate PIP5K membrane localization and activity in cells.

Recently, our lab established supported lipid bilayers (SLBs) and Total Internal Reflection Fluorescence Microscopy (TIRF-M) to directly visualize PIP5K membrane binding dynamics with single molecule resolution. We discovered that human PIP5KB binds cooperatively to its product, $PI(4,5)P_2$, which enhances PIP5K membrane localization through a $PI(4,5)P_2$-mediated positive feedback loop [69]. Positive feedback is based on an increased affinity for PIP5K to $PI(4,5)P_2$ lipids (**Fig. S1**), driving localization as $PI(4,5)P_2$ is synthesized, leading to a greater density of PIP5K on the membrane. This membrane-bound PIP5K has an increased likelihood to encounter PI(4)P lipids in a conformational state ideal for productive binding and catalysis (Amos et al.) leading to an increased apparent activity of PIP5K enzymes. Further, we've shown that when PIP5K crosses a threshold membrane surface density it can also dimerize, which potentiates lipid kinase activity

[71]. This suggests that the site of $PI(4,5)P_2$ binding may be an important step for plasma membrane localization in cells, as $PI(4,5)P_2$ lipids exist almost exclusively at the plasma membrane. Currently, the residues or motif that regulates high affinity $PI(4,5)P_2$ binding remains unknown.

To date, much work has been done to define PIP5Ks enzymatic activity, including identifying motifs that regulate substrate specificity, ATP binding, and hydrolysis [63,66,67]. Structural biochemistry has helped elucidate the mechanism controlling PIP5K substrate recognition [63,67]. X-ray crystallography of zebrafish PIP5K (zPIP5K) determined that PIP5K binds to its substrate, PI(4)P, through the DLKGSxxxR motif, which is also referred to as the PI(4)P or substrate binding motif [63,64]. Mutations in the PI(4)P binding motif (PIPBM) of PIP5Ks abolishes lipid kinase activity [63]. PIP5K substrate specificity has been found to be mediated by a structural motif referred to in the literature as either the activation loop or specificity loop. Structural analysis of zPIP5KA using nuclear magnetic resonance (NMR) suggests that the specificity loop exchanges between a disordered and an alpha helical conformation [67]. Membrane-lipid interactions are hypothesized to shift the equilibrium to favor the alpha helical conformation, allowing hydrophobic residues in the specificity loop to insert into a lipid bilayer [67]. Mutating lysine residues in the specificity loop have been shown to disrupt plasma membrane localization [65]. Mutations that break the alpha helical character, but preserve the overall basic charge, have also been shown to disrupt catalysis [67]. In both cases, loss PIP5K function has been attributed to perturbing the PI(4)P binding interaction. While these studies have revealed which motifs are critical for PIP5K lipid kinase activity, we do not currently understand how these motifs contribute to the cooperative $PI(4,5)P_2$ binding, membrane mediated dimerization, and positive feedback. Deciphering these mechanisms could help explain why PIP5K is predominantly localized and activated at the plasma membrane.

Here we present a mutational analysis and single molecule TIRF-M study of PIP5K, which reveals the sequence of molecular interactions that control PIP5K membrane docking and $PI(4,5)P_2$ engagement. The initial membrane interaction is regulated by the specificity loop, which plays an important first step for membrane binding but is not essential for productive membrane docking. Using a set of chimeric proteins that contain different specificity loops, we show that the initial binding step of PIP5K can be mediated by interactions with either PI(4)P or $PI(4,5)P_2$ lipids. Our findings are consistent with the previously reported substrate specificity for PIP5K. Interactions with the lipid product, $PI(4,5)P_2$, were also paradoxically mediated through region of the kinase commonly referred to as the PI(4)P binding motif (PIPBM) or substrate binding motif. We discovered that the PIPBM is a broad anionic lipid sensor that can associate with lipids including phosphatidylserine and all types of PIP lipids. Overall, the strength of lipid interactions with the PIPBM is strongly correlated with the valency of phosphorylation on the PIP lipid head group, with triply phosphorylated PIP lipids exhibiting the strongest interaction. Supporting that the PIPBM controls membrane localization in addition to catalysis, we find that PIPBM mutants can still phosphorylate PI(4)P when localized to bilayers artificially. Finally, we used new insight about PIP5Ks membrane binding mechanism to validate separation of function mutants that are catalytically dead but retain their ability to localize to $PI(4,5)P_2$ containing membranes. Overall, this work improves our understanding of the molecular mechanisms underlying $PI(4,5)P_2$-mediated recruitment of PIP5K to the cellular plasma membrane.

RESULTS

The specificity loop regulates PIP5K localization to PI(4,5)P_2 containing membranes

Previous studies indicate that PIP5K substrate recognition is regulated by the specificity loop [63,65–67]. Positioned within ~20Å of the active site, the specificity loop is thought to help organize the active site to orient the substrate, PI(4)P, for catalysis [63]. Nuclear magnetic resonance (NMR) experiments also suggest that membrane docking of PIP5K causes the unstructured specificity loop to adopt an alpha helical conformation, which reportedly inserts into lipid membranes [67]. Membrane insertion of an amphipathic helix is predicted to significantly enhance the membrane dwell time of PIP5K, which could contribute to the positive feedback mechanism involving cooperative membrane binding of PIP5K to the lipid product, PI(4,5)P_2 [69] (**Fig. S1**). To determine how the specificity loop contributes to PIP5K localization and positive feedback, we disrupted alpha helix formation in the specificity loop by introducing a W365P mutation in PIP5KB (**Fig. 2.1A**). A homologous mutation (i.e. W393P) was previously shown to reduce the catalytic activity of zebrafish PIP5KA 25-fold relative to the wild type kinase [67]. Consistent with previous observations, PIP5KB (W365P) displayed a 50-fold reduction in lipid kinase activity compared to wild type PIP5KB when measured on supported lipid bilayers (SLBs) using TIRF microscopy (**Fig. 2.1B**). By contrast, the PIP5KB (W365A) mutant displayed a less dramatic decrease in catalytic activity (**Fig. S2A**), suggesting that preservation of the specificity loop alpha helical character or hydrophobicity is important for PIP5K catalysis. This is consistent with the zPIP5KA (W393G) mutant reportedly having similar kinase activity to wild type zPIP5KA [67].

To determine the extent to which the reduced activity of PIP5KB (W365P) is due to defects in membrane localization, we used sortase-mediated peptide ligation to fluorescently label PIP5KB with Alexa Fluor 647 (AF647) and visualized the mutant kinase localization in vitro on

reconstituted supported lipid bilayers (SLBs). Unlike wild type and dimerization deficient (i.e. D51R) AF647-PIP5KB, localization of AF647-PIP5KB (W365P) did not exhibit cooperative membrane recruitment that was coupled to production of PI(4,5)P_2 lipids (**Fig. 2.1C, Fig. S1B-S1C,** and **Fig. S2B**). Overall, the reduced PIP5KB (W365P) activity was strongly correlated with a decrease in membrane localization.

Figure 2.1

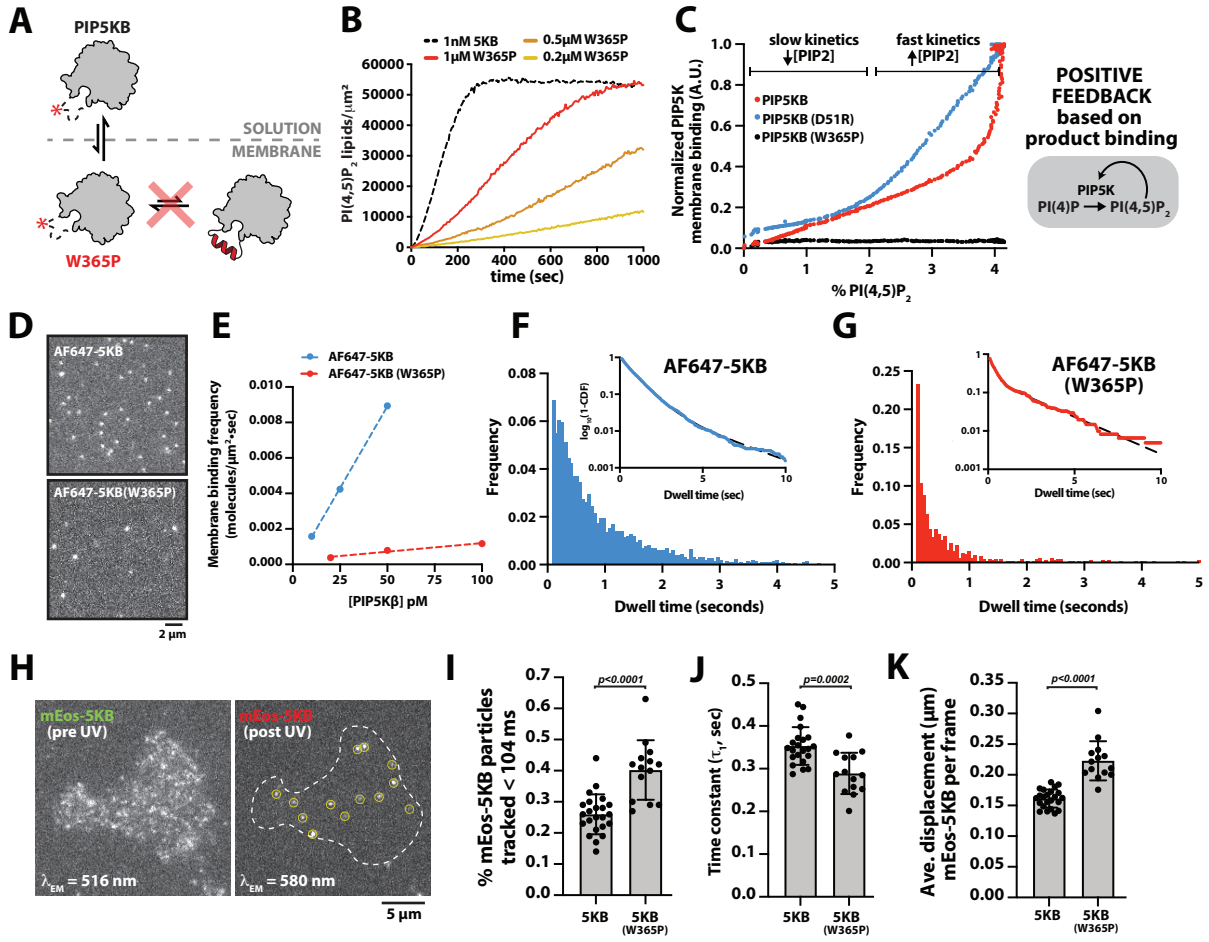

Figure 2.1
The specificity loop regulates the membrane association and dissociation rate constants.
(A) Cartoon illustrating how the W365P mutation disrupts the specificity loop alpha helical conformation in PIP5KB. **(B)** Representative lipid kinase activity traces measured in the presence of PIP5KB and PIP5KB (W365P). Production of PI(4,5)P_2 was monitored in the presence of 20 nM Cy3-PLCδ and the indicated concentration of PIP5KB. **(C)** PIP5KB (WT and D51R) but not PIP5KB (W365P) display cooperative

$PI(4,5)P_2$ dependent changes in supported membrane localization. Phosphorylation of PI(4)P and membrane localization of PIP5KB were monitored in the presence of 5 nM AF647-PIP5KB, 5 nM mNG-PIP5KB (D51R), or 5 nM AF647-PIP5KB (W365P). The production of PI(4,5)P2 was visualized using 20 nM Cy3-PLCδ in each kinase reaction. **(B-C)** Initial membrane composition: 96% DOPC, 4% PI(4)P. **(D)** Representative TIRF-M images showing membrane localization in the presence of 100 pM AF647-PIP5KB or AF647-PIP5KB (W365P). **(E)** Experimental measure of membrane binding frequency in the presence of 10-50 pM AF647-PIP5KB (k_{ON} = 184/μM•μm^2•sec) and 20-100 pM AF647-PIP5KB (W365P, k_{ON} = 9.68/μM•μm^2•sec). **(F-G)** Single molecule dwell time distributions measured in the presence of either AF647-PIP5KB (t_1 = 0.815 ± 0.054s, t_2 = 3.09 ± 0.35s, α = 0.95 ± 0.014, n = 14950) or AF647-PIP5KB (W365P) (t_1 = 0.296 ± 0.11s, t_2 = 2.82 ± 0.71s, α = 0.77 ± 0.056, n = 2389). **(D-G)** Membrane composition: 98% DOPC, 2% $PI(4,5)P_2$. **(H)** Representative TIRF-M images of mEos-PIP5KB plasma membrane localization before and after following photoconversion with 405 nm light in HEK293T cells. **(I)** A larger fraction of mEos-5KB W365P (40%) display transient membrane binding events < 104 ms, compared to the wild type mEos-5KB (26%). Each data point equals the average number of transient molecules detected per cell (N = 14-23 cells). **(J)** The mean dwell time of mEos-PIP5KB (W365P) (t_1 = 0.289 ± 0.05s, N = 14 cells, n = 5662 molecules) is shorter compared to mEos-PIP5KB (t_1 = 0.353 ± 0.04s, N = 23 cells, n = 19087 molecules). Each data point is derived from a single exponential fit to a dwell time distribution from a single cell. **(I-J)** Each data point equals the average number of transient molecules or time constant (t_1, sec) calculated per cell (N = 14-23 cells). **(K)** mEos-PIP5KB (W365P) is more diffuse in the cellular plasma membrane compared to mEos-PIP5KB. Average single molecule displacement during 52 ms time interval is greater for mEos-PIP5KB W365P (0.223 ± 0.03 μm, N = 14 cells) compared to mEos-PIP5KB (0.161 ± 0.01 μm, N = 23 cells). Each data point is the average displacement measured for a single cell. **(I-K)** P value calculated by unpaired Student's t-test.

Since membrane binding of AF647-PIP5KB (W365P) was unresponsive to the generation of $PI(4,5)P_2$ lipids, we hypothesized that the specificity loop directly senses $PI(4,5)P_2$ lipids, in addition to playing a critical role in substrate recognition. When we compared the single molecule localization of AF647-PIP5KB and AF647-PIP5KB (W365P) we observed a striking difference in the total number of membrane binding events on $PI(4,5)P_2$ containing bilayers (**Fig. 2.1D-2.1E**). To quantify this difference, we measured the single molecule membrane binding frequency of AF647-PIP5KB and AF647-PIP5KB (W365P) (**Fig. 2.1E** and **Fig. S2C-S2D**). Mutating the specificity loop resulted in a 19-fold decrease in the association rate constant (k_{ON}) compared to wild type PIP5KB (**Fig. 2.1E**). A similar reduction in the membrane binding frequency was observed for mNG-PIP5KB (W365A) (**Fig. S2E**). In addition to the observed reduction in k_{ON} for AF647-PIP5KB (W365P), disrupting the specificity loop reduced the single molecule dwell time in the presence of $PI(4,5)P_2$ (**Fig. 2.1F-2.1G**). Considering that the specificity loop has been

proposed to penetrate directly into membranes [67], we expected to observe a more dramatic decrease in the membrane dwell time. Mutations that preserve the alpha helical character of the specificity loop (i.e. W365A and L61E/W365R) but reduce the hydrophobicity, displayed similarly modest decreases in the dwell time on $PI(4,5)P_2$ containing membranes (**Fig. S2F**). Together, these findings suggest that while binding frequency and dwell time were diminished, the PIP5K specificity loop mutants could still dock on $PI(4,5)P_2$ containing membranes.

The single molecule supported membrane binding experiments are excellent platform for measuring individual proteins-lipid interactions, however, they lack some of the complexity of the cell plasma membrane. For example, the supported bilayers described here lack sterol lipids and various peripheral membrane binding proteins that could modulate membrane localization of PIP5K. To determine whether membrane binding of PIP5KB (W365P) was similarly altered in living cells, we established conditions to visualize the plasma membrane localization of PIP5KB in HEK293T cells with single molecule resolution using TIRF-M. For these experiments, genes encoding either mEos-tagged PIP5KB or PIP5KB (W365P) were transiently expressed in HEK293T cells under a heat shock promoter, which yielded a near single molecule membrane density of fluorescently tagged kinase localized to the plasma membrane (**Fig. 2.1H**). Following a short pulse of 405 nm light, a fraction of the mEos-tagged PIP5K were photoconverted from the green to red fluorescent state, which provided the spatial resolution needed to track single PIP5K molecules (**Fig. 2.1H**). Based on measurements across multiple cells, we classified significantly more transient localization events (i.e. < 104 ms) in the presence of mEos-PIP5KB (W365P). Excluding these brief localization events from our data set, we still consistently measured average dwell times of mEos-PIP5KB (W365P) that were shorter compared to mEos-PIP5KB (**Fig. 2.1J**). The observed membrane binding frequency of mEos-PIP5KB (W365P) was also reduced.

However, calculating the k_{ON} for mEos-PIP5KB (WT and W365P) in cells was impractical due to cell-to-cell variation in protein expression and differences in the fraction of photoconverted mEos, which make it challenging to calculate the cellular concentration of PIP5K. Overall, our cellular measurements agree with our in vitro observations that the specificity loop facilitates PI(4,5)P_2 binding but is not essential for membrane localization.

The PIP5K specificity loop enhances PI(4)P and PI(4,5)P_2 specificity of chimeric proteins

Previous research indicates that the specificity loop controls membrane docking of PIP5K through substrate specificity [63,65,67]. This is supported by molecular dynamics simulations that indicate membrane docking relies on the initial engagement of PI(4)P by the specificity loop, which then transitions to the active site for catalysis [99]. Based on our single molecule dwell time analysis of AF647-PIP5KB on SLBs, the specificity loop regulates the rate of membrane association (k_{ON}) on PI(4,5)P_2 containing membranes (**Fig. 2.1E**). Given these findings, we hypothesize that the specificity loop can directly interact with PI(4,5)P_2 lipids, a function previously uncharacterized. One question that arises with this hypothesis is whether the specificity loop functions as a broad anionic lipid binding domain or if it has specificity for certain PIP lipids. Given that the specificity loop has been previously shown to favor PI(4)P binding and block PI(5)P binding, we would hypothesize that the specificity loop does not act as a broad anionic binding domain. Testing these hypotheses with the full PIP5K protein, however, would be difficult due to multiple areas of high electro positivity on the protein that play their own role in membrane binding. To isolate the question of whether the specificity loop can function as a specific PI(4)P and PI(4,5)P_2 lipid sensor, we created a chimeric mNeonGreen (mNG) fusion protein containing the PIP5K specificity loop fused to the pleckstrin homology (PH) domain derived from

phospholipase C-δ1 (i.e. mNG-5K(SL)-PLCδ) (**Fig. 2.2A**). Characterization of the mNG-5K(SL)-PLCδ membrane binding properties in the context of PLCδ provided an approach for measuring the potential gain in PIP lipid specificity and enhanced membrane binding affinity due to the addition of the PIP5KB specificity loop. Using single molecule TIRF-M we examined whether mNG-5K(SL)-PLCδ acquired membrane binding specificity for either PI(4)P or PI(5)P lipids (**Fig. 2.2B**). Consistent with PH-PLCδ lacking specificity for either PI(4)P or PI(5)P, mNG-PLCδ did not strongly interact with either lipid on supported membranes (**Fig. 2.2B**). By contrast, we observed an increase in the single molecule dwell time for mNG-5K(SL)-PLCδ in the presence of PI(4)P, but not PI(5)P (**Fig. 2.2B**). This result supports that the PIP5K specificity loop can discriminate between PI(4)P and PI(5)P, even when fused to a different peripheral membrane binding protein. Note that we also attempted to visualize membrane interactions of mNG fused to the PIP5K specificity loop (i.e. mNG-5K-SL), however, this chimeric protein displayed very transient membrane interactions that were not quantifiable. Presumably, the additional weak electrostatic interactions provided by PH-PLCδ facilitated membrane association in the presence of 5K(SL). As a control, we performed these same single molecule tracking experiments on PI(4)P and PI(5)P with both mNG-PIP5KB and the mNG-PIP5KB (W365P) specificity loop mutant (**Fig. S3A-S3C**). Overall, we observed similar trends as Figure 1D-E, mutating the specificity loop had a more dramatic effect on the dwell times measured in the presence of PI(4)P (**Fig. S3B-S3C**).

Figure 2.2

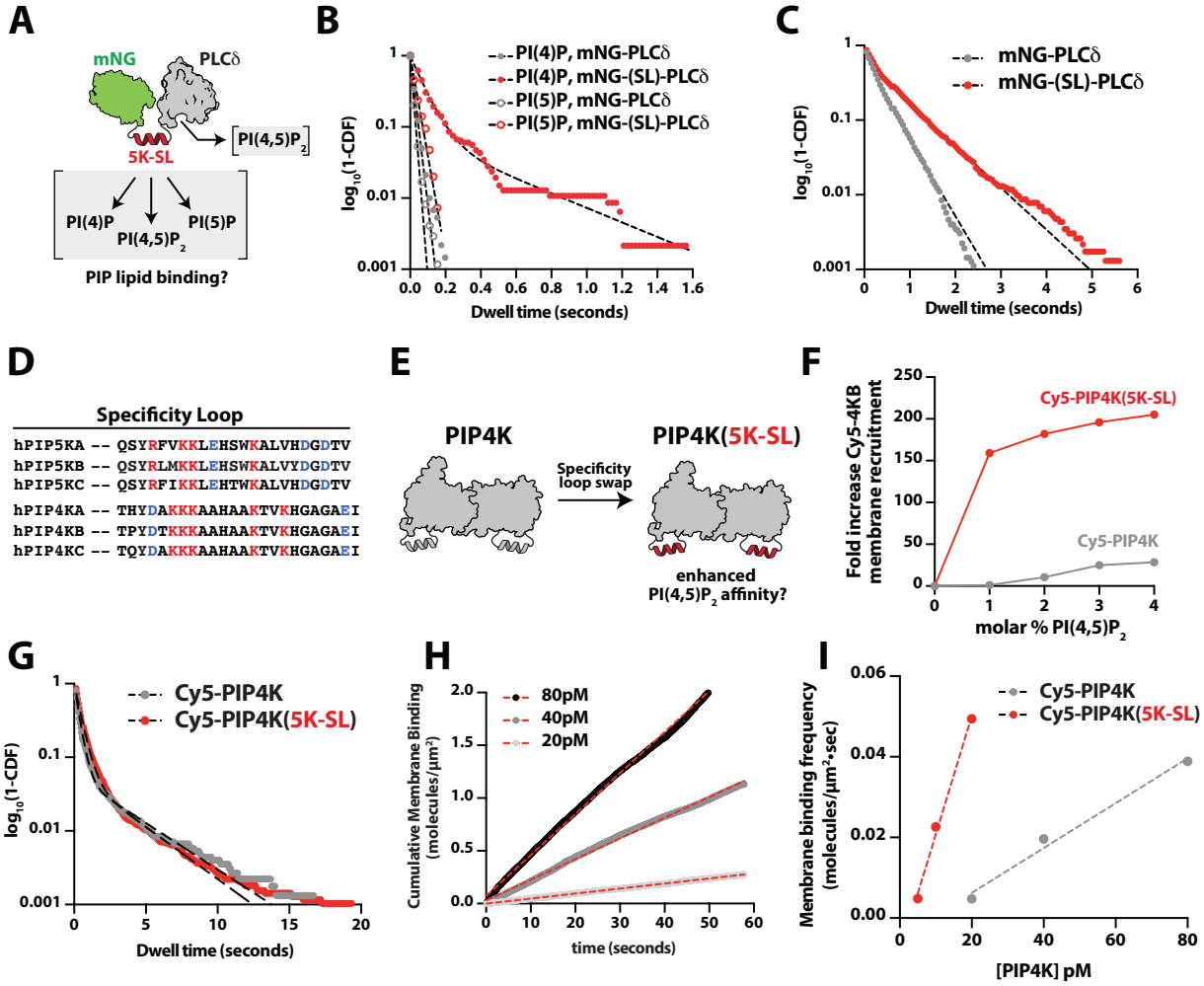

Figure 2.2

The PIP5K specificity loop enhances PI(4,5)P_2 lipid binding.

(A) Cartoon showing the structure of the mNG-PIP5K specificity loop-PLCδ chimeric protein. The expected PIP lipid binding interactions are indicated. **(B)** Single molecule dwell time distributions of mNG-PLCδ measured on membranes containing either PI(4)P (t_1 = 20 ± 1 ms, n = 6456) or PI(5)P (t_1 = 26 ± 10 ms, n = 2872). Single molecule dwell time analysis of mNG-(5K-SL)-PLCδ yield the following time constants: PI(4)P (t_1 = 42 ± 34 ms, t_2 = 314 ± 271 ms, α = 0.81 ± 0.13, n = 4274) or PI(5)P (t_1 = 82 ± 13 ms, n = 855). In both cases, dwell times were measured on membrane containing 4% PI(4)P or 4% PI(5)P. **(C)** Single molecule dwell time distributions of mNG-PLCδ (t_1 = 0.346 ± 0.041s, n = 5414) and mNG-(5K-SL)-PLCδ (t_1 = 0.127 ± 0.059 s, t_2 = 0.797 ± 0.066 s, α = 0.47 ± 0.06, n = 3082) measured on membranes containing 4% PI(4,5)P_2. **(D)** Sequence alignment of PIP5K and PIP4K specificity loops. **(E)** Cartoon showing the PIP4K to PIP5K specificity loop swap. **(F)** Quantification of the fold increase in localization of Cy5-PIP4K and Cy5-PIP4K(5K-SL) on membranes containing different molar concentrations of PI(4,5)P_2. The fold change was calculated relative to the measured membrane density in the absence of PI(4,5)P_2. **(G)** Single molecule dwell time distributions of Cy5-PIP4K (t_1 = 0.248 ± 0.021 s, t_2 = 1.82 ± 0.16 s, α = 0.81 ± 0.04, n = 13117 molecules) and Cy5-PIP4K(5K-SL) (t_1 = 0.431 ± 0.067 s, t_2 = 8.77 ± 4.9 s, α = 0.84 ± 0.05, n = 12720 molecules) measured on membranes containing 4% PI(4,5)P_2. **(H)** Plots showing the cumulative membrane binding events measured in the presence of 20-80 pM Cy5-PIP4K. The slope of

each curve was calculated by linear regression yielding a binding frequency for each concentration of Cy5-PIP4K. **(I)** Experimental measure of membrane binding frequency in the presence of 20-80 pM Cy5-PIP4K (k_{ON} = 0.56/nM•μm^2•sec) or 5-10 pM Cy5-PIP4K(5K-SL) (k_{ON} = 2.93/nM•μm^2•sec).

In addition to regulating substrate recognition, our results indicate that the specificity loop controls PI(4,5)P_2 lipid binding and contributes to the positive feedback loop observed during PIP5K mediated production of PI(4,5)P_2. To determine if the PIP5K specificity loop can generally enhance the affinity of other membrane binding proteins we compared the single molecule dwell times of mNG-PLCδ and mNG-5K(SL)-PLCδ on PI(4,5)P_2 containing membranes (**Fig. 2.2C**). Both mNG-PLCδ and mNG-5K(SL)-PLCδ displayed transient dwell times that were nearly identical, due to both proteins sharing the common PH-PLCδ domain (**Fig. 2.2C**). Looking at the dwell time distribution of mNG-5K(SL)-PLCδ, we observed a second population of longer dwelling molecules, consistent with the specificity loop enhancing PI(4,5)P_2 association (**Fig. 2.2C**).

Our recent membrane binding study of the type II phosphatidylinositol-5-phosphate 4-kinase (PIP4K) revealed that a threshold membrane density of ~3% PI(4,5)P_2 lipids was required to observe robust PIP4K localization on supported lipid bilayers [76]. By contrast, PIP5K strongly localizes to membranes containing only 1% PI(4,5)P_2 [69,76]. To determine whether the difference in PI(4,5)P_2 dependent membrane association is related to the specific loop sequence variation between PIP4K and PIP5K (**Fig. 2.2D**), we generated a PIP4KB to PIP5KB specificity loop swap referred to as PIP4K(5K-SL) (**Fig. 2.2E**). We quantified the difference in Cy5-PIP4K and Cy5-PIP4K(5K-SL) bulk membrane recruitment on supported membranes containing varying concentrations of PI(4,5)P_2 (**Fig. 2.2F-2.2G and Fig. SF2**). In the presence of 1% PI(4,5)P_2, Cy5-PIP4K(5K-SL) reached a final equilibrium membrane surface density that was 160-fold greater than Cy5-PIP4K (**Fig. 2.2F**). Visualization of the single molecule membrane binding properties of

Cy5-PIP4K and Cy5-PIP4K(5K-SL) revealed that the two kinases had similarly long dwell times (**Fig. 2.2G**). Swapping the specificity loop, however, increased the association rate constant (k_{ON}) Cy5-PIP4K(5K-SL) by 5-fold (**Fig. 2.2H-2.2I**). This is consistent with the role the specificity loop serves in enhancing PIP5K membrane localization to PI(4,5)P_2 containing membranes. Considering that the PIP4KB to PIP5KB specificity loop swap reduces the isoelectric from 9.7 to 8.4, the observed enhancement in membrane localization for Cy5-PIP4K(5K-SL) cannot be attributed solely to a change in net positive charge. Overall, these data confirm that the PIP5K specificity loop can sense both PI(4)P and PI(4,5)P_2 lipids. This data also provides one explanation for why PIP4K has a reduced capacity to localize to PI(4,5)P_2 lipids compared to PIP5K both in vivo and in vitro.

Molecular basis of the PIP5K high affinity PI(4,5)P_2 lipid interaction

Having established that the specificity loop serves an important role in regulating the initial membrane docking step of PIP5K, we sought to identify residues responsible for the high affinity PI(4,5)P_2 lipid binding interaction. We hypothesized the existence of this interaction site based on the ability of AF647-PIP5K (W365P) to stably associate with PI(4,5)P_2 containing membranes (**Fig. 2.1**). PIP5K contains numerous basic amino acids on the membrane binding interface that could promote interactions with anionic lipids [68,100]. Structural biochemistry studies of zPIP5KA protein crystals soaked with selenate resolved a SeO_4^{2-} molecule bound to basic residues (i.e. K238 and R244) near the ATP binding pocket [63]. These residues are part of a conserved sequence, DLKGSxxxR, which is referred to as the PIP binding motif (PIPBM) or substrate binding motif [63] (**Fig. 2.3A**). The PIPBM is considered part of the kinase domain active site and plays an important role in positioning PI(4)P near the ATP γ-phosphate for efficient lipid phosphorylation [63].

Consistent with this model, molecular dynamic (MD) simulations have shown that zPIP5KA interacts with PI(4)P lipids through the PIPBM (Amos et al. 2019). Mutations of R244 have been shown to reduce zPIP5KA lipid kinase activity, but paradoxically does not affect the intrinsic ATP hydrolysis rate of zPIP5KA in solution [63].

Figure 2.3

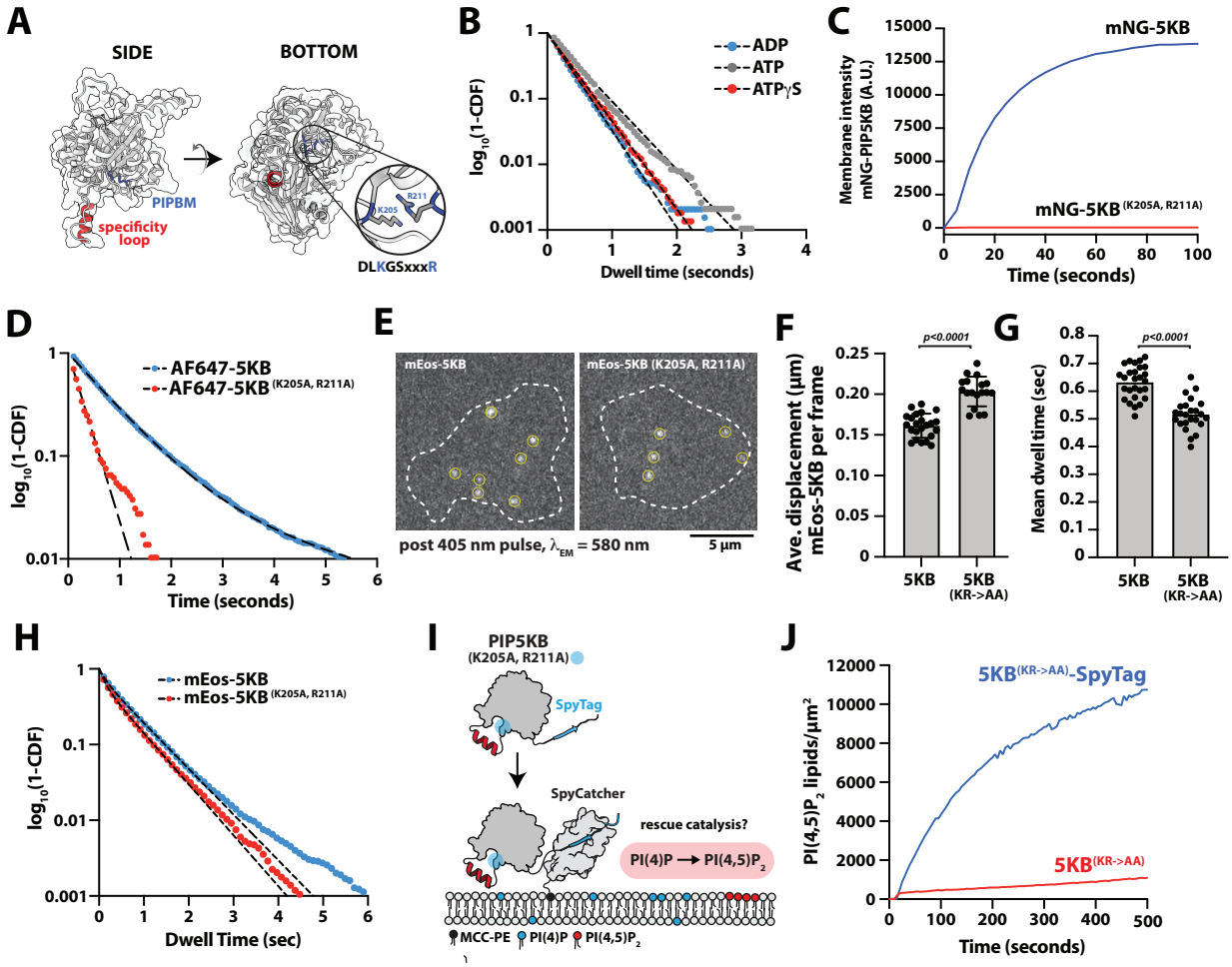

Figure 2.3
PIP5K can engage PI(4,5)P_2 lipids through the substrate binding motif.
(A) AlphaFold structure of human PIP5KB validated against zPIP5Kα (5E3U.pdb). Structure highlights the specificity loop (red) and the PIP lipid (or substrate) Binding Motif (PIPBM, blue). **(B)** Single molecule dwell time distributions of AF647-PIP5KB measured in the buffer containing 1 mM ATP (t_1=0.463 ± 0.16 sec, n = 6377), ADP (t_1=0.365 ± 0.11 sec, n = 10543), or ATPγS (t_1=0.329 ± 0.004 sec, n = 6231). **(C)** Bulk membrane recruitment of either 25nM mNG-PIP5KB or mNG-PIP5KB (K205A/R211A). (B-C) Membrane composition: 98% DOPC, 2% PI(4,5)P_2. **(D)** Single molecule dwell time distribution comparing AF647-

PIP5KB and AF647-PIP5KB (K205A/R211A, t_1 = 0.306 ± 0.19 sec, n = 684). Membrane composition: 98% DOPC, 2% PI(4,5)P_2. **(E)** Representative TIRF-M images showing the localization of the mEos-PIP5KB (WT and K205A/R211A) expressed in HEK293T cells. **(F)** mEos-PIP5KB (K205A,R211A) is more diffuse in the cellular plasma membrane compared to mEos-PIP5KB. Average single molecule displacement during 52 ms time interval is greater for mEos-PIP5KB K205A,R211A (0.203 ± 0.02 μm, *N* = 18 cells) compared to mEos-PIP5KB (0.161 ± 0.01 μm, *N* = 23 cells). Each data point is the average displacement measured for a single cell. **(G)** The mean dwell time of mEos-PIP5KB K205A/R211A (0.516 ± 0.06s, *N* = 24 cells) is shorter compared to mEos-PIP5KB (0.632 ± 0.06s, *N* = 27 cells). Each data point is derived from a single cell. (F-G) *P* value calculated by unpaired Student's *t*-test. **(H)** Significantly more transient interactions observed for mEos-PIP5KB K205A/R211A (t_1 = 0.142 s, t_2 = 0.645 s, α = 0.34, n = 15162 molecules, *N* = 24 cells) compared to mEos-PIP5KB (t_1 = 0.159 s, t_2 = 0.719 s, α = 0.22, n = 19450 molecules, *N* = 27 cells). Dwell time distribution was fit using all single molecule binding events measured across all cells. **(I)** Schematic showing SpyTag-PIP5KB (K205A/R211A) and SpyCatcher kinase activity assay. **(J)** Kinetics of lipid phosphorylation measured for membrane tethered and non-tethered SpyTag-PIP5KB (K205A/R211A). Production of PI(4,5)P_2 was monitored in the presence of 20 nM Cy3-PLC*δ*. Initial membrane composition: 98% DOPC, 2% PI(4)P.

Does the PIPBM regulate PI(4,5)P_2 binding? Structural modeling of PI(4)P bound to the PIPBM previously suggested that the inositol 5-phosphate of PI(4,5)P_2 would sterically clash with the γ-phosphate of ATP [63]. However, when we measured the single molecule dwell times AF647-PIP5KB in TIRF-M imaging buffer containing either ADP, ATP, or nonhydrolyzable ATPγS, we found that the kinase could associate with PI(4,5)P_2 membranes independent of the nucleotide chemistry (**Fig. 2.3B**). In fact, the presence of ATP caused AF647-PIP5KB to dwell slightly longer (t_1=0.463 ± 0.16 sec) on membranes compared to kinases visualized in the presence of ADP (t_1=0.365 ± 0.11 sec) or ATPγS (t_1=0.329 ± 0.004 sec). This suggests that nucleotide binding does not sterically occlude the interaction between PIP5K and PI(4,5)P_2, which led us to hypothesize that the conserved PIPBM could potentially regulate PI(4,5)P_2 lipid binding. To test whether the PIPBM is required for the PI(4,5)P_2 lipid interactions, we introduced mutations that were homologous to zPIP5KA (i.e. K238 and R244) into human PIP5KB (i.e. K205A and R211A). We found that disrupting the PIPBM strongly diminished bulk membrane binding of PIP5K on PI(4,5)P_2 containing membranes (**Fig. 2.3C**). Consistent with our bulk membrane localization experiment, single molecule characterization of AF647-PIP5KB (K205A/R211A) revealed a 2.4-

fold decrease in the average dwell time compared to AF647-PIP5KB (**Fig. 2.3D**). Interestingly, while we did see greatly diminished dwell time, we did not observe a complete loss of PI(4,5)P_2 binding. This shorter dwell time could be explained by the remaining specificity loop binding interaction. To determine if our in vitro membrane binding results are consistent with in vivo membrane binding dynamics, we expressed mEos-PIP5KB (K205A, R211A) in HEK293T cells and quantified the single molecule plasma membrane dwell time (**Fig. 2.3E**). Consistent with the mutant having a reduced frictional drag coefficient in the plasma membrane due to fewer lipid interactions, the average single molecule displacement of mEos-PIP5KB (K205A/R211A) was significantly larger compared to mEos-PIP5KB (**Fig. 2.3F**). The average single molecule dwell time for mEos-PIP5KB (K205A/R211A) was also shorter compared to mEos-PIP5KB (**Fig. 3G**). Fitting all the observed single molecule binding events revealed that a larger fraction of mEos-PIP5KB (K205A/R211A, 34%) molecules displayed a transient membrane binding behavior compared to mEos-PIP5KB (22%) (**Fig. 2.3H**). This data suggests that the PIPBM serves an important role in regulating PIP5K plasma membrane localization in cells.

Previous biochemical characterization of the zPIP5KA (R244A) mutant revealed that the PIPBM is critical for phosphorylating PI(4)P to generate PI(4,5)P_2 [63]. Our data also suggests that mutations in the PIPBM reduce PIP5K localization to membranes containing PI(4,5)P_2. This led us to hypothesize that the previously observed loss in zPIP5KA kinase activity could be partially due to a disruption in membrane binding. This would be consistent with zPIP5KA (R244A) displaying no change in the ATP hydrolysis rate measured in solution [63]. To test this hypothesis, we utilized the SpyTag-SpyCatcher interaction [101,102] to rescue PIP5KB (K205A/R211A) membrane localization and measure lipid kinase activity (**Fig. 2.3I**). For these experiments, SpyCatcher was conjugated to a bilayer via a maleimide lipid. SpyTag-mNG-PIP5KB

(K205A/R211A) was then flowed over the supported membrane in buffer lacking ATP and allowed to form an isopeptide bond with membrane conjugated SpyCatcher. Unbound kinase in solution was washed out of the sample chamber before initiating the kinase reaction by adding ATP containing buffer and the $PI(4,5)P_2$ biosensor, Cy3-PLCδ. Consistent with the previous characterization of zPIP5KA (R244A), we found that non-membrane tethered SpyTag-PIP5KB (K205A/R211A) mutant was unable to catalyze $PI(4,5)P_2$ production in solution (**Fig. 2.3J**). However, upon tethering to SpyTag-PIP5KB (K205A/R211A) to SLBs via SpyCatcher we were able to localize and rescue $PI(4,5)P_2$ production. Taken together, these data confirm that the site of high affinity binding and positive feedback come from binding $PI(4,5)P_2$ lipids in the PIP lipid binding motif (PIPBM). This high affinity binding interactions controls membrane localization of PIP5K both in vitro and in vivo.

The PIPBM displays broad specificity for anionic lipids

While the canonical activity of PIP5K is the phosphorylation of PI(4)P to produce $PI(4,5)P_2$, PIP5K can also phosphorylate PI(3)P and PI(5)P, albeit less efficiently compared to PI(4)P [63,66]. In addition, PIP5K has also been shown to catalyze the synthesis of the important signaling lipid $PI(3,4,5)P_3$ using $PI(3,4)P_2$ as a substrate. Having established that the PIPBM regulates membrane interactions with $PI(4,5)P_2$, we aimed to determine whether the PIPBM controls broad specificity for anionic lipids. For this, we created supported lipid bilayers and performed single particle tracking of mNG-PIP5K in the presence of various types of PIP lipids (**Fig. 2.4A** and **Table 2.1**). We found that mNG-PIP5K bound singly phosphorylated PI(4)P and PI(5)P lipids with a similarly low affinity, while interactions with either doubly or triply

phosphorylated PIP lipids (PI(3,4)P_2, PI(4,5)P_2, and PI(3,4,5)P_3) displayed longer dwell times (**Fig. 2.4A** and **Table 2.1**).

Figure 2.4

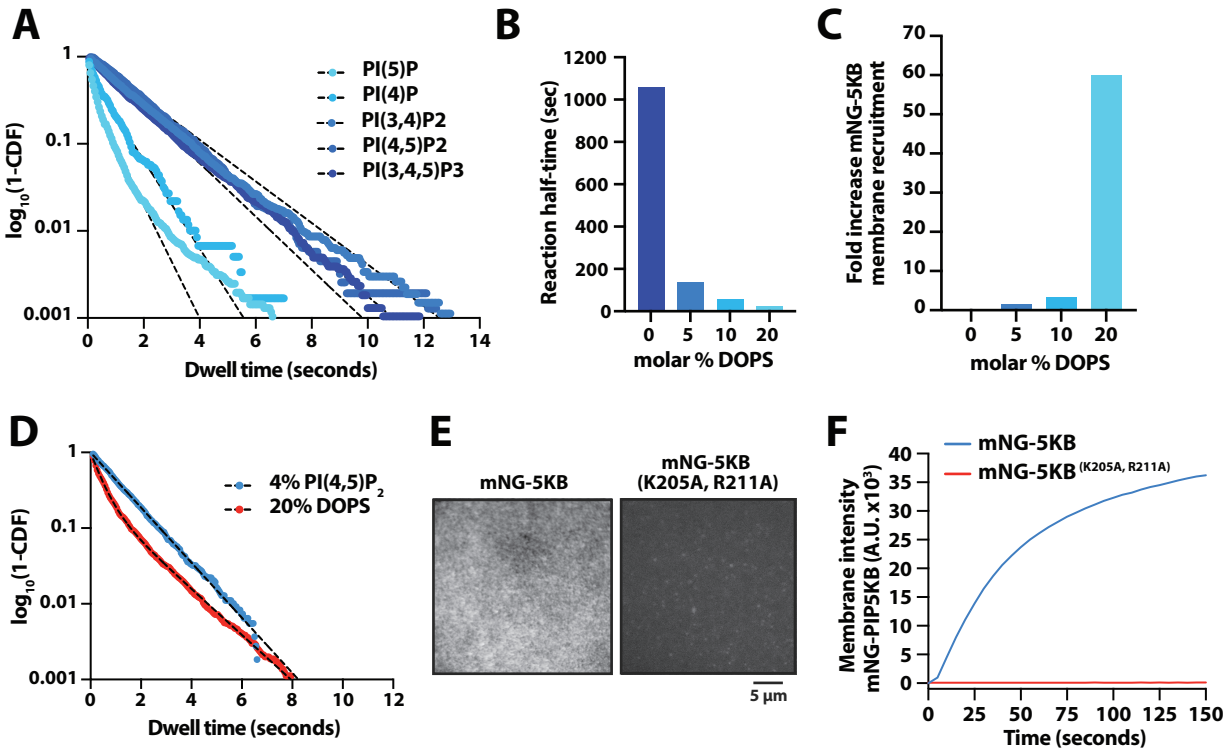

Figure 2.4
The PIP5K PIPBM exhibits broad specificity for anionic lipids.
(A) Single molecule dwell time distributions measured in the presence of mNG-PIP5KB on SLBs containing 4% of the indicated PIP lipid. **(B)** Kinetics of PIP5KB dependent lipid phosphorylation measured in the presence of 0-20% DOPS. All membranes contain 2% PI(4)P and reactions were monitored using 20 nM Cy3-PLCδ. Kinetics were quantified by comparing the half-time for reaction completion. **(C)** Quantification of the fold increase of membrane recruitment measured in the presence of 15 nM mNG-PIP5KB on SLBs containing 0-20% DOPS. The fold increase in membrane binding we calculated relative to the membrane intensity of mNG-PIP5K measured in the absence of DOPS. **(D)** Single molecule dwell time analysis of mNG-PIP5KB in the presence of 4% PI(4,5)P_2 or 20% DOPS. **(E)** Representative TIRF-M images showing the membrane localization of 15 nM mNG-PIP5K or mNG-PIP5K (K205A/R211A). Membrane composition: 20% DOPS, 80% DOPC. **(F)** Quantification of bulk recruitment data shown in (E). See Table 2.1 for single molecule dwell times (t_1 and t_2) and statistics.

To test whether PIP5KB prefers to bind doubly and triply phosphorylated PIP lipids due to the structure of the inositol head group versus the total negative charge, we examined the membrane binding properties of mNG-PIP5KB in the presence of PS lipids. We chose phosphatidylserine (PS) because its headgroup has a distinct chemical structure compared to PIP lipids but retains a negative charge. PS lipids have also previously been shown to activate PIP5K, though the molecular basis of this activation was not understood [103]. In agreement with published data, we found that increasing the molar percentage of PS enhanced PIP5K activity, with a physiologically relevant concentration of 20% PS lipids increasing the kinase activity 42.5-fold compared to membranes that contained 2% PI(4)P and no PS lipids (**Fig. 2.4B**). Correlated with the observed increase in kinase activity, mNG-PIP5KB localization displayed a nonlinear response to PS membrane density. At the physiologically relevant concentration of 20% PS, mNG-PIP5KB membrane localization increased 60-fold compared to membranes lacking PS lipids (**Fig. 2.4C**). Next, we compared the single molecule dwell times of mNG-PIP5KB associated with supported membranes containing either 4% PI(4,5)P_2 or 20% PS lipids. In the presence of either of these lipid species, mNG-PIP5KB displayed similarly long membrane dwell times (**Fig. 2,4D** and **Table 1**). To determine if the interaction with PS lipids was mediated by the PIPBM, we measured the bulk membrane localization of mNG-PIP5K (K205A, R211A). Like our characterization of mNG-PIP5K (K205A, R211A) membrane binding in the presence of PI(4,5)P_2 (**Fig. 2.3C**), the PIPBM mutant was unable to localize to membranes containing 20% PS lipids (**Fig. 2.4E-2.4F**). Taken together, these data demonstrate that PIP5K is localized to PS through association of the lipid with

the PIPBM, supporting a model in which the PIPBM functions as a broad specificity anionic lipid sensor.

Deciphering the relationship between PIP5K membrane recruitment and catalysis

Our membrane binding studies of the PIPBM mutant revealed that residues that have previously been shown to be critical for lipid kinase activity also regulate PIP5K membrane localization. This raised questions about whether other commonly studied "kinase dead" mutants are defective in membrane binding. For this reason, we aimed to isolate a PIP5K "kinase dead" mutant that lacks lipid phosphorylation activity, but retains the membrane binding dynamics characteristic of the wild type enzyme. To validate a separation of function mutant, we rationalized that PIP5K must have a functional specificity loop and PIPBM. Looking at existing structural biochemistry data of zPIP5KA [63], we found that residue D350 helps coordinate a Mg^{2+}/Mn^{2+} ions in the active site in PIP5KB (**Fig. 2.5A**).

Figure 2.5

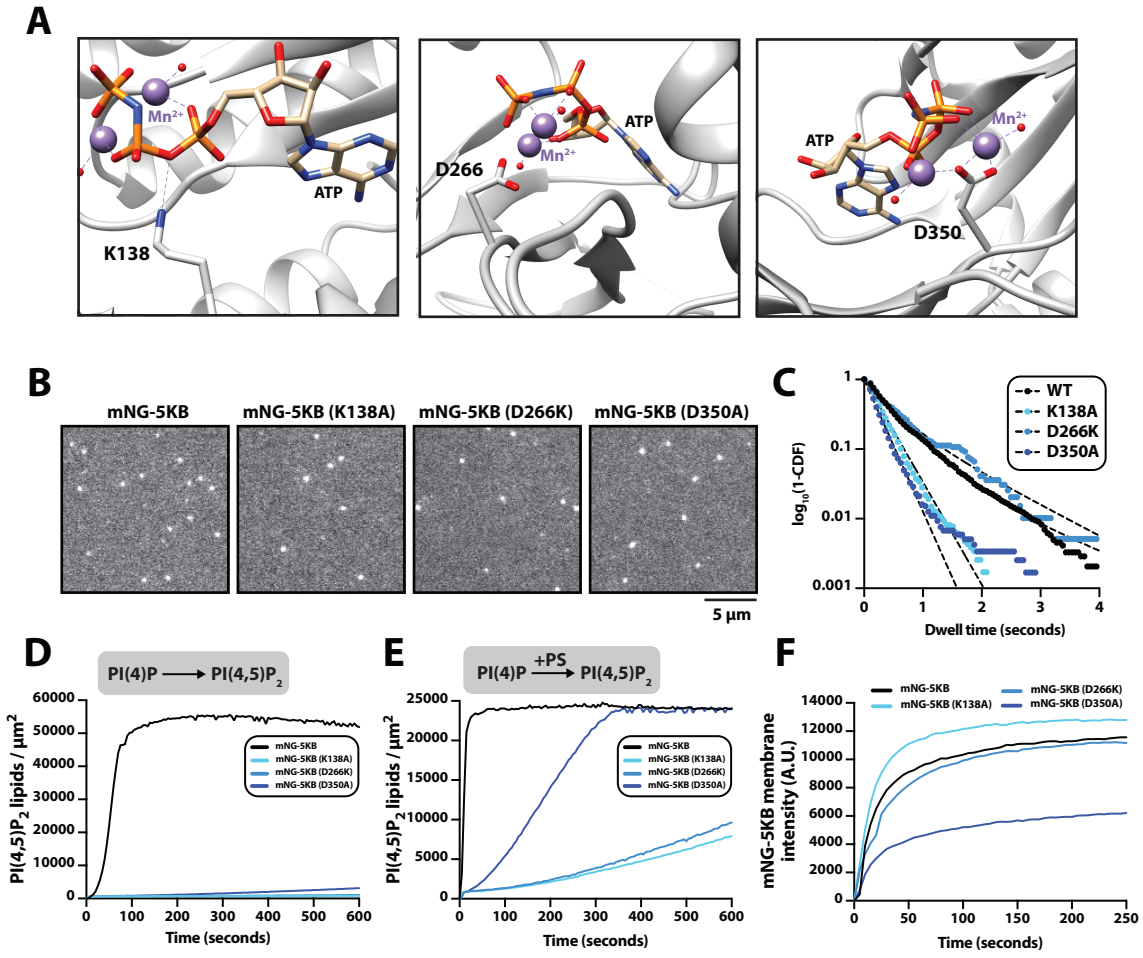

Figure 2.5

Deciphering the relationship between PIP5K catalysis and membrane recruitment.

(A) Structure of zPIP5KA (5E3U.pdb) showing the position of residues that are important for catalysis. Residue numbers represent human PIP5KB amino acids that are homologous to the zPIP5KA residues shown in the structure. **(B)** Representative TIRF-M images showing the localization of mNG-PIP5KB (WT and mutants). **(C)** Single molecule dwell time distributions for mNG-PIP5KB (WT and mutants) measured. See Table 1 for single molecule dwell times (t_1) and statistics. (B-C) Membrane composition: 98% DOPC, 2% $PI(4,5)P_2$. **(D)** Bulk membrane recruitment measured by TIRF-M in the presence of 20 nM mNG-PIP5KB (WT and mutants). Membrane composition: 98% DOPC, 2% $PI(4,5)P_2$. **(E-F)** Lipid kinase activity measured using TIRF-M in the presence of 10 nM PIP5KB (WT and mutants). Production of $PI(4,5)P_2$ was monitored in the presence of 20 nM Cy3-PLCδ. (E) Membrane composition: 96% DOPC, 4% PI(4)P. (F) Membrane composition: 78% DOPC, 2% PI(4)P, 20% DOPS.

Mutations in this residue are predicted to destabilize the transition state following nucleophilic attack of the ATP gamma phosphate. In addition, residues K138 and D266 of PIP5KB serve important roles in stabilizing ATP in the active site. Using the mNG-PIP5K single molecule TIRF assay we quantified the membrane binding properties of fluorescently labeled PIP5KB (K138A, D266A, and D350A) on supported membranes containing 2% $PI(4,5)P_2$ (**Fig. 2.5B**). We found that only the D266K mutant exhibits membrane binding properties that phenocopy the wild type PIP5KB (**Fig. 2.5C**). This was observed when we measured the single molecule dwell times (**Fig. 2.5C** and **Table 1**) and bulk membrane recruitment (**Fig. 2.5D**). Next, we measured the catalytic efficiency of each mutant on supported membranes containing an initial concentration of 4% PI(4)P and no additional anionic lipids. Under these conditions, none of the mutants displayed significant levels of activity compared to wild type PIP5KB (**Fig. 2.5E**). When we repeated these experiments on supported membranes containing 20% PS lipids, we were able to stimulate the activity of PIP5KB (D350A) through enhanced membrane localization (**Fig. 2.5F**). However, the K138A and D266K mutants still displayed weak activity even though their membrane localization dynamics were similar to wild type PIP5KB. Together, these results indicate that some PIP5K "kinase dead" mutants are defective in catalysis due to the inability to bind to anionic lipids, which controls membrane localization.

DISCUSSION

Previous structural biochemistry studies have implicated both the specificity loop and PIP lipid binding motif (also known as the substrate binding motif) of PIP5K in regulating substrate specificity and kinase activity [63,65–67]. These molecular details contribute to two potential models that describe PIP5K membrane docking and catalysis. In a single binding pocket model, the

specificity loop adopts a helical conformation positioned near the PIP lipid binding motif (PIPBM). These two motifs function in concert to form a single unified PIP lipid binding site responsible for substrate specificity. This model is supported by mutational analysis and chemical crosslinking studies that show the specificity loop and PIPBM move into close proximity of each other following substrate binding [63]. Alternatively, in a two-step binding model, the specificity loop regulates the initial membrane sensing and docking step, while the substrate binding and PI(4)P phosphorylation is mediated by the PIPBM [70]. In this model, the specificity loop holds the PIP5K enzyme at the membrane until the PI(4)P lipid interaction is repositioned to interact with the PIPBM. This model is supported by molecular dynamics simulations showing that PI(4)P binds to the specificity loop prior to engaging the PIPBM [99]. Through the direct visualization of fluorescently labeled PIP5K on supported lipid bilayers using TIRF microscopy, we found that mutating either the specificity loop or PIPBM disrupts PIP5K lipid kinase activity and positive feedback. In support of the two-step membrane recruitment mechanism, we find that mutating the specificity loop reduces the membrane binding frequency (k_{ON}), but only moderately affects the dissociation rate constant (k_{OFF}) of PIP5K. The ability of the PIPBM to facilitate membrane association in the absence of a functional specificity loop provides support for a two-step membrane recruitment mechanism. Although membrane recruitment of PIP5K is more robust in the presence of both a functional specificity loop and PIPBM, each motif can individually contribute to membrane binding.

Previous research has established the specificity loop as the determinative motif that controls substrate specificity of the type I and II PIP kinases, PIP4K and PIP5K [63,65–67]. Studies have identified specific residues in the PIP4K and PIP5K specificity loops that can be swapped to switch substrate recognition and modulate catalysis [63,66]. The structural basis of sequence

dependent changes in lipid specificity PIP4K and PIP5K, however, remains unclear. Our characterization of chimeric fusion proteins revealed that the PIP5K specificity loop can confer specificity for either PI(4)P and PI(4,5)P_2 when attached to another peripheral membrane binding protein. Fusing the PIP5KB specificity loop to the pleckstrin homology (PH) domain of PLCδ enhanced the ability of the mNG-(5K-SL)-PLCδ chimeric protein to interact with PI(4)P and PI(4,5)P_2 lipids, but not PI(5)P (**Fig. 2**). These findings support a model in which the specificity loop has preferred PIP lipid interactions, rather than functioning as a broad lipid membrane sensor.

The PIPBM has previously been described as the active site of the type I, II, and III PIP lipid kinases [63]. The finding that the PIPBM also strongly binds PI(4,5)P_2 lipids raises questions concerning how PIP5K can exhibit positive feedback based on product binding when PI(4,5)P_2 appears to function as competitive inhibitor. If PI(4,5)P_2 binds to the "active site", we expect to observe attenuated lipid kinase activity following PI(4)P phosphorylation. One mechanism that could resolve this paradox is through membrane-mediated dimerization of PIP5K. We previously reported that PIP5K dimerizes in a density-dependent manner and that dimerization potentiates lipid kinase activity through a mechanism consistent with allosteric regulation [71]. Molecular dynamics simulations have shown that only a single kinase domain of a PIP5K dimer is able to associate with membrane lipids [99]. Quantitative analysis of monomeric and dimeric mNG-PIP5K membrane surface densities also support a model in which only a single kinase domain can engage PI(4,5)P_2 on a membrane [71]. This may allow dimeric PIP5K to bypass PI(4,5)P_2 dependent inhibition by toggling membrane engagement of kinase domains between cycles of catalysis. Additional biochemical and molecular dynamics simulations are required to understand the mechanism for bypassing competitive inhibition.

Catalytically dead PIP5K mutants are often used in cellular PIP5K studies [76,104–106]. Many studies, however, used mutations to the PIPBM to achieve their "catalytically dead" PIP5K mutants. This is unideal, as we show in this study that mutation of the PIPBM leads to a dramatic decrease in membrane localization. We sought to identify candidate catalytically dead PIP5K mutants for the field to use in future in vivo studies. We used single molecule TIRF microscopy to characterize several catalytically dead PIP5K mutants (i.e. K138A, D266K, and D350A) with mutations outside of the PIPBM have previously been used in cell biological studies [73,75,76,104–112]. We found that PIP5KB (D266K) was the ideal separation of function mutant because it displayed single molecule membrane binding properties that were nearly identical to the wild type kinase while showing no discernable activity on PI(4)P membranes, and greatly reduced activity in the presence of a physiologically relevant concentrations of PS lipids. It's important to note that in the presence of 20% phosphatidylserine, none of the "catalytically dead" PIP5K mutants were fully inactive. Considering that the cellular environment contains a variety of antagonists, including PIP lipid phosphatases and PIP4K, the basal level of activity displayed by the PIP5KB (D266K) mutant will likely be suppressed in vivo.

Previous studies have shown that PIP5K enzymes target the inner leaflet of the cellular plasma membrane [68,76]. The prevailing hypothesis in the field is that PIP5K targets the membrane through direct association with the lipid substrate, PI(4)P, and interactions with peripheral membrane binding proteins [45,64,72,88,113]. But if PIP5K preferentially binds to its substrate lipid, PI(4)P, why does it target the inner leaflet of the plasma membrane and not other PI(4)P containing intracellular membranes? Previous characterization by immunofluorescence has shown that a large abundance of cellular PI(4)P exists at the Golgi cisternae [114–116]. The overall lack of strong PIP5K localization to the Golgi suggests that it's substrate, PI(4)P, is not the major lipid interaction that

promotes plasma membrane localization of PIP5K. Our data provides a different explanation for preferential inner leaflet targeting. First, we show that PIP5K binds $PI(4,5)P_2$ lipids with higher affinity than PI(4)P lipids (**Fig. 4A**), consistent with previous findings [69,71]. Previous work, however, demonstrated that disrupting $PI(4,5)P_2$ lipid concentrations diminishes, but does not fully abolish plasma membrane localization of PIP5K[68]. Our study explains this result by establishing that PIP5K recruits to membranes containing high molar concentrations of anionic lipids like phosphatidylserine. However, unlike $PI(4,5)P_2$ binding, which occurs even at low molar percentages, phosphatidylserine must be present at high molar concentrations >15% before we detect robust membrane recruitment of PIP5K (**Fig. 4C**). This switch-like recruitment to phosphatidylserine provides a possible explanation for PIP5K inner leaflet targeting. In mammalian cell membranes, despite phosphatidylserine being present at all intracellular membranes, it is only highly abundant (>15%) at the inner leaflet [117].

Researchers recently discovered that PIP4K negatively regulates PIP5K activity, which establishes a homeostatic mechanism for maintaining stable $PI(4,5)P_2$ levels at the plasma membrane [54,76]. Plasma membrane recruitment of PIP4K requires elevated levels of $PI(4,5)P_2$, where it then attenuates PIP5K catalytic activity through an unknown mechanism [76]. In vitro experiments have confirmed that PIP4K requires a higher molar concentration of $PI(4,5)P_2$ lipids for membrane localization compared to PIP5K [76]. Why PIP4K had a decreased sensitivity to $PI(4,5)P_2$ lipids compared to PIP5K was unclear. Here, we report that the difference in $PI(4,5)P_2$ lipid sensitivity can be attributed to the divergence in the PIP4K and PIP5K specificity loop sequences. Swapping specificity loops enhanced the membrane binding frequency of PIP4K, even on supported lipid bilayers containing 1% $PI(4,5)P_2$. Overall, our results show that the PIP4K and PIP5K specificity loop is a major factor that controls sensitivity to $PI(4,5)P_2$ lipids. These findings

reveal intricate mechanisms underlying membrane targeting and lipid kinase activity within the phosphoinositide signaling pathway, offering insights into potential avenues for modulating cellular PI(4,5)P_2 levels by PIP4K and PIP5K during cell signaling.

TABLE 2.1

Protein visualized	Membrane	$\tau_1 \pm SD$ (sec)	$\tau_2 \pm SD$ (sec)	$\alpha \pm SD$	*N*	*n*
mNG-PIP5KB	4% PI(4)P	0.469 ± 0.22	—	—	3	6251
mNG-PIP5KB	4% PI(5)P	0.557 ± 0.14	—	—	3	21425
mNG-PIP5KB	4% PI(3,4)P_2	0.854 ± 0.32	—	—	3	5461
mNG-PIP5KB	4% PI(4,5)P_2	1.05 ± 0.13	—	—	3	3993
mNG-PIP5KB	4% PI(3,4,5)P_3	0.503 ± 0.07	1.419 ± 0.028	0.42 ± 0.085	3	16930
mNG-PIP5KB	20% PS	0.322 ± 0.19	1.414 ± 0.49	0.74 ± 0.23	3	11351
mNG-PIP5KB	2% PI(4,5)P_2	0.468 ± 0.019	—	—	3	7075
mNG-PIP5KB (K138A)	2% PI(4,5)P_2	0.285 ± 0.004	—	—	3	7423
mNG-PIP5KB (D266K)	2% PI(4,5)P_2	0.619 ± 0.071	—	—	3	4667
mNG-PIP5KB (D350A)	2% PI(4,5)P_2	0.228 ± 0.004	—	—	3	3546

SD = standard deviation from the indicated number of technical replicates

N = # of SLBs or cells used for calculating the mean dwell times (i.e. technical replicates)

n = total number of molecules tracked across all of the indicated number of technical replicates (*N*)

alpha (a) = fraction of molecules with characteristic dwell time (t_1)

membrane composition equals DOPC plus the indicated molar percentage of PIP or PS lipids.

MATERIALS AND METHODS

Molecular Biology. The gene coding the PH domain derived from human phospholipase C-δ1 (PLCδ Accession #P51178.2), human phosphatidylinositol 4-phosphate 5-kinase type-1 beta (hPIP5KB; Uniprot #O14986) and human phosphatidylinositol 5-phosphate 4-kinase type-2 beta (hPIP4KB; Uniprot #P78356) were derived from codon optimized genes synthesized by GeneArt (Invitrogen). The gene encoding mEos3.2 [118] was PCR amplified and cloned in-frame with PIP5KB to create a N-terminal fusion for mammalian cell expression. Gene sequences were subcloned into either bacterial, insect cell, or mammalian expression vectors using Gibson assembly [119]. Plasmids containing PIP5KB mutations (i.e. W365A, W365P, D51R, K205A, R211A, K138A, D350A, D266K, etc.) were generated through site-directed mutagenesis using the PfuUltra High-Fidelity DNA polymerase (Agilent, cat# 600380). Chimeric mNG-PIP5K, mNG-PLCδ, and mNG-Specificity Loop-PLCδ were created using PCR amplification of genes via AccuPrime *Pfx* Master Mix (ThermoFisher, Cat#12344040) then combined with a digested plasmid using Gibson Assembly. The complete open reading frame of all vectors used in this study were sequenced by Azenta (formerly Genewiz) and Plasmidsaurus (University of Oregon) to ensure constructs lacked deleterious mutations. Each protein expression construct was screened for optimal yield and solubility in either bacteria (BL21 DE3 Star, Rosetta, etc.) or *Spodoptera frugiperda* (Sf9) insect cells. See Supplementary file for the amino acid sequences used during recombinant protein expression or transient transfection in HEK293T cells. Note that there have previously been inconsistencies in nomenclature between human and mouse PIP5K paralogs. In this manuscript, PIP5KB refers to the human PIP5KB paralog. All plasmids created and used within this manuscript function under this human nomenclature.

Protein purification

PIP5KB and mNG-PIP5K. Wild type and mutant PIP5K proteins were recombinantly expressed and purified as previously described [69,71]. Gene sequences encoding PIP5KB and mutants (i.e. W365P, D51R, and K205A/R211A) were cloned into FastBac1 vectors in frame with a N-terminal his_6-MBP-TEV-GGGGG or his_6-TEV-mNG-GGGGG and expressed under the polyhedrin (pH) promoter. BACMIDS and baculoviruses were generated as previously described [69]. For large protein expression, high five cells were infected with baculovirus using an optimized multiplicity of infection (MOI), typically 2% vol/vol. Infected insect cells were grown for 48 hours at 27ºC in ESF 921 Serum-Free Insect Cell Culture medium (Expression Systems, Cat# 96-001-01). Cells were then harvested by centrifugation, washed with 1x PBS [pH 7.2], resuspended in cell storage buffer (1x PBS [pH 7.2], 10% glycerol, 2x Sigma protease inhibitor table), and then stored in the -80ºC freezer. For purification, frozen insect cell pellets for 2-4 liters of liquid culture were thawed at room temperature in a water bath and lysed into buffer containing 50 mM Na_2HPO_4 [pH 8.0], 10 mM imidazole, 400 mM NaCl, 1 mM PMSF (added twice, once before homogenization and once after), 5 mM BME, 100 µg/mL DNase, SIGMAFAST protease inhibitor cocktail tablets, EDTA-free (Sigma, Cat# S8830-20TAB) per 100 mL lysis buffer. Cells in this buffer were lysed using a dounce homogenizer. Lysate was clarified by centrifugation at 36,000 rpm (140,000 x *g*) for 60 minutes under vacuum using a Beckman Ti-45 rotor at 4ºC. Lysate was then batch bound to 5 mL of Ni-NTA Agarose (Qiagen, Cat# 30230) resin at 4ºC for 2 hours in a beaker set on a stir plate. Resin was then collected in 50 mL tubes, centrifuged, and washed with buffer containing 50 mM Na_2HPO_4 [pH 8.0], 10 mM imidazole, 400 mM NaCl, and 5 mM BME and centrifuged again

before being transferred to gravity flow column in more wash buffer. Ni-NTA resin with his_6-MBP-TEV-GGGGG-PIP5K bound was then eluted into buffer containing 500 mM imidazole. Peak fractions were pooled, combined with 200 µg/mL his6-TEV(S291V) protease, and dialyzed against 4 liters of buffer containing 20 mM Tris [pH 8.0], 200 mM NaCl, 2.5 mM BME for 16-18 hours at 4ºC. Dialysate was then combined 1:1 with 20 mM Tris [pH 8.0], 1 mM TCEP (~100 mM NaCl final). Precipitation was removed by centrifugation and 0.22 µm syringe filtration. Clarified dialysate was then bound to a MonoS cation exchange column (GE Healthcare, Cat# 17-5168-01) equilibrated in 20 mM Tris [pH 8.0], 100 mM NaCl, 1 mM TCEP buffer. Proteins were resolved over a 10-100% linear gradient (0.1-1 M NaCl, 45 CV, 45 mL total, 1 mL/min flow rate). PIP5K homologs and paralogs typically eluted from the MonoS column in the presence of 370-450 mM NaCl. Peak fractions containing PIP5K were pooled, concentrated in a 30 kDa MWCO Vivaspin 6 centrifuge tube (GE Healthcare, Cat# 28-9323-17), and loaded onto a 24 mL Superdex 200 10/300 GL (GE Healthcare, Cat# 17-5174-01) size exclusion column equilibrated in 20 mM Tris [pH 8.0], 200 mM NaCl, 10% glycerol, 1 mM TCEP. Peak fractions were concentrated in a 30 kDa MWCO Vivaspin 6 centrifuge tube and snap frozen at a final concentration of 10-40 µM using liquid nitrogen. GGGGG-PIP5KB (WT and mutants) were labeled with Alexa647-LPETGG using sortase mediated peptide ligation as previously described [69].

PIP4K2B and PIP4K2B (5K-SL). Codon optimized gene sequence encoding human PIP4K2B isoform 2 (Uniprot # P78356) was cloned into a pETM derived bacterial expression vector to create the following fusion protein: his_6-SUMO3-GGGGG-PIP4K2B (1-416aa). Recombinant PIP4K2B was expressed in BL21(DE3) Star *E. coli* as previously described [76]. Using 2-4 liters of Terrific Broth, bacterial cultures were grown at 37ºC until OD_{600}=0.6. Cultures were then shifted to 18ºC

for 1 hour to cool down. Protein expression was induced with 50 μM IPTG and bacteria expressed protein for 20 hours at 18ºC before being harvested by centrifugation. For purification, cells were lysed into buffer containing 50 mM Na_2HPO_4 [pH 8.0], 400 mM NaCl, 0.4 mM BME, 1 mM PMSF (add twice, 15 minutes intervals), DNase, 1 mg/mL lysozyme using a microtip sonicator. Lysate was centrifuged at 16,000 rpm (35,172 x *g*) for 60 minutes in a Beckman JA-17 rotor chilled to 4ºC. Lysate was circulated over 5 mL HiTrap Chelating column (GE Healthcare, Cat# 17-0409-01) that had been equilibrated with 100 mM $CoCl_2$ for 1 hour, washed with MilliQ water, and followed by buffer containing 50 mM Na_2HPO_4 [pH 8.0], 400 mM NaCl, 0.4 mM BME. Recombinant PIP4K2B was eluted with a linear gradient of imidazole (0-500 mM, 8 CV, 40 mL total, 2 mL/min flow rate). Peak fractions were pooled, combined with 50 μg/mL of his6-SenP2 (SUMO protease), and dialyzed against 4 liters of buffer containing 25 mM Na_2HPO_4 [pH 8.0], 400 mM NaCl, and 0.4 mM BME for 16-18 hours at 4ºC. Following overnight cleavage of the SUMO3 tag, dialysate containing his6-SUMO3, his6-SenP2, and GGGGG-PIP4K2B was recirculated for at least 1 hr over a 5 mL HiTrap(Co^{+2}) chelating column. Flow-through containing GGGGG-PIP4K2B was then concentrated in a 30 kDa MWCO Vivaspin 6 before loading onto a Superdex 200 size exclusion column equilibrated in 20 mM HEPES [pH 7], 200 mM NaCl, 10% glycerol, 1 mM TCEP. In some cases, cation exchange chromatography was used to increase the purity of GGGGG-PIP4K2B before resolving on the Superdex 200 column. In those cases, we equilibrated a MonoS column 20 mM HEPES [pH 7], 100 mM NaCl, 1 mM TCEP buffer. PIP4K2B (pI = 6.9) bound to the MonoS was resolved over a 10-100% linear gradient (0.1-1 M NaCl, 30 CV, 30 mL total, 1.5 mL/min flow rate). Peak fractions collected from the Superdex 200 were concentrated in a 30 kDa MWCO Vivaspin 6 centrifuge tube and snap frozen at a final concentration of 20-80 μM using liquid nitrogen.

Codon optimized gene sequence encoding human PIP4K2B isoform 2 (Uniprot # P78356) was modified by PCR based insertion to swap the PIP4K2B specificity loop (372-384aa; DTKKKAAHAAKTVKHGAGAEI) for the PIP5KB specificity loop (353-373aa; RLMKKLEHSWKALVYDGDTV). This produced a chimeric PIP4K2B enzyme with a PIP5K specificity loop, which is referred to as PIP4K2B (5K-SL). The his_6-SUMO3-GGGGG-PIP4K2B (5K-SL) protein was purified as described above for wild type PIP4K2B. Both PIP4K2B and PIP4K2B (5K-SL) were labeled on a N-terminal GGGGG motif with Cy5-LPETGG using sortase mediated peptide ligation [69,71,120]. Following labeling, Cy5-PIP4KB and Cy5-PIP4KB (5K-SL) were resolved on a Superdex 200 size exclusion column equilibrated in 20 mM HEPES [pH 7], 200 mM NaCl, 10% glycerol, 1 mM TCEP. This removed free Cy5-LPETGG, Sortase (16 kDa), and a small amount of aggregated Cy5-PIP4KB. Peak fractions were pooled from the Superdex 200 column and concentrated using a 30 kDa MWCO Vivaspin 6 centrifuge tube before being snap frozen in liquid nitrogen at a final concentration of 10-20 μM.

PLCδ-PH domain. This protein was expressed and purified as previously described [69]. Briefly, human PLCδ-PH domain (11-140aa) was expressed in BL21 (DE3) Star *E. coli* as a his_6-SUMO3-$(Gly)_5$-PLCδ11-140aa) fusion protein. Following growth at 37ºC in Terrific Broth to an OD_{600} of 0.8, cultures were shifted to 18ºC for 1 hour, induced with 0.1 mM IPTG, and allowed to express protein for 20 hours at 18ºC before being harvested. Cells were lysed into 50 mM Na_2HPO_4 [pH 8.0], 300 mM NaCl, 0.4 mM BME, 1 mM PMSF, 100 μg/mL Dnase using a microfluidizer. Lysate was then centrifuged at 16,000 rpm (35,172 x *g*) for 60 minutes in a Beckman JA-17 rotor chilled to 4ºC. Lysate was circulated over 5 mL HiTrap Chelating column (GE Healthcare, Cat# 17-0409-01) charged with 100 mM $CoCl_2$ for 1 hour. Bound protein was then eluted with a linear gradient

of imidazole (0-500 mM, 8 CV, 40 mL total, 2 mL/min flow rate). Peak fractions were pooled, combined with SUMO protease (50 µg/mL final concentration), and dialyzed against 4 liters of buffer containing 50 mM Na_2HPO_4 [pH 8.0], 300 mM NaCl, and 0.4 mM BME for 16-18 hours at 4ºC. Dialysate containing SUMO cleaved protein was recirculated for 1 hr over a 5 mL HiTrap Chelating column. Flow-through containing $(Gly)_5$-PLCδ (11-140aa) was then concentrated in a 5 kDa MWCO Vivaspin 20 before being loaded on a Superdex 75 size exclusion column equilibrated in 20 mM Tris [pH 8.0], 200 mM NaCl, 10% glycerol, 1 mM TCEP. Peak fractions containing $(Gly)_5$-PLCδ (11-140aa) were pooled and concentrated to a maximum concentration of 75 µM (1.2 mg/mL) before snap freezing with liquid nitrogen and storage at -80ºC. As previously described, GGGGG-PLCδ11-140aa) was labeled with either AF488 or Cy3 using sortase mediated peptide ligation [69,71].

mNG-PLCδ-PH and mNG-(5K-SL)-PLCδ-PH. Genes encoding chimeric mNeonGreen-hPLCδ-PH domain (11-140aa) and mNeonGreen-hPIP5K Specificity Loop (353-373aa)-hPLCδ-PH domain (11-140aa) were cloned into bacterial expression vectors. Each construct was expressed in BL21 (DE3) Star *E. coli* as his_{10}-TEV fusion proteins. Bacteria were grown at 37ºC in Terrific Broth to an OD_{600} of 0.8. Cultures were induced with 0.1 mM IPTG and allowed to express protein for 20 hours at 18ºC before being harvested. Cells were lysed into 50 mM Na_2HPO_4 [pH 8.0], 400 mM NaCl, 0.5 mM BME, 1 mM PMSF, 100 µg/mL DNase using tip sonication (45% amplitude, 5 seconds on, 10 seconds off). Lysate was then centrifuged at 16,000 rpm (35,172 x *g*) for 60 minutes in a Beckman JA-17 rotor chilled to 4ºC. Lysate was circulated over 5 mL HiTrap Chelating column (GE Healthcare, Cat# 17-0409-01) charged with 100 mM $CoCl_2$ for 1 hour. Bound protein was then eluted with a linear gradient of imidazole (0-500 mM, 8 CV, 40 mL

total, 2 mL/min flow rate). Peak fractions were pooled and combined with 200 µg/mL his6-TEV(S291V) protease and dialyzed against 4 liters of buffer containing 50 mM Na_2HPO_4 [pH 8.0], 400 mM NaCl, and 0.4 mM BME for 16-18 hours at 4ºC. Dialysate containing cleaved His_{10}-TEV protein was recirculated for 1 hr over a 5 mL HiTrap Chelating column. Flow-through containing mNG-PLCδ or mNG-(5K-SL)-PLCδ were then concentrated in a 50 kDa MWCO Vivaspin 20 before being loaded on a Superdex 75 size exclusion column equilibrated in 25 mM Tris [pH 8.0], 150 mM NaCl, 10% glycerol, 1 mM TCEP. Peak fractions containing either mNG-PLCδ or mNG-(5K-SL)-PLCδ were pooled and concentrated to 4-20 µM before snap freezing with liquid nitrogen and storage at -80ºC.

Preparation of small unilamellar vesicles. The following lipids were used to generated small unilamellar vesicles (SUVs): 1,2-dioleoyl-sn-glycero-3-phosphocholine (18:1 DOPC, Avanti # 850375C), L-α-phosphatidylinositol-4-phosphate (Brain PI(4)P, Avanti Cat# 840045X), 1,2-dioleoyl-sn-glycero-3-phospho-(1'-myo-inositol-5'-phosphate) (PI(5)P, Avanti Cat# 850152P), L-α-phosphatidylinositol-4,5-bisphosphate (Brain $PI(4,5)P_2$, Avanti Cat# 840046X), D-myo-phosphatidylinositol 3,4,5-trisphosphate ($PI(3,4,5)P_3$ diC16, Echelon Cat# P-3916-100ug), D-myo-phosphatidylinositol 3,4-bisphosphate ($PI(3,4)P_2$ diC16, Echelon Cat# P-3416-100ug), 1,2-dioleoyl-*sn*-glycero-3-phospho-L-serine (18:1 DOPS, Avanti Cat# 840035C), 1,2-dioleoyl-sn-glycero-3-phosphoethanolamine-N-[4-(p-maleimidomethyl)cyclohexane-carboxamide] (18:1 MCC-PE, Avanti Cat# 780201C). To make liposomes, 2 µmoles total lipids are combined in a 35 mL glass round bottom flask with 2 mL of chloroform. Lipids were dried to a thin film using rotary evaporation with the glass round-bottom flask submerged in a 42ºC water bath. The lipid film was then resuspended in 2 mL of PBS [pH 7.2], getting a final concentration of 1 mM total lipids. All

lipid mixtures expressed as percentages (e.g. 98% DOPC, 2% PI(4)P) are equivalent to molar fractions. To generate SUVs, 1 mM total lipid mixture was extruded through a 0.05 μm pore size 19 mm polycarbonate membrane (Avanti, Cat# 610002) with filter supports (Avanti, Cat# 610014) on both sides of the polycarbonate membrane. Extruding hydrated lipids a total of 11 times achieved the desired SUV size of ~50 nm.

Preparation of supported lipid bilayers. Supported lipid bilayers are formed on 25x75 mm coverglass (IBIDI, Cat# 10812). Coverglass first is cleaned with 2% Hellmanex III (Fisher, Cat# 14-385-864) heated to 60-70ºC in a glass coplin jar. This was incubated for at least 30 minutes. Once incubated, the coverglass was washed thoroughly with MilliQ water. Once cleaned, the coverglass was then etched in Pirahna solution (1:3, hydrogen peroxide:sulfuric acid) for 10-15 minutes the same day SLBs were formed. Once etched coverglass was again thoroughly rinsed with MilliQ water before being rapidly dried with nitrogen glass. Once dried, glass was adhered to a 6-well sticky-side chamber (IBIDI, Cat# 80608). SLBs were formed by flowing 30 nm SUVs diluted in PBS [pH 7.2] to a total lipid concentration of 0.25 mM and incubated for 30 minutes. IBIDI chambers were then washed with 5 mL of PBS [pH 7.2] to remove non-absorbed SUVs. Membrane defects are blocked for 15 minutes with a 1 mg/mL beta casein (ThermoFisher, Cat# 37528) diluted in 1x PBS [pH 7.4]. Before use as a blocking protein, frozen 10 mg/mL beta casein stocks were thawed, centrifuged for 30 minutes at 21370 x *g*, and 0.22 μm syringe filtered. After blocking SLBs with beta casein, membranes were washed again with 1mL of PBS, followed by 1 mL of kinase buffer before TIRF-M.

Membrane conjugation of SpyCatcher. Following beta-casein blocking of SLBs, membranes that contained MCC-PE lipids were washed into 1x PBS [pH 7.2] containing 0.1 mM TCEP. MCC-PE lipids were used to covalently couple SpyCatcher protein onto supported bilayers. For these SLBs, 100 µL of 30 µM SpyCatcher diluted in a 1x PBS [pH 7.2] and 0.1 mM TCEP buffer was added to the IBIDI chamber and incubated for 2 hours at 23ºC. Once the coupling period passed, SLBs with MCC-PE lipids were then washed with 2 mL of 1x PBS [pH 7.2] containing 5 mM beta-mercaptoethanol (BME) and incubated in this buffer for 15 minutes to quench the unreacted maleimide headgroups. SLBs were then washed with 2 mL of 1x PBS to remove unbound protein. Membranes were stored for up to 2 hours in 1x PBS before being washed into imaging buffer to initiate TIRF-M measurements.

Assay for measuring the kinetics of PI(4,5)P_2 production. The kinetics of PI(4)P phosphorylation were measured on SLBs formed in IBIDI chambers and visualized using TIRF microscopy as previously described [69,71]. Imaging or reaction buffer contained 20 mM HEPES [pH 7.0], 150 mM NaCl, 1 mM ATP, 5 mM $MgCl_2$, 0.5 mM EGTA, 20 mM glucose, 200 µg/mL beta casein (ThermoScientific, Cat# 37528), 20 mM BME, 320 µg/mL glucose oxidase (Serva, Cat# 22780.01 *Aspergillus niger*), 50 µg/mL catalase (Sigma, Cat# C40-100MG Bovine Liver), and 2 mM Trolox (UV treated as previously described by Hansen et al. 2019). Perishable reagents (i.e. glucose oxidase, catalase, and Trolox) were added 5-10 minutes before image acquisition. For all experiments, we monitored the change in PI(4)P or PI(4,5)P_2 membrane density using a solution concentration of 20 nM AF488-GGGGG-PLCδ or Cy3-GGGGG-PLCδ. Density of PIP lipids (lipids/µm^2) was calculated assuming a footprint of 0.72 nm^2 for DOPC lipids [69,121].

Cell culture and live cell imaging. Human embryonic kidney (HEK) 293T cells were cultured in DMEM + GlutMAX + High Glucose (4.5 g/L) + sodium pyruvate (110 mg/L) (Life Technologies, cat #10569010) supplemented with 10% FBS (Sigma, cat# F4135-500ML), penicillin (100 units/ml), and streptomycin (100 µg/ml). Cells were grown in 10 cm dishes in humidified incubators at 37°C in the presence of 5% CO_2 and split at a confluency of 80-90% every 2-3 days. HEK293T cells were split using using 1.5mL of 0.25% Trypsin. Trypsin was that quenched with 8.5 mL complete DMEM media containing 10% FBS. Cells were diluted 1:10 and seeded on a new 10 cm dish containing a total volume of 10 mL complete DMEM media warmed to 37°C.

HEK293T cells were prepared for imaging by seeding cells at a confluency of 30% in an 18-well glass bottom chamber (IBIDI, Cat# 81817) 48-hours before imaging. Cells were transfected 24-hours before imaging with 0.1 µg of plasmid DNA using Lipofectamine 2000 (ThermoFisher, Cat# 11668027). Prior to imaging cells, the complete DMEM media containing phenol red was aspirated from the chamber and replaced with 1x HBSS (20 mM HEPES [pH 7.2], 150 mM NaCl, 4 mM KCl, 1 mM $MgCl_2$, 10 mM glucose). The chamber was mounted on an inverted Nikon Ti2 microscope with an OKO Touch heated stage. Cells were imaged through a 100x Nikon objective (1.49 NA) oil immersion TIRF objective with a heated flexible collar with temperature control. The correction collar on the 100x objective was adjusted for 37ºC imaging.

Single molecule imaging of PIP5KB in HEK293T utilized a N-terminal fusion of monomeric Eos3.2 [118], referred to as mEos throughout the manuscript. Photoconversion of mEos-PIP5KB from the green (516 nm l_{peak}) to the red fluorescent (580 nm l_{peak}) state was accomplished by exposing cells in the desired field of view to a 50 ms pulse of 0.5-1 mW of 405 nm light. The intensity of 405 nm light was measured through the objective using a Newport light meter.

Following photoconversion, single cells were imaged for 30-60 seconds with a time resolution of 52-102 ms to visualize the membrane binding dynamics of mEos-PIP5KB.

Microscope hardware and imaging acquisition. Single molecule imaging experiments were performed on an inverted Nikon Ti2 microscope using a 100x Nikon objective (1.49 NA) oil immersion TIRF objective. The x-axis and y-axis positions were manually controlled using a Nikon motorized stage and joystick. All images were acquired using an iXion Life 897 EMCCD camera (Andor Technology Ltd., UK). Fluorescently labeled proteins were excited with either a 405 nm, 488 nm, 561 nm, or 637 nm diode laser (OBIS laser diode, Coherent Inc. Santa Clara, CA) controlled by a Vortran laser drive with acousto-optic tunable filters (AOTF) control. The power output measured through the objective for single particle imaging was 1-3 mW. For dual color imaging of mNG-PIP5K localization during Cy3-PLCδ monitored $PI(4,5)P_2$ synthesis, samples were excited with 1 mW 488 nm and 1 mW 561 nm light, as measured through the objective. Excitation light was passed through the following dichroic filter cubes before illuminating the sample: (1) ZT488/647rpc and (2) ZT561rdc (ET575LP) (Semrock). Fluorescence emission was detected on an ANDOR EMCCD camera position after a Sutter emission filter wheel housing the following emission filters: ET525/50M, ET600/50M, ET700/75M (Semrock). All in vitro experiments were performed at room temperature (23ºC). Single molecule imaging in living cells was performed at 37ºC using an OKO Touch heated stage and heated objective collar. Microscope hardware was controlled using Nikon NIS elements.

Single particle tracking. Fluorescent protein detection and tracking was performed using the ImageJ/Fiji TrackMate plugin [122]. Data in the form of .nd2 files were loaded in ImageJ. Before

being analyzed using TrackMate, data brightness was adjusted for molecules to be easily identifiable. TrackMate was then used to identify and track molecular tracks in these steps: Particles were first identified using the LoG detector option based on brightness and signal-to-noise ratio. Once identified, particles were tracked for their full lifetime using the LAP tracker. This LAP tracker follows molecular displacement as a function of time. Particle trajectories were filtered based on Track Start (removed trajectories that began in first frame), Track End (removed trajectories present in last frame), Duration (removed trajectories ≤ 2 frames and singular extra-long tracks), Track displacement (removed immobilized particles displacement <0.1), and X - Y location (removed particles near the edge of the images). The TrackMate output files were analyzed using PRISM 9 (GraphPad) to calculate characteristic dwell times and diffusion coefficients.

Step size distribution of single particle trajectories were plotted in Prism as frequency versus step size (μm). For all analysis presented in this manuscript, the bin size for the step size distribution equals 0.01 μm. For curving fitting, the step-size distributions were plotted as probability density versus step size (μm). This was achieved by dividing the frequency distribution (i.e. y-axis values) by the bin size (0.01 μm). The probability density versus step size plots were fit to the following one- or two-species distributions:

Single species model:

$$f(r) = \frac{r}{2D\tau} e^{-\left(\frac{r^2}{4D\tau}\right)}$$

Two species model:

$$f(r) = \alpha \frac{r}{2D_1\tau} e^{-(\frac{r^2}{4D_1\tau})} + (1-\alpha) \frac{r}{2D_2\tau} e^{-(\frac{r^2}{4D_2\tau})}$$

Variables are defined as the D1=diffusion coefficient species 1 (μm^2/sec), D2=diffusion coefficient species 2 (μm^2/sec), alpha (α_1 = % of species 1, r = step size (μm), α_2 = time interval between steps (sec). Final step size distribution plots were generated in PRISM graphing software and using the following equations: (1 species model): f(x) = x/(2*D1*t)*exp(-(x^2/(4*D1*t))), (2 species model): f(x) = alpha*(x/(2*D1*t)*exp(-(x^2/(4*D1*t))))+(1-alpha)*(x/(2*D2*t)*exp(-(x^2/(4*D2*t)))).

To calculate the single molecule dwell times for Cy5-PIP4K2B, Cy5-PIP4K2B(5K-SL), AF647-PIP5K (and mutants), mNG-PIP5K (and mutants), mNG-PLCδ, and mNG-(5K-SL)-PLCδ we generated a cumulative distribution frequency (CDF) plot using the frame interval as the bin size (e.g. 50 ms). The $\log_{10}$(1-CDF) was plotted against the dwell time and fit to either a single or double exponential decay curve.

Single exponential model:

$$f(t) = e^{(-x/\tau)}$$

Two exponential model:

$$f(t) = \alpha * e^{(-x/\tau 1)} + (1 - \alpha) * e^{(-x/\tau 2)}$$

Fitting procedure initiated with a single exponential. In cases of a low-quality single exponential fit, a maximum of two species model was used. For double exponential fit, alpha (α) represents the fraction of fast dissociating population of molecules characterized by the time constant, α_1.

Image analysis, curve fitting, and statistics. Image analysis was performed on ImageJ. PRISM 9 (GraphPad) was used for curve fitting. Single molecule dwell time and step size presented in this manuscript represent combined data from 3 technical replicates with 2-3 movies acquired from multiple fields of view for each experimental condition. Dwell time distributions and curve fits were generated with n = 1000-3000 particle trajectories. Step size distribution plots and curve fits represent 10,000-30,000 measured displacements. When fitting single particle dwell time distributions derived from visualizing mEos-PIP5KB (WT and mutants) in HEK293T cells we generate a single dwell time distribution for all the molecules tracked in a single cell. The average dwell time for single molecule measurements performed in cells represents the average for all the cells (n = 14-23).

Bridge to Chapter III

In the previous Chapter, we demonstrated that product-binding by PIP5K is mediated by the specificity loop and PIP lipid binding motif. Further, we were able to show that the specificity loop functions as a specific PIP lipid binding motif, able to bind PI(4)P and PI(4,5)P_2 lipids. This result challenged the prevailing theory that the specificity loop was only able to bind the substrate PI(4)P lipid. I then showed that this is a unique capability of the PIP5K specificity loop, and showed that the PIP4K specificity loop does not facilitate binding to PI(4,5)P_2 lipids. Using a combination of bulk fluorescence and single molecule binding, I showed that the PIPBM is a broad anionic lipid binding motif, able to bind to each PIP lipid, preferring doubly and triply phosphorylated lipids. These findings provide a structural understanding of the previously described PIP5K product-binding phenotype, as well as providing a potential mechanism for why PIP5K specifically targets the inner leaflet of the plasma membrane in cells. Chapter II focuses on how PIP5K gets to the membrane, while Chapter III of this thesis focuses on studying the dynamics of PIP5K post membrane binding. In a previous study, we showed that PIP5K dimerizes in a density-dependent fashion following membrane binding. As the membrane concentration of PI(4,5)P_2 rises, more PIP5K is recruited onto the lipids. As the density of membrane bound PIP5K rises, the oligomerization state of PIP5K shifts from primarily monomeric to dimeric. However, the techniques used to show membrane-mediated dimerization of PIP5K enzymes relied on using biophysical characteristics of the protein to infer oligomerization state. There existed no assay to track PIP5K dimerization in real-time. In Chapter III, we use rational design principles to create a PIP5K dimerization FRET biosensor. The biosensor is a PIP5K enzyme engineered with a

fluorescent dye near the dimer interface such that when two PIP5K FRET construct enzymes dimerize, their complementary dyes can undergo FRET. I characterized this sensor and performed controls to confirm that the FRET output seen is the result of dimerization. Using this biosensor, I was able to better define the lifetime of PIP5K dimerization, and characterize the diffusion of PIP5K FRET dimers. Using the FRET assay, I was able to demonstrate that PIP5K paralogs can homodimerize (e.g. PIP5KB-PIP5KB) and heterodimerize (e.g. PIP5KA-PIP5KB) due to their conserved dimer interface. Finally, I use a combination of the FRET assay complemented with in vitro biochemistry assays to show that the mechanism by which PIP5K is inhibited by PIP4K is via blocking the dimer interface, competing with the aspartic acid necessary to form the dimer salt bridge during PIP5K dimerization.

CHAPTER III

A novel FRET biosensor for visualizing membrane-mediated dimerization of PIP5K

This chapter includes unpublished material. Experiments and synthesis of this manuscript were completed by me.

INTRODUCTION

Despite being only a minor component of eukaryotic cell membranes, phosphatidylinositol-4,5-bisphosphate ($PI(4,5)P_2$) plays a major functional role in membrane signaling pathways[3,123]. $PI(4,5)P_2$ lipids function as molecular scaffolds that recruit numerous peripheral membrane binding proteins to the inner leaflet of the plasma membrane. This scaffolding role has been shown to be critical for the progress of many signaling pathways, from cell-type specific pathways including neuronal ion channel gating critical for muscular function and macrophage phagocytosis, to more broad and fundamental cellular functions including cytoskeletal anchoring, membrane permeability, and nutrient uptake and membrane protein recycling through mediation of endocytic events[24,43,124–128]. But $PI(4,5)P_2$ lipids don't only play a primary signaling role, they also exist as a critical precursor for the formation of $PI(3,4,5)P_3$ lipids, which regulate cell fate determination, migration, neurogenesis, and adhesion[129–131]. These key roles make $PI(4,5)P_2$ lipids fundamental to the functioning of eukaryotic membranes, and mutations that deplete $PI(4,5)P_2$ in embryos lead to lethality, demonstrating the necessity of this lipid for life to function[132]. Less severe mutations that modulate the regulation of $PI(4,5)P_2$ lipids in cells leads to various disease states including cardiomyopathies, cataract development,

intellectual disability formation, and some cancers[133,134]. Overall, the importance of PI(4,5)P_2 lipids to cell function is self-evident, though our understanding of how PI(4,5)P_2 levels are stably maintained in cells is less well understood.

Studies of PI(4,5)P_2 levels in different cell types and have shown that the concentration of these lipids at the plasma membrane is kept tightly controlled in resting cells[135,136]. This can be attributed to their role as both precursor for other signaling pathways, as well as their function in constitutive signaling events occurring at the membrane surface[137]. However, studies have also shown that PI(4,5)P_2 lipids can be rapidly synthesized in response to specific cell signaling pathways[138–140]. Some examples that have directly shown this cell signaling-rapid PIP_2 synthesis are Wnt signalosome formation, FcγR-mediated phagocytosis, and calcium influx[138,140,141]. In each of these pathways, surface receptor activation leads to a rapid increase in PI(4,5)P_2 levels. How PI(4,5)P_2 synthesis can transition from steady-state levels to rapid formation in response to extracellular cues is poorly defined, but likely relies on changes to the catalytic efficiency of the enzymes that synthesize PI(4,5)P_2 in these different cell signaling states.

Mammalian cells contain two sets of kinases that can regulate the synthesis of PI(4,5)P2 lipids: type I phosphatidyl-4-phosphate 5-kinase (PIP5K) enzymes and type II phosphatidyl-5-phosphate 4-kinase (PIP4K) enzymes. Type I PIP5K enzymes have the primary substrate of phosphatidylinositol-4-phosphate (PI(4)P), and function as a lipid kinase, phosphorylating the 5-OH on the PI(4)P inositol ring[142–144]. Conversely, type II PIP4K enzymes specifically utilize phosphatidylinositol-5-phosphate (PI(5)P) lipids as their substrate [51,145]. Despite the existence of these separate two pathways, studies have shown that PIP5K enzymes are the main driver of PI(4,5)P_2 synthesis in mammalian cells[61,123,146]. This enzyme family is comprised of three paralogs (A, B, and C), each of which play non-redundant roles in signaling events and have various tissue-

specific expression profiles[61,147,148]. Knockout studies in mice show variable response to the deletion of these PIP5K paralogs. For example, deletion of the neuronal-specific PIP5KC paralog leads to either perinatally or embryonic lethal phenotypes, demonstrating the importance of this enzyme during neurogenesis [132]. In contrast, PIP5KB knockout mice show no developmental abnormalities, but have severe autoimmune responses to histamine stimulation due to actin malformations in their immune cells[149]. Functioning in concert with PIP5KB, PIP5KA knockout studies show a similar actin malformations in immune cells that cripples phagocytic pathways[148], suggesting that these two paralogs may both play complementary roles in these cells. Despite this suggestion, if and how PIP5K paralogs are able to interact is not well understood. Studies that knockout the other more minimal PI(4,5)P_2 synthesis pathway, knockouts of PIP4K, have shown that PI(4,5)P_2 levels rise in response to depletion of PIP4K enzymes[150]. Follow up biochemical studies have shown that the increase in PI(4,5)P_2 levels is the direct response of PIP4K enzymes inhibit PIP5K enzymatic activity through an unknown mechanism[151].

PIP5K is critical for the rapid synthesis of PIP_2 in response to signaling pathways[58,138]. How PIP5K activity can rapidly change during signaling events is still an open question from a biochemical standpoint. Some studies have tried to tie PIP5K activation to effector molecules like GTPases including Rac1 and ARF family proteins[74,152,153], though in vitro biochemistry hasn't readily deciphered these interactions. Overexpression studies of PIP5K enzymes triggers higher densities of PI(4,5)P_2 lipids to be synthesized [151,154,155]. Interestingly, however, overexpression of catalytically dead PIP5K enzymes still bolster PI(4,5)P_2 levels, despite not contributing to the synthesis catalytically[151]. The mechanism that allows for catalytically dead PIP5K's to stimulate other PIP5K enzymes remains unknown. This finding suggests that activation of PIP5K to catalyze rapid PI(4,5)P_2 synthesis may be facilitated through intrinsic mechanisms. Our recent studies into

PIP5K activity have provide possible explanations for how PIP5K activity can be potentiated during signaling events. First, we showed that PIP5K has a robust positive feedback mechanism via increase affinity for binding to membranes containing PI(4,5)P_2 lipids[143,156]. Further, we've recently shown that PIP5K exists in solution as a monomer but has the ability to dimerize on membranes in a density-dependent manner[157]. This is a potentially critical point for PIP5K activity regulation, as dimeric PIP5K is stimulated through an allosteric mechanism, potentiating PIP5K lipid kinase activity 20-fold[71]. How cells modulate PIP5K dimerization through targeted interactions remains unclear. Addressing these questions have been technically challenging until now, as PIP5K dimerization is transient in nature and difficult to resolve using single molecule imaging. Quantifying the fraction of membrane dimerized PIP5K molecules in the presence of potential regulatory factors requires new experimental approaches.

Here, we address the challenge of visualizing PIP5K dimerization by establishing a novel Forster Resonance Energy Transfer (FRET) assay to measure PIP5K dimerization with single molecule resolution. FRET is a longstanding and well-established method for tracking binding dynamics between two molecules in real-time and has been recently used by various fields to determine changes in structural characteristics between binding partners[158–160]. We used rational design principles to create a FRET biosensor that allows us to watch PIP5K dimerization for the first time in real-time and track the dynamics of dimerization. We validated this biosensor by showing that mutations that abolish dimerization are unable to show FRET signal. We then use this biosensor to measure heterodimerization of PIP5K paralogs, which revealed a mechanism for PIP5K paralogs to synergistically enhance overall lipid kinase activity in cells. We finish by using our FRET biosensor to show that PIP4K enzymes inhibit PIP5K enzymes by blocking PIP5K dimerization when present at physiologically relevant concentrations. Overall, this work

establishes an assay for studying PIP5K dimerization in real-time and uses this assay to uncover mechanisms by which PIP5K dimerization can be enriched or blocked via protein-protein interactions. The assay created in this manuscript can be broadly applicable to scientists seeking to study how proteins or small molecules enhance or diminish PIP5K dimerization.

RESULTS

Designing a biosensor for PIP5K dimerization

Previously, we demonstrated that PIP5K dimerizes in a density-dependent manner. Tracking dimerization in real-time was difficult, as at single molecule densities PIP5K primarily existed as a monomer, with only around five percent of total single particles exhibiting a molecular brightness consistent with a homodimer. Because PIP5K dimerization is transient and requires high protein densities that are not compatible with single molecule tracking, visualization, and quantification of PIP5K is technically challenging. As well, because our studies relied on using biophysical proxies like extended dwell times and reduced molecular diffusion as a read out for dimerization, determining if a secondary factor (such as another protein or peptide) can enhance or discourage dimerization difficult without a way to directly quantify the change in dimerization frequency. To address this challenge, we designed a single-molecule FRET assay that allows us to view PIP5K dimerization in real-time and quantify biophysical parameters of dimerization (**Figure 3.1A**).

Figure 3.1

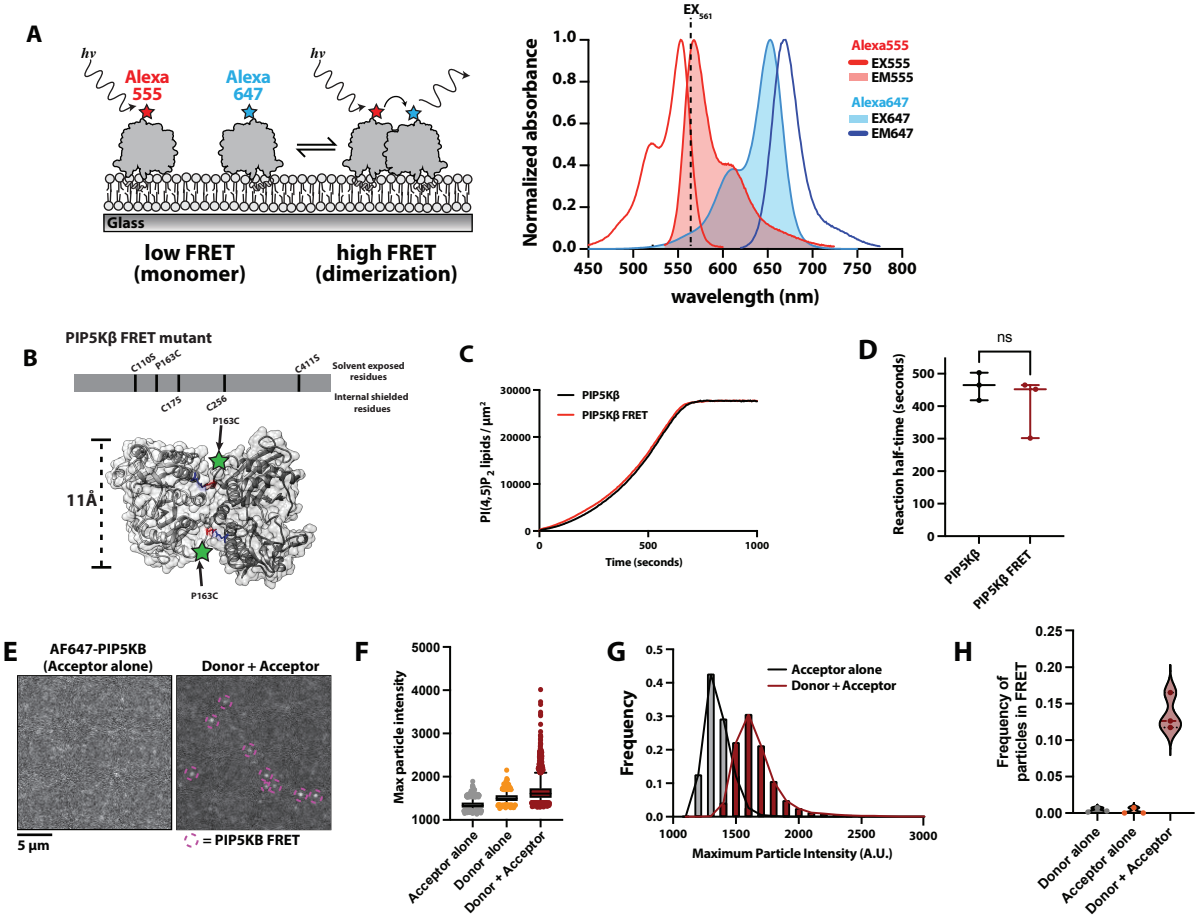

Figure 3.1
Designing a biosensor for PIP5K dimerization.
(A) Schematic representation of FRET assay to track PIP5K dimerization in real-time (left). Excitation-Emission spectra of AF555 and AF647 used for the FRET assay. Dashed black line represents excitation laser (561 nm). **(B)** PIP5KB FRET construct gene with indicated location of buried and solvent-exposed cysteine residues determine by ESI-MS (Top). Kinase domain orientation of the zebrafish PIP5KA homodimer, the aspartic acid residues (red) that form a salt bridge with arginine residues (blue). Green stars indicate the location of engineered cysteine locations for maleimide labeling. These residues reside ~41Å apart when dimerized (Bottom). **(C)** Representative kinase activity trace tracking the production of $PI(4,5)P_2$ lipids over time using 20 nM Cy3-PLCδ PH domain sensor comparing the activity of wildtype PIP5KB and our PIP5KB FRET construct (PIP5KB C110S, P163C, C411S). **(D)** Reaction half-times comparing the activity of PIP5KB and PIP5KB FRET (n=3). A Student's T-test with Welch's correction was performed to determine no significant difference between the reaction half-time of wildtype PIP5Kβ and our PIP5Kβ FRET constructs (p=0.41). **(E)** TIRF-M Stills using FRET imaging conditions (excitation with 561 laser, collected emission through a 700 nm Bandpass filter) in the presence of either 1nM Acceptor alone (AF647-PIP5KB FRET, right) or 5nM AF555-PIP5KB FRET donor and 1 nM AF647-PIP5KB FRET acceptor together (right). **(F)** Representative max particle intensities for 1 nM AF647-PIP5KB FRET

acceptor alone, 5 nM AF555-PIP5KB FRET donor alone, or donor and acceptor together. Particles tracked and identified using TRACKMATE software as described in methods section. **(G)** Frequency of maximum particle intensities shown in Figure 1F to demonstrate the existence of population of particles in donor + acceptor condition brighter than just acceptor alone condition. **(H)** Frequency of particles in FRET in either donor alone condition, acceptor alone, or donor + acceptor conditions (all n=3). Frequency was determined by taking the number of particles brighter than 99% of donor alone or acceptor alone conditions, whichever had brighter molecules.

FRET is a distance-dependent physical process that necessitates that the two dyes transferring energy are physically close to one another, with the dyes ideally positioned closer than the Forester Radius (R_0). To minimize spectral overlap while maximizing the R_0 distance, we chose to use the fret pair Alexa Flour 555 (AF555) and Alexa Fluor 647 (AF647) which have an R_0 of ~51 Å. With the knowledge that we needed to position the dyes on the PIP5K enzyme closer than 51 Å apart when PIP5K is dimerized, we modeled the PIP5K dimer using the available zebrafish PIP5K crystal structure (PDB: 4TZ7) similarly to previous studies[157,161]. Doing so, we identified a proline at site 163 on the PIP5KB protein calculated 43Å apart when dimerized (**Figure 3.1B**). We sought to utilize maleimide-thiol chemistry to conjugate a fluorescent dye to PIP5K at this designed position, to do this we mutated the identified proline to a cysteine residue (PIP5KB P163C). However, maleimide-thiol chemistry is nonspecific, and if we only made this mutation and attempted to dye PIP5KB P163C we would inevitably get off target dyeing of the protein at other solvent-exposed cysteine residues. To address this challenge, we utilized electrospray ionization mass spectroscopy (ESI-MS) to identify which cysteine residues on PIP5KB are solvent-exposed, and which were internal and shielded from the maleimide-fluorophore reagent. We mutated the two cysteine residues found by ESI-MS to non-reactive serine residues and created the PIP5KB mutant which we fluorescently labeled and used in the FRET experiments in this study (PIP5KB C110S, P163C, C411S; referred to as PIP5KB FRET construct). To confirm that these mutations did not perturb the catalytic efficiency of PIP5K, we

performed lipid kinase assays to compare the production of $PI(4,5)P_2$ lipids to wild type PIP5K (**Figure 3.1C and 3.1D**). We observed no significant change in the catalytic efficiency our PIP5K FRET construct compared to wildtype.

Quantifying FRET output

With our FRET sensor designed, purified, and confirmed to have minimal perturbation compared to wildtype, we next established conditions to quantify the dynamics of PIP5K dimerization using single molecule FRET (smFRET) on supported lipid bilayers. Using Total Internal Reflection Fluorescence Microscopy (TIRF-M), we optimized conditions to excite AF555-PIP5KB (donor) and readout the emission of AF647-PIP5KB (acceptor) with minimal direct excitation of AF647 either a 532 or 561 nm laser. Because we sought to track dimerization events via single particle tracking, bleed through of donor emission or direct excitation of the acceptor fluorophore was a major concern in this study. As discussed earlier, dimerization occurs at membrane surface densities that prevent single molecules from being resolved. Consequently, we relied on sensitized emission of the acceptor fluorophore while undergoing dimerization-dependent FRET to quantify dimerization. Overall, we found that using 5 nM AF555-PIP5KB FRET to 1nM AF647-PIP5KB FRET gave us the optimal FRET to resolve single dimerization events via single particle tracking of excited acceptor molecules (**Figure 3.1E**).

To quantify the single molecule acceptor fluorescence seen during our FRET assay, we tracked single FRET dimers to determine the lifetime, brightness, and diffusion of molecules[162]. To discriminate particles that are FRET from any bleed through via either direct excitation of the acceptor dye or captured emission of excited donor fluorophores, we used homogenous particle identification parameters for our experimental conditions (addition of both donor and acceptor

PIP5K FRET proteins) and our control conditions (either donor PIP5K FRET alone or acceptor PIP5K FRET alone). By comparing the molecular brightness of particles identified in our controls to our experimental FRET condition, we were able to identify particles based on a threshold molecular brightness of the acceptor emission that far exceeded the brightest particles in our control conditions (**Figure 3.1F**, highlighted box). We then plot the frequency of particle brightness and divided the number of molecules brighter than 99% of particles in the donor and acceptor alone controls to the total number of tracked particles (Frequency = #bright molecules/#total molecules) to determine the frequency of particles seen in smFRET (**Figure 3.1G and 3.1H**). This workup allows us to quantify the amount of FRET we are seeing using our single molecule FRET assay and compare different experimental conditions to determine how other molecules modulate the frequency of PIP5K dimers observed by smFRET (**Figure 3.1H**).

Validating the dimerization biosensor

We've demonstrated that we can track and quantify FRET using single particle tracking via TIRF-M using our PIP5KB FRET construct, next we sought to validate that FRET signal seen is due to PIP5K FRET constructs dimerizing and not the result of another PIP5K-PIP5K interaction. We started by titrating in dark PIP5K into our FRET assay (**Schematic shown in Figure 3.2A**). Addition of 10nM unlabeled PIP5KB into reaction mixture led to a significant decrease in the frequency of particles in FRET seen in our assay (**Figure 3.2B and Figure 3.2C**). This makes sense, as we are increasing the possible interactions that can be made between the PIP5K molecules in solution, making it less likely that an AF555-PIP5KB FRET protein engages an AF647-PIP5KB FRET protein. In contrast, when we added a mutant PIP5K that is unable to form dimers[157,161], PIP5KB D51R, we saw no discernable decrease in the frequency of molecules

in FRET tracked (**Figure 3.2B and 3.2C**). This finding suggests that PIP5K molecules added to solution that are unable to make contacts with the dimer interface of PIP5K are unable significantly disrupt dimerization in our assay.

Figure 3.2

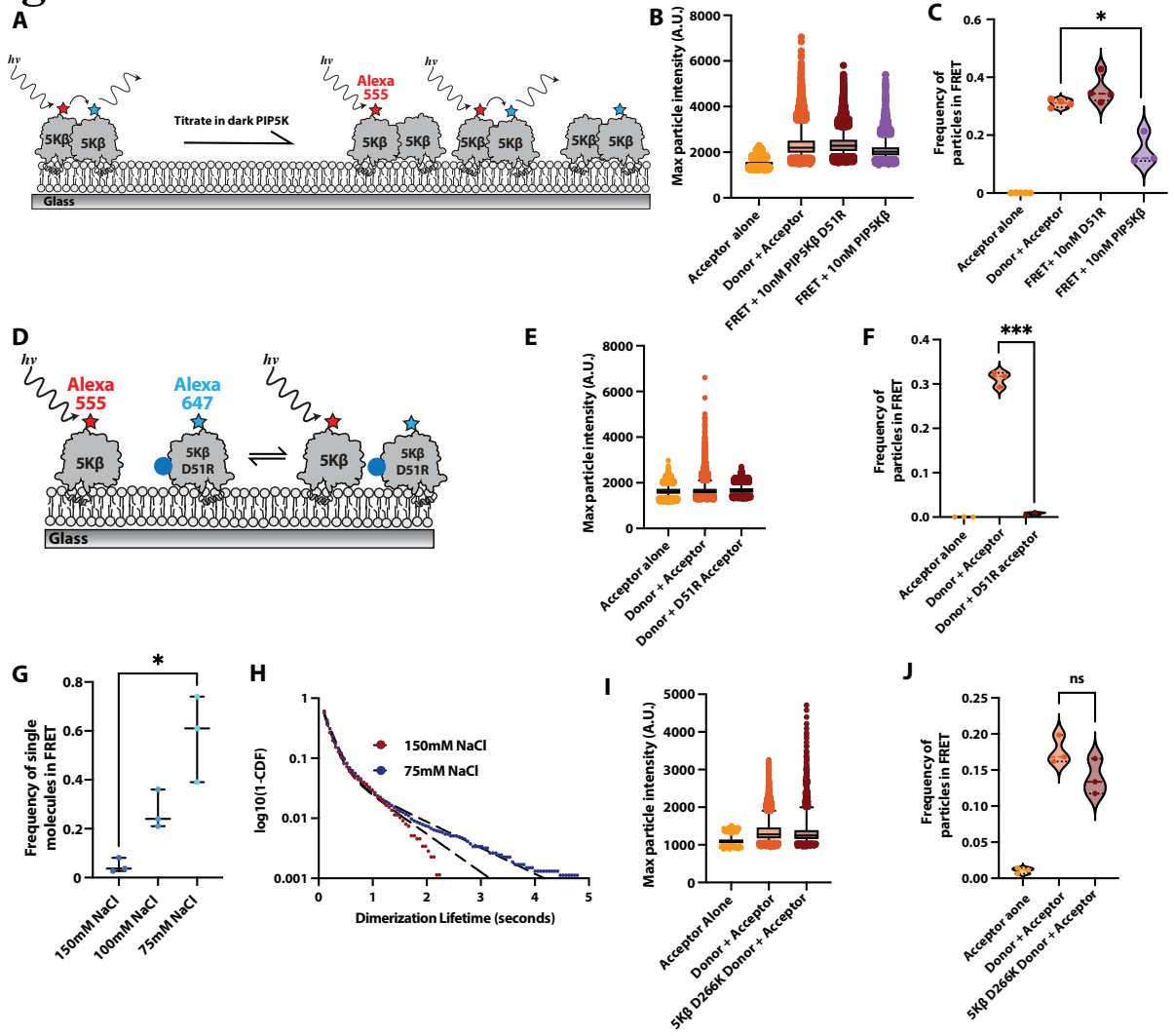

Figure 3.2
Membrane-mediated dimerization of PIP5K visualized by smFRET.
(A) Schematic describing the experimental setup for figure 2B and 2C, PIP5K FRET assay was performed, followed by the addition of unlabeled PIP5KB enzymes to determine the effect on frequency of FRET observed. **(B)** Representative maximum particle intensities for acceptor alone, donor + acceptor, donor + acceptor + 10nM dark monomeric PIP5KB D51R mutant, or donor + acceptor + 10nM dark wildtype PIP5KB. **(C)** Frequency of particles in FRET for acceptor alone (n=5), donor + acceptor (n=4), donor + acceptor + 10nM unlabeled monomeric PIP5KB D51R (n=4), and donor + acceptor + 10nM unlabeled wildtype PIP5KB (n=3). Student's T-test with Welch's correction was performed to show statistically

significant decrease in frequency of FRET seen when comparing donor + acceptor and +10nM PIP5KB conditions (p=0.027). **(D)** Schematic describing the experimental setup for Figure 2E and 2F, PIP5K FRET assay was performed with AF555-PIP5KB FRET construct donor and a monomeric AF647-PIP5KB FRET D51R (PIP5KB D51R, C110S, P163C, C411S) acceptor. **(E)** Representative maximum particle intensity graph for a single experiment of acceptor alone, AF555-PIP5KB FRET donor + AF647-PIP5KB FRET acceptor condition, or AF-555 PIP5KB FRET + AF647-PIP5KB D51R FRET construct acceptor. **(F)** Frequency of particles in FRET for acceptor alone (n=3), donor + acceptor (n=3), and donor + D51R FRET acceptor (n=3). Student's T-test with Welch's correction was performed to show statistically significant difference in the average frequency of particles in FRET when comparing donor + acceptor and donor + D51R FRET acceptor conditions (p=0.0008). **(G)** Frequency of particles in FRET in standard donor + acceptor (5nM AF555-PIP5KB FRET + 1nM AF647-PIP5KB FRET) conditions in the presence of 150mM NaCl (n=3), 100mM NaCl (n=3), or 75mM NaCl (n=3). Student's T-test with Welch's correction performed to show significant difference between 150mM NaCl and 75mM NaCl conditions (p=0.034). **(H)** Representative dimerization lifetime distributions using TIRF-M FRET assay (Figure 1A) in the presence of 150mM NaCl or 75mM NaCl in reaction buffer. **(I)** Representative maximum particle intensities for acceptor alone, donor + acceptor, and AF555-PIP5KB FRET D266K (PIP5KB C110S, P163C, D266K, C411S) donor + acceptor conditions. **(J)** Frequency of particles in FRET for acceptor alone (n=3), donor + acceptor (n=3), and AF555-PIP5KB FRET D266K donor + acceptor conditions (n=3). Student's T-test with Welch's correction was performed to demonstrate no significant difference between donor + acceptor and D266K donor + acceptor conditions (p=0.1127).

We next sought to disrupt dimerization in our FRET assay by mutating the acceptor PIP5KB proteins in our assay. We took our PIP5KB FRET construct and added a mutation to fully disrupt the ability for PIP5K to dimerize (PIP5KB D51R, C110S, P163C, C411S: referred to a monomeric PIP5KB FRET herein), creating a monomeric PIP5KB FRET construct (**Figure 3.2D**). We performed our FRET assay with our AF555-PIP5KB FRET donor and monomeric AF647-PIP5KB FRET acceptor. We found a significant decrease in the frequency of FRET seen when using a monomeric PIP5KB FRET acceptor compared to the standard FRET pair assay (**Figure 3.2E**). We did find some molecules in FRET compared to our control, approximately 0.5-1% of molecules were brighter than acceptor or donor alone controls. We expect that this finding is the result of AF555-PIP5KB donor and monomeric AF647-PIP5KB FRET acceptor molecules interacting nonspecifically while bound to the supported bilayers, as is expected when working at nanomolar concentrations in our assay. Overall, these findings demonstrate that our PIP5KB FRET

biosensor is both sensitive and specific towards PIP5K dimerization, functioning as a readout of real-time dimerization of PIP5K molecules.

Characterizing properties of PIP5K dimerization

Elucidating mechanisms that could enrich or diminish PIP5K dimerization in cells is critical for understanding how dimerization regulates cellular pathways. PIP5KC, for example, is the neuronal-specific PIP5K paralog, critical for producing the $PI(4,5)P_2$ lipids that regulate ion channel function and modulation of salt gradients required for action potential firing. Indeed, modulation of local salt concentration is a common signaling requirement to produce, dampen, or extend signaling events[163,164]. Additionally, dimerization is facilitated through a salt bridge formed between an aspartic acid and arginine residues on PIP5K molecules, two previous studies have shown that disrupting the salt bridge is sufficient for blocking homodimerization, suggesting that this salt bridge is critical for dimerization (**Figure 3.1B**)[157,161]. For these reasons, we sought to test how fluctuating the salt concentration in our reaction buffer affected the frequency of FRET in our assay. We found that lowering salt concentration greatly stimulates the amount of dimerization observed (**Figure 3.2G**). This finding is expected, as lowering the amount of salt ions present in solution causes lower shielding of the arginine and aspartic acid side chains. Still, this finding suggests the ability to make local areas of low salt in cells may stimulate PIP5K dimerization.

Previous work that structurally demonstrated PIP5K dimerization and subsequent studies that determined the mechanism of membrane-mediated homodimerization each were able to demonstrate dimerization, however neither were able to determine the lifetime of dimerization[157,161]. Understanding dimerization lifetime is important, as previous work assumed that PIP5K enzymes existed as constitutive dimers, while follow up studies suggest that

dimerization is transient, not constitutive[157]. Our FRET assay using TIRF-M was ideal to study dimerization lifetime, as using supported lipid bilayers paired with TIRF-M allowed us to recruit PIP5KB FRET constructs to membranes containing 4% $PI(4,5)P_2$ at nanomolar concentrations, facilitating dimerization. We were able to track single FRET events due to the high signal-to-noise ratio of our assay (**Figure 3.1E**) and tracking the duration of these single-event tracks allowed us to plot a distribution of dimerization lifetimes (**Figure 3.2H**). Overall, our data agreed with previously published data suggesting that PIP5K homodimerization is transient in nature. We found that in buffer containing 75mM NaCl, FRET lifetimes were best described by a double exponential fit, with characteristic dwell times (τ) of τ_1= 0.17s, τ_2= 1.00s, α= 0.94, suggesting that the oligomerization state of PIP5K molecules rapidly exchanges between monomer and dimer.

As discussed earlier, one previous study showed that overexpression of catalytically dead PIP5K in HeLa cells lead to a significant increase in the total plasma membrane $PI(4,5)P_2$ lipid concentration[151]. We hypothesized that this could be facilitated through dimerization of catalytically dead PIP5KB enzymes with wildtype PIP5KB expressed in cells. We sought to use our FRET assay to test the ability of PIP5KB FRET construct (PIP5KB C110S, P163C, C411S) to dimerize with catalytically dead PIP5K FRET constructs (PIP5KB C110S, P163C, D266K, C411S). Using an AF555-PIP5KB FRET D266K as the donor molecule, we were able to show that we could resolve molecules in FRET with similar frequencies between our standard donor + acceptor condition when compared to the AF555-PIP5KB FRET D266K donor plus AF647-PIP5KB FRET acceptor conditions (**Figure 3.2I and 3.2J**). These data provide a suggestive mechanism for why overexpressing catalytically dead PIP5K can increase the total plasma membrane $PI(4,5)P_2$ levels in cells, through dimerization of catalytically dead PIP5K with endogenous PIP5K, potentiating kinase activity through allostery.

Membrane-mediated heterodimerization of PIP5K paralogs

Tissue specific expression profiles of the PIP5K paralogs shows near homogenous overlap in expression between the human PIP5K paralogs[62]. Previously it was suggested that overlapping PIP5K paralog expression could be due to different subcellular localization patterns[61]. However, many localization studies suggest that all three PIP5K paralogs localize to the plasma membrane of cells[124,151,165]. Some studies have shown non-overlapping functions to these paralogs, but few have assessed whether these enzymes are able to interact with each other to synergistically stimulate $PI(4,5)P_2$ lipid production. Co-immunoprecipitation studies using HEK293T cell lysate showed that PIP5K paralogs β and γ were able to associate, though the proposed mechanism for this interaction has later been shown to be erroneous[166]. Here, we sought to test if PIP5KA and PIP5KB paralogs can heterodimerize. Sequence alignment of human PIP5K paralogs shows conservation of the dimer interface (**Figure 3.3A**). Previously, we established that dimeric PIP5KB displays unique single particle dwell time and diffusion characteristics compared to monomeric PIP5KB[157]. Working from these findings, we used single molecule tracking experiments performed at low kinase densities (i.e. 10 pM). At this density, PIP5K exists primarily as a monomer on membranes[157]. By tracking the dwell time (**Figure 3.3B**, yellow) and the diffusion (Figure 3D, yellow), of low density AF647-PIP5KB molecules we were able to determine the biophysical parameters of the monomeric PIP5K. We then increased the solution concentration of unlabeled PIP5KA to high densities to promote heterodimerization (i.e. 50 nM PIP5KA). When high densities of PIP5KA were added we saw a distinct increase in the dwell time of AF647-PIP5KB enzymes (**Figure 3.3B**, orange) and a decrease in the characteristic diffusion (**Figure 3.3D**, orange). These findings suggest that PIP5KA molecules in solution are interacting with our

low-density AF647-PIP5KB molecules in a manner consistent with dimerization. To confirm that the interaction we were seeing is due to dimerization and not a result of another protein-protein interaction or molecular crowding, we performed control studies that tracked low densities of monomeric AF647-PIP5KB (D51R), this mutation was previously shown to abolish homodimerization of PIP5KB. When repeating the above experiments with our control AF647-PIP5KB (D51R), addition of high concentrations of unlabeled PIP5KA had no effect on the characteristic dwell time or diffusion of single molecules we tracked (**Figure 3.3C**). This data together supports that PIP5KB and PIP5KA enzymes can heterodimerize.

Figure 3.3

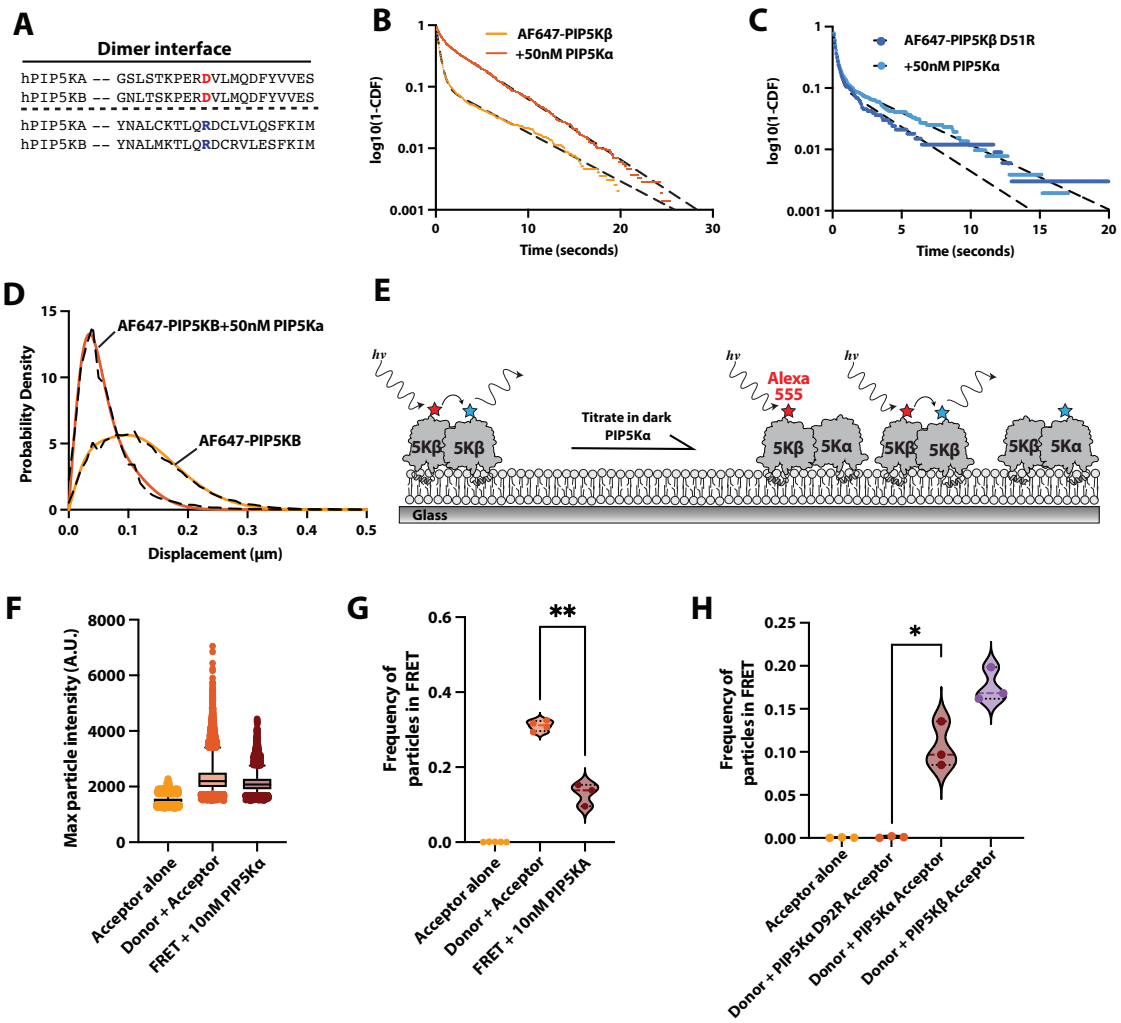

Figure 3.3:
Membrane-mediated heterodimerization of PIP5K paralogs
(A) Sequence alignment between hPIP5KA and PIP5KB demonstrates conservation of the dimer interface of these enzymes. **(B)** Representative single molecule dwell time distributions of 10pM AF647-PIP5KB alone (yellow) or in the presence of 50nM unlabeled PIP5KA (orange) demonstrates the change in dwell time when PIP5KB can interact with PIP5KA enzymes. **(C)** Representative single molecule dwell time distributions of 300 pM monomeric AF647-PIP5KB D51R alone (darkest blue) or in the presence of 50 nM unlabeled PIP5KA (light blue) demonstrates that disrupting the dimer interface disrupts the ability for PIP5KB:PIP5KA interaction seen in Figure 3B. **(D)** Dimerization shortens diffusion of AF647-PIP5KB molecules. Representative diffusion plot of 10 pM AF647-PIP5KB alone (yellow) or in the presence of 50 nM unlabeled PIP5KA (orange). **(E)** Schematic showing experiments performed in Figure 3F and 3G. Standard FRET assay was performed with donor and acceptor before titrating in unlabeled PIP5KA enzymes to determine effect on the frequency of FRET observed. **(F)** Representative maximum particle intensities of acceptor alone, donor + acceptor, and donor + acceptor + 10nM PIP5Kα conditions. **(G)**

Frequency of particles in FRET for acceptor alone (n=5), donor + acceptor (n=4), and donor + acceptor + 10nM PIP5Kα (n=3) conditions. Student's T-test with Welch's correction was performed to demonstrate statically significant difference in frequency of particles in FRET observed comparing donor + acceptor to donor + acceptor + 10nM PIP5Kα conditions (p=0.0036). **(H)** Frequency of particles in FRET for acceptor alone (n=3), donor (AF555-PIP5Kβ FRET) + 647-PIP5Kα D92R acceptor, donor + 647-PIP5Kα acceptor, and donor + acceptor conditions. Student's T-test with Welch's correction was performed to demonstrate statistically significant difference between the frequency of particles in FRET when comparing donor +1nM 647-PIP5Kα acceptor condition to the donor + 1nM 647-PIP5Kα D92R acceptor condition (p= 0.021).

Having established our FRET biosensor is able to specifically read out PIP5KB dimerization, we sought to determine if competition based on PIP5K paralogs binding at the dimer interface could perturb homodimerization. We performed our FRET assay first as normal, but then proceeded to titrate in dark PIP5KA. If PIP5KA can heterodimerize with our PIP5KB FRET constructs in our assay, we should expect to see some change in the frequency of particles in FRET, i.e. frequency of dimerization, seen in our assay (**schematic in Figure 3.3E**). Indeed, when comparing our standard donor + acceptor condition to a condition where we've titrated in 10nM of unlabeled PIP5KA, we do see a significant reduction in the frequency of particles in FRET tracked (**Figure 3.3F and 3.3G**). This result suggests that our FRET assay is indeed sensitive to perturbations that block PIP5KB homodimerization. To follow up, we sought to confirm that the interactions made between PIP5KB and PIP5KA were due to dimerization via their shared dimer interfaces, and not the result of interaction through another binding interface. To do so, we performed our FRET assay using our standard AF555-PIP5KB FRET donor, but this time we chose to use an N-terminally labeled AF647-PIP5KA acceptor. We chose to use an N-terminal label instead of creating a PIP5KA FRET mutant that could be labeled at a specifically engineered site to assess the possibility of using N-terminal labels in the future. Two N-terminal labels (one on each the donor and acceptor) would reside approximately 14 nanometers apart, just outside the window for efficient energy transfer to occur[167]. However, one N-terminal dye on the acceptor

AF647-PIP5KA is calculated to be approximately 9.8 nanometers away from the engineered cysteine on our donor AF555-PIP5KB FRET mutant, within the allotted distance for FRET to occur[167]. We modified our acceptor to be an N-terminal labeled AF647-PIP5KA enzyme and mixed it with our standard AF555-PIP5KB FRET donor to determine if we could establish a FRET assay that able to sense heterodimerization between PIP5KB and PIP5KA (**Figure 3.3H**, red violin plot). We compared this heterodimerization FRET sensor to our standard PIP5KB FRET homodimerization and saw no significant change in the frequency of particles in FRET (**Figure 3.3H**, red compared with purple). To confirm that the FRET signal seen between PIP5KB donor and PIP5KA acceptor was the result of dimerization and not due to the high surface density of enzymes on the membranes or through unspecified protein-protein interactions, we mutated the dimer interface of the PIP5KA enzyme to create a strictly monomeric AF647-PIP5KA (D92R) acceptor molecule. When performing our FRET with AF555-PIP5KB FRET donor and AF647-PIP5KA D92R acceptor, we saw little to no particles in FRET, suggesting that interactions made between PIP5KB and PIP5KA are the result of heterodimerization. Overall, this biochemical and FRET assay data support the hypothesis that PIP5K paralogs can heterodimerize.

PIP4K enzymes inhibit PIP5K enzymes by competing with homodimerization

Type II phosphatidylinositol-5-phosphate 4-kinase (PIP4K) are a family of enzymes able to produce PI(4,5)P_2 via the substrate PI(5)P[61]. However, this pathway is thought to contribute only a small portion of the total plasma membrane pool of PI(4,5)P_2 due to the low abundance of PI(5)P in cells. However, studies that have knocked out PIP4K enzymes from human cells show a marked increase in PI(4,5)P_2 levels at the plasma membrane[150,151]. This paradoxical result was confirmed, and was determined that PIP4K enzymes are able to inhibit PIP5K through a currently

unknown mechanism[151]. To attempt to map the interaction site between PIP4K and PIP5K enzymes we modeled potential interactions using Alphafold multimer[168]. One fascinating outcome was an arginine at site 104 of PIP4KIIA interacting with the aspartic acid of the dimer interface of PIP5KB (D51) (**Supplemental Figure B2A**). We followed up on this proposed interaction by mutating the PIP4KIIA arginine to an aspartic acid, flipping the charge and hopefully abolishing a salt bridge that could be made between PIP4KIIA and PIP5KB. We tested this mutant but found that the PIP4KIIA R104D mutant was still able to interact and inhibit PIP5KB enzymes (**Supplemental Figure B2B-B2D**). While this result discredited the predicted interaction site from Alphafold multimer, we didn't discount the hypothesis that PIP4KIIA could be binding to PIP5K enzymes via the dimer interface (**Figure 3.4A**). We tested this hypothesis first through determining if monomeric PIP5KB D51R is able to recruit PIP4K to low densities of $PI(4,5)P_2$. Using a bilayer comprised of low concentrations of $PI(4,5)P_2$ lipids (2% $PI(4,5)P_2$, 98% DOPC), we first flowed in 50nM AF488-PIP4KIIA over the supported bilayer and imaged using TIRF-M. We saw some small basal amount of recruitment (**Figure 3.4B**, light blue and **Figure 3.4C**, top panel). Then we spiked in 10nM of wildtype unlabeled PIP5KB to the reaction mixture and saw PIP5KB recruit our AF488-PIP4KIIA to the bilayer (**Figure 3.4B**, red line and **Figure 3.4C**, bottom left panel) as a positive control. In congruence with previously published work, wildtype PIP5KB is able to recruit more AF488-PIP4KIIA to the membrane[151]. Next, we attempted to recruited AF488-PIP4KIIA with 30nM of PIP5KB D51R. We used three-fold more PIP5KB D51R in our experiments to control for previously reported differences in overall membrane surface density between PIP5KB wildtype and PIP5KB D51R[157]. We saw little to no change in the overall amount of AF488-PIP4KIIA recruited to the membrane upon addition of unlabeled PIP5KB D51R, suggesting that the interaction between PIP4KIIA and PIP5KB is facilitated through the dimer

interface of PIP5KB (**Figure 3.4B**, dark blue and **Figure 3.4C**, bottom right panel). We performed this experiment again with PIP5KA and PIP5KA D92R, to test if the interaction site between PIP4KIIA is homogenous with other PIP5K paralogs and found, again, that monomeric PIP5KA D92R was unable to recruit PIP4KIIA to membranes (**Figure 3.4D**).

Figure 3.4

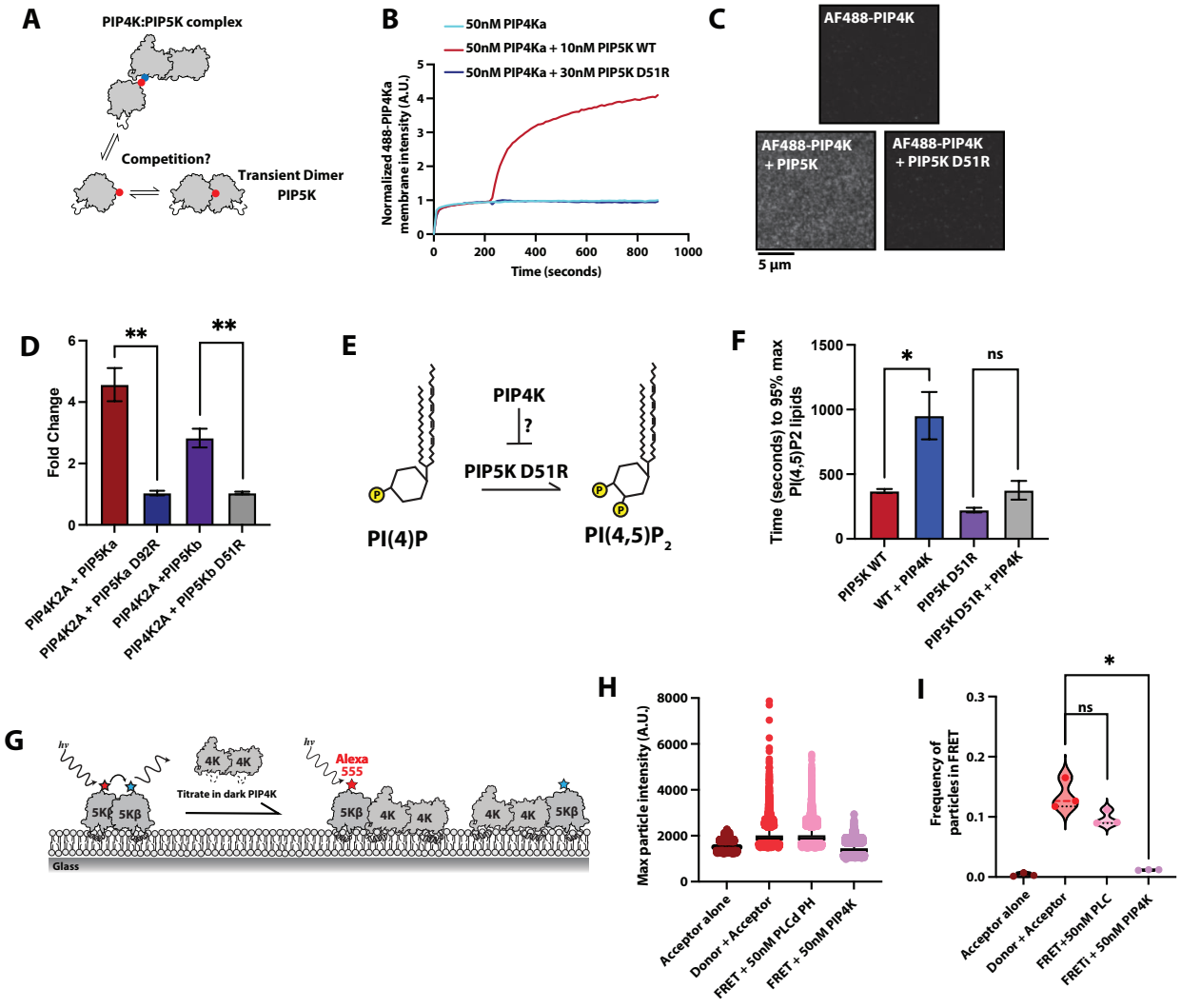

Figure 3.4
PIP4K inhibits PIP5K enzymes by blocking dimerization.

(A) Cartoon illustrating the proposed mechanism for inhibition of PIP5K by PIP4K. PIP5K is able to transiently dimerize with other PIP5K enzymes on membranes, however, the residues critical for PIP5K homodimerization are also able to facilitate heterooligomerization with PIP4K homodimers through unknown contacts on PIP4K. These two oligomeric states (PIP5K:PIP5K homodimer and PIP5K:PIP4K:PIP4K heterotrimer) compete, and thus leads to a decrease in PIP5K activity through blockage of homodimerization. **(B)** representative fold-change of 50nM AF488-PIP4K2A membrane binding alone (light blue), in the presence of 10nM wildtype unlabeled PIP5KB (red), or in the presence of 30nM monomeric, unlabeled, PIP5KB D51R (dark blue). PIP5KB was added at 250 seconds. All reactions performed on 2% PI(4,5)P_2, 98% DOPC bilayers. **(C)** Representative TIRF-M stills showing basal membrane recruitment of 50nM 488-PIP4K2A alone (top), in the presence of 10nM unlabeled PIP5KB (bottom left), or in the presence of 30nM unlabeled monomeric PIP5KB D51R (bottom right). **(D)** Fold change in 50nM AF488-PIP4K2A recruitment to 2% PI(4,5)P_2, 98% DOPC bilayers in the presence of 10nM PIP5Kα (n=3), 30nM PIP5KA D92R (n=3), 10nM PIP5KB (n=3), or 30nM PIP5KB D51R (n=3). Students T-tests with Welch's corrections were performed to determine differences between +PIP5KA and +PIP5KA D92R conditions (p= 0.007) and to determine differences between +PIP5KB and +PIP5KB D51R conditions (p=0.009). **(E)** Cartoon illustrating the questions being asked in Figure 1F, if PIP4K inhibits PIP5K via blocking dimerization, does PIP4K no longer significantly decrease PIP5K activity of a monomeric PIP5KB D51R unable to either dimerize, or make a ternary heterocomplex with PIP4K2A. **(F)** Time to 95% max PI(4,5)P_2 lipids in the presence of 1nM wildtype PIP5KB (n=3), 1nM wildtype PIP5KB + 50nM PIP4K2A (n=3), 10nM PIP5KB D51R (n=3), and 10nM PIP5KB D51R + 50nM PIP4K2A (n=3). Student's T-tests with Welch's corrections were performed to determine differences between PIP5KB and PIP5KB + PIP4K2A conditions (p=0.031) and between PIP5KB D51R and PIP5KB D51R + PIP4K2A conditions (p=0.06). **(G)** Schematic of experiment performed in Figure 3.4H and 3.4I. Standard FRET assay was performed before titrations of dark PIP4K2α homodimers were titrated to determine the effect on frequency of PIP5Kβ homodimerization determined by particles in FRET. **(H)** Representative Maximum particle intensities of acceptor alone, donor + acceptor (5nM AF555-PIP5KB FRET construct + 1nM AF647-PIP5KB FRET construct), donor + acceptor + 50nM PLCδ PH domain (negative control), and donor + acceptor + 50nM PIP4K2A. **(I)** Frequency of particles in FRET for acceptor alone (n=3), donor + acceptor (n=3), donor + acceptor + 50nM PLCδ PH domain (n=3), and donor + acceptor + 50nM PIP4K2A conditions. Student's T-tests were performed to determine difference between Frequency of particles in FRET when comparing donor + acceptor and FRET + 50nM PIP4K2A conditions (p=0.014) and to determine differences between donor + acceptor and FRET + 50mM PLCδ PH domain (p=0.1).

We next sought to confirm that the interaction found was responsible for the decrease in PI(4,5)P_2 lipid synthesis via inhibition of PIP5K seen in previous studies (**Figure 3.4E**). We compared the rate of PI(4,5)P_2 production for wild type PIP5K and monomeric PIP5KB (D51R) in the presence or absence of physiologically relevant concentrations of PIP4KIIA. Previously, it was reported that the most drastic change in PI(4,5)P_2 synthesis occurs at 95% max PI(4,5)P_2 lipid concentration, not at the reaction half-time, so we reported our results this way[151]. In concordance with the previous study, we found a statistically significant decrease in the rate of PI(4,5)P_2

synthesis when 50nM PIP4KIIA was added to the PIP5KB lipid kinase assays (**Figure 3.4F**, red and blue bars). This decrease in the rate of $PI(4,5)P_2$ production was significant when we measured lipid kinase activity in the presence of monomeric PIP5KB (D51R) (**Figure 3.4F**, purple and grey bars). It's important to note that we did see a small, but reproducible, decrease in activity in the presence of 50 nM PIP4KIIA. This small decrease is likely due to PIP4KIIA binding to $PI(4,5)P_2$ lipids as they are produced, blocking membrane availability for PIP5KB (D51R) enzymes despite no direct interaction between the enzymes.

These results suggest that PIP4K inhibits PIP5K by binding to the dimer interface, thus creating a PIP5K-$(PIP4K)_2$ (PIP4K is a constitutive dimer) ternary complex that competes for the same binding site as the $(PIP5K)_2$ homodimer. We sought to confirm this result using our validated FRET assay. We started by performing our standard FRET assay for dimerization before titrating in 50 nM PIP4KIIA to determine if the frequency of PIP5K dimerization was altered (**Figure 3.4G**). Consistent with our previous biochemical results, $(PIP5K)_2$ FRET measured in the presence of 50 nM PIP4KIIA showed a significant decrease in the frequency of PIP5K dimerization. While 50 nM PIP4KIIA is a physiologically relevant concentration of protein in cells, it's possible that the decrease in FRET we see is due to molecular crowding on our supported bilayer, and not the result of a direct PIP4K-PIP5K interaction. To control for this, we performed our standard FRET assay in the presence of 50 nM PLCδ PH domain, a $PI(4,5)P_2$ lipid binding domain that populates the membrane without interacting specifically with the donor or acceptor labeled PIP5KB. We found that there was a small decrease in the amount of FRET seen, but not a statistically significant difference. This shows that the decrease we see from the addition of 50 nM PIP4KIIA in our FRET assay is the result of direct blockage of the dimer interface and isn't the result of crowding of molecules on the supported bilayer. Taken together, these data support the hypothesis that PIP4K

inhibits PIP5K activity through blocking PIP5K dimerization by competing for binding at the dimer interface (**schematic in Figure B2**).

DISCUSSION

Here, we developed a novel FRET sensor able to track membrane-mediated dimerization of PIP5K in real-time. Before this work, the field relied on using biophysical characteristics like molecular dwell time and single particle diffusion to act as a proxy for PIP5K dimerization [157]. Without the ability to track dimerization in real-time, it was difficult to easily discern if other proteins directly modulate PIP5K dimerization, or if they are disrupting lipid kinase activity through an allosteric mechanism. Using this biosensor, we found that dimerization is transient in nature, quickly dissociating from dimeric to monomeric state (**Figure 3.2H**). This finding is in concordance with our recent publication that demonstrated PIP5K exists in solution in a primarily monomeric state but can shift equilibrium to a dimeric conformation when bound to membranes at high density. These findings run counter to the previously held belief in the field that PIP5K exists as a constitutive dimer, similar to PIP4K enzymes[64].

Having a biosensor and assay to quickly assess if a protein or small molecule blocks membrane-mediated dimerization of PIP5K enzymes could prove useful in structure-based drug design. Recent studies have implicated PIP5K activity being necessary for tumor progression in both prostate and breast cancers[98,169]. Further, metastatic properties of cancer cells often relies on upregulation of phosphatidylinositol-3,4,5-trisphosphate ($PI(3,4,5)P_3$) signaling pathways, for which the product of PIP5K enzymatic activity, $PI(4,5)P_2$, is a critical precursor lipid[170–172]. Previous studies have shown that blocking PIP5K activity lowers the surface level $PI(4,5)P_2$ lipids on the inner leaflet, leading to lowered levels of $PI(3,4,5)P_3$ signaling pathway output[53,54]. We

recently showed that dimerization bolsters PIP5K lipid kinase activity 20-fold[71]. Identifying factors that block PIP5K dimerization, and attenuate lipid kinase activity, could be a fruitful route for treatment of some cancers. Recent headway made in de novo structure design provide a potential route for designing small peptides to bind to and block the dimer interface of PIP5K[173].

Recent studies that address dimerization of PIP5K have been focused on in vitro biochemistry[64,71]. Only one study, to date, has tracked PIP5K dimerization in cells[166]. Researchers used FRET to show that PIP5KB and PIP5KC isoforms underwent dimerization in HEK293T cells. The findings in this paper are considered dubious due to their incorrect assertion that the N-terminal region of PIP5K is sufficient for dimerization. The residues identified and mutated to disrupt dimerization are not the actual residues required for the electrostatic bridge that we and other researchers have previously shown mediate dimerization[64,71]. The FRET in this paper is hard to understand, as the methods section doesn't describe what promoter these constructs were transiently expressed on. As well, there are no controls in this paper to determine that the FRET the authors see is specifically due to dimerization, and not the result of other possible interactions. That said, the authors of this paper do conclude that PIP5KB and PIP5KC paralogs are able to heterodimerize. This conclusion is most strongly supported by co-immunoprecipitation from cell lysate containing overexpress PIP5K paralogs. Here, we show that heterodimerization is also possible between PIP5KA and PIP5KB using a combination of single molecule characteristics, biochemical assays, and our in vitro FRET assay (**Figure 3.3**). What is clearly lacking, however, is a demonstration that dimerization occurs at physiologically relevant concentrations in vivo. While our in vitro work was performed with physiologically relevant concentrations of PIP5K paralogs (between 10-20nM)[174], our reductionist experiments do not mimic the complex environment found within a cell. Dimerization may be a key factor regulating the activity of PIP5K

in cells, but we cannot make a conclusion until further work is performed addressing this question. The work in this paper demonstrates that FRET is a useful technique to track dimerization in real time and may be a useful technique for future researchers to bridge this in vivo gap. However, if researchers wish to make a compelling case using FRET in vivo, they must perform complex controls that the only resulting FRET signal seen could be due to dimerization. In the supplement of this study, we describe an orthogonal dimer interface set of mutations (PIP5KB D51R, R254D) that is unable to heterodimerize (**Supplemental Figure B1**). This mutant would be an ideal control for studying dimerization in an in vivo context, as it will be unable to dimerize with endogenous PIP5K.

PIP5K activity has been shown to be greatly enhanced during some signaling pathways, namely the Wnt pathway and during phagocytosis[46,124,138]. How PIP5K activity is enhanced during these processes is not well understood, though dimerization provides a plausible explanation. Dimerization could be facilitated through a tertiary interaction with GTPases like Rac1 or Arf6, or by other proteins that have been shown to directly interact with PIP5K like Daam2 or Dishevelled[58,64,72,74]. These proteins could cluster PIP5K into distinct signalosomes on the inner leaflet that promoted density-dependent dimerization. Future studies that attempt to describe PIP5K dimerization in vivo should explore dimerization in terms of cell signaling pathways like Wnt to attempt to describe a functional role for dimerization.

Recently, a handful of studies have shown that $PI(4,5)P_2$ lipid synthesis is inhibited by PIP4K expression[53,54,76]. Follow up studies established a direct interaction between PIP4K and PIP5K and show that this interaction leads to inhibition of PIP5K[76]. Recent advances in modeling protein-protein interactions via artificial intelligence led us in this study to attempt to model the interaction between PIP5K and PIP4K via Alphafold3 (**Supplementary Figure B2**)[168]. While the

direct interaction predicted by alphafold multimer (residue D51 PIP5K forms a salt bridge with R104 of PIP4K) was incorrect, it suggested to us that the mechanism of inhibition could be based on blocking PIP5K dimerization. Using a combination of biochemical assays and our FRET biosensor, we were able to show that PIP4K can block PIP5K dimerization, and that monomeric PIP5K is not significantly inhibited by PIP4K (**Figure 3.4**). We were unable, however, to determine the exact residues able to mediate the PIP4K-PIP5K interaction. Structural characterization using techniques such as hydrogen-deuterium exchange mass spectrometry may be more successful in determining how PIP4K binds to the dimer interface of PIP5K. The finding the dimer interface is blocked by PIP4K does, when taken with previous in vivo studies, suggest that there exist mechanisms in the cell that antagonize PIP5K dimerization.

MATERIALS AND METHODS

Molecular Biology. The gene coding the PH domain derived from human phospholipase C-δ1 (PLCδ Accession #P51178.2), human phosphatidylinositol 4-phosphate 5-kinase type-1 beta (hPIP5KB; Uniprot #O14986) and human phosphatidylinositol 5-phosphate 4-kinase type-2 alpha (hPIP4KA; Uniprot #P48426) were derived from codon optimized genes synthesized by GeneArt (Invitrogen). Subcloning of gene sequences were performed using methods previously described[22,71,143]. Plasmids containing PIP5KB mutations (i.e. C110S, D51R, D266K, P163C, C411S), PIP4KIIA (R104D), and PIP5KA (D92R) were generated through site-directed mutagenesis using the PfuUltra High-Fidelity DNA polymerase (Agilent, cat# 600380). The PIP5KB FRET construct contains the following point mutations: C110S, P163C, and C411S. The complete open reading frame of all vectors used in this study were sequenced by Azenta (formerly Genewiz) and Plasmidsaurus (University of Oregon) to ensure constructs lacked deleterious mutations. Each protein expression construct was screened for optimal yield and solubility in either bacteria (BL21 DE3 Star, Rosetta, etc.) or *Spodoptera frugiperda* (Sf9) insect cells. In this manuscript, PIP5KB refers to the human PIP5KB paralog (this is the murine PIP5KA paralog due to naming inconsistencies). All plasmids created and used within this manuscript function under this human nomenclature.

Protein purification

PIP5KB and PIP5KB mutants. Gene sequences encoding PIP5KB were cloned into FastBac1 vectors in frame with a N-terminal his_6-MBP-TEV-GGGGG and expressed under the polyhedrin (pH) promoter. BACMIDS and baculoviruses were generated as previously described[71,143].

Briefly, high five insect cells were infected with 2% vol/vol baculovirus for an optimized multiplicity of infection (MOI). After 48 hours of growth at 27ºC in ESF 921 Serum-Free Insect Cell Culture medium (Expression Systems, Cat# 96-001-01), cells were harvested by centrifugation before washing and storing at -80 ºC in storage buffer (1x PBS [pH 7.2], 10% glycerol, 2x Sigma protease inhibitor table). For purification, after thawing, cells were lysed via dounce homogenizer as previously described[71]. Clarification was done via centrifugation for 60 minutes at 140,000 x *g* under vacuum using a Beckman Ti-45 rotor. Using 5 mL of Ni-NTA Agarose (Qiagen, Cat# 30230) resin at 4ºC, lysate was batch bound for 2 hours in a beaker set on a stir plate. To collect protein-bound resin, resin was centrifuged in 50mL tubes and washed with buffer containing 50 mM Na_2HPO_4 [pH 8.0], 10 mM imidazole, 400 mM NaCl, and 5 mM BME. After another centrifugation round, resin was applied to a gravity flow column in more wash buffer. Ni-NTA resin with his_6-MBP-TEV-GGGGG-PIP5K bound was then eluted into buffer containing 500 mM imidazole. Peak fractions were pooled, combined with 200 µg/mL his6-TEV(S291V) protease, and dialyzed against 4 liters of buffer containing 20 mM Tris [pH 8.0], 200 mM NaCl, 2.5 mM BME for 16-18 hours at 4ºC. Dialysate was then combined 1:1 with 20 mM Tris [pH 8.0], 1 mM TCEP (~100 mM NaCl final). Precipitation was removed by centrifugation and 0.22 µm syringe filtration. Clarified dialysate was then bound to a MonoS cation exchange column (GE Healthcare, Cat# 17-5168-01) equilibrated in 20 mM Tris [pH 8.0], 100 mM NaCl, 1 mM TCEP buffer. Proteins were resolved over a 10-100% linear gradient (0.1-1 M NaCl, 45 CV, 45 mL total, 1 mL/min flow rate). PIP5K paralogs typically eluted from the MonoS column in the presence of 370-450 mM NaCl. Peak fractions containing PIP5K were pooled, concentrated in a 30 kDa MWCO Vivaspin 6 centrifuge tube (GE Healthcare, Cat# 28-9323-17), and loaded onto a 24 mL Superdex 200 10/300 GL (GE Healthcare, Cat# 17-5174-01) size exclusion column

equilibrated in 20 mM Tris [pH 8.0], 200 mM NaCl, 10% glycerol, 1 mM TCEP. Peak fractions were concentrated in a 30 kDa MWCO Vivaspin 6 centrifuge tube and snap frozen at a final concentration of 10-40 μM using liquid nitrogen.

PIP5KB FRET constructs (C103S, P163, C411S) were fluorescently labeled via their singular surface exposed cysteine residue with either Alexa647-C2-maleimide or Alexa555-C2-maleimide. Once labeled, excess unreacted dye was extracted using a Cytiva NAP-25 column (Fisher scientific, Cat# 10004064) before being loaded onto a 24 mL Superdex 200 10/300 (GE Healthcare, Cat# 17-5174-01) size exclusion column equilibrated in 20 mM Tris [pH 8.0], 200 mM NaCl, 10% glycerol, 1 mM TCEP. Peak fractions were concentrated in a 30 kDa MWCO Vivaspin 6 centrifuge tube and snap frozen at a final concentration of 1-30 μM using liquid nitrogen.

PIP5KA and PIP5KA mutants. Gene sequences encoding PIP5KA and PIP5KA D92R were cloned into FastBac1 vectors in frame with an N-terminal his6-MBP-$(Asn)_{10}$-TEV-GGGGG. Protein expression in High Five insect cells was constitutive under the polyhedrin (pH) promoter. High Five cells were infected with baculovirus using an optimized MOI, typically 1.5–2% vol/vol, was determined empirically from small-scale test expression (25–50 mL culture). Infected cells were grown at 27°C for 48 hours in ESF 921 Serum-Free Insect Cell Culture medium (Expression Systems, Cat# 96-001-01). Cells were harvested by centrifugation, washed with 1× PBS (pH 7.2), and then stored in the –80°C freezer. For purification, frozen insect cell pellets for 4–6 L of liquid culture were thawed in an ambient water bath and lysed into buffer containing 50 mM Na_2HPO_4 (pH 8.0), 10 mM imidazole, 400 mM NaCl, 1 mM PMSF, 5 mM BME, 100 μg/mL

DNase, 1 Sigma protease inhibitor cocktail EDTA free per 100 mL lysis buffer using a dounce homogenizer. Lysate was centrifuged using a Beckman Ti-45 rotor at 4°C at 35,000 rpm (140,000 × *g*) for 60 min under vacuum. Lysate was then batch bound to 5 mL of Ni-NTA Agarose (QIAGEN, Cat# 30230) resin at 4°C for 1–2 hr in a beaker set on a stir plate. Resin was then collected in 50 mL tubes, centrifuged, and washed with buffer containing 50 mM Na_2HPO_4 (pH 8.0), 10 mM imidazole, 400 mM NaCl, and 5 mM BME before being transferred to gravity flow column. NiNTA resin with his6-MBP-$(Asn)_{10}$-TEV-GGGGG-PIP5K was then washed with 100 mL of 50 mM Na_2HPO_4(pH 8.0), 30 mM imidazole, 400 mM NaCl, and 5 mM BME buffer and then eluted into buffer containing 500 mM imidazole. Peak fractions were pooled, combined with 200 µg/mL his6-TEV(S291V) protease, and dialyzed against 4 L of buffer containing 20 mM Tris (pH 8.0), 200 mM NaCl, 2.5 mM BME for 16–18 hr at 4°C. Dialysate was then combined 1:1 with 20 mM Tris (pH 8.0), 1 mM DTT (~100 mM NaCl final). Precipitation was removed by centrifugation and 0.22 µm syringe filtration. Clarified dialysate was then bound to a MonoS cation-exchange column (GE Healthcare, Cat# 17-5168-01) equilibrated in 20 mM Tris (pH 8.0), 100 mM NaCl, 1 mM TCEP buffer. Proteins were resolved over a 10–100% linear gradient (0.1–1 M NaCl, 45 CV, 45 mL total, 1 mL/min flow rate). PIP5K homologs and paralogs typically eluted from the MonoS column in the presence of 370–450 mM NaCl. Peak fractions containing PIP5K (or Mss4) were pooled, concentrated in a 30 kDa MWCO Vivaspin 6 centrifuge tube (GE Healthcare, Cat# 28-9323-17), and loaded onto a 24 mL Superdex 200 10/300 GL (GE Healthcare, Cat# 17-5174-01) size-exclusion column equilibrated in 20 mM Tris (pH 8.0), 200 mM NaCl, 10% glycerol, 1 mM TCEP. Peak fractions were concentrated in a 30 kDa MWCO Vivaspin 6 centrifuge tube and snap-frozen at a final concentration of 20–40 µM using liquid nitrogen.

PIP4KIIA and PIP4KIIA (R104D). Codon optimized gene sequence encoding human PIP4KIIA (Uniprot # P48426) was cloned into a pETM-derived bacterial expression vector to create the following fusion protein: his_6-SUMO3-GGGGG-PIP4K2A (1-416aa). Expressed in BL21(DE3) Star *E. coli* as previously described [76]. Bacterial cultures (grown in 2-4 liters of Terrific Broth) were grown at 37ºC until OD_{600}=0.6. Protein expression was induced with 50 μM IPTG and bacteria expressed protein for 20 hours at 18ºC before being harvested by centrifugation. For purification, cells were lysed into buffer containing 50 mM Na_2HPO_4 [pH 8.0], 400 mM NaCl, 0.4 mM BME, 1 mM PMSF, DNase, 1 mg/mL lysozyme using a microtip sonicator. Lysate was centrifuged at 16,000 rpm (35,172 x *g*) for 60 minutes in a Beckman JA-17 rotor chilled to 4ºC. Lysate was circulated over 5 mL HiTrap Chelating column (GE Healthcare, Cat# 17-0409-01) that had been equilibrated with 100 mM $CoCl_2$ for 1 hour, washed with MilliQ water, and followed by buffer containing 50 mM Na_2HPO_4 [pH 8.0], 400 mM NaCl, 0.4 mM BME. Recombinant PIP4K2B was eluted with a linear gradient of imidazole (0-500 mM, 8 CV, 40 mL total, 2 mL/min flow rate). Peak fractions were pooled, combined with 50 μg/mL of his6-SenP2 (SUMO protease), and dialyzed against 4 liters of buffer containing 25 mM Na_2HPO_4 [pH 8.0], 400 mM NaCl, and 0.4 mM BME for 16-18 hours at 4ºC. Following overnight cleavage of the SUMO3 tag, dialysate containing his6-SUMO3, his6-SenP2, and GGGGG-PIP4K2B was recirculated for at least 1 hr over a 5 mL HiTrap(Co^{+2}) chelating column. Flow-through containing GGGGG-PIP4K2B was then concentrated in a 30 kDa MWCO Vivaspin 6 before loading onto a Superdex 200 size exclusion column equilibrated in 20 mM HEPES [pH 7], 200 mM NaCl, 10% glycerol, 1 mM TCEP. In some cases, cation exchange chromatography was used to increase the purity of GGGGG-PIP4K2B before resolving on the Superdex 200 column. In those cases, we equilibrated a MonoS column 20 mM HEPES [pH 7], 100 mM NaCl, 1 mM TCEP buffer. PIP4K2B (pI = 6.9)

bound to the MonoS was resolved over a 10-100% linear gradient (0.1-1 M NaCl, 30 CV, 30 mL total, 1.5 mL/min flow rate). Peak fractions collected from the Superdex 200 were concentrated in a 30 kDa MWCO Vivaspin 6 centrifuge tube and snap frozen at a final concentration of 20-80 µM using liquid nitrogen.

PLCδ-PH domain. This protein was expressed and purified as previously described [69]. Briefly, human PLCδ-PH domain (11-140aa) was expressed in BL21 (DE3) Star *E. coli* as a his_6-SUMO3-$(Gly)_5$-PLCδ 11-140aa) fusion protein. Following growth at 37ºC in Terrific Broth to an OD_{600} of 0.8, cultures were shifted to 18ºC for 1 hour, induced with 0.1 mM IPTG, and allowed to express protein for 20 hours at 18ºC before being harvested. Cells were lysed into 50 mM Na_2HPO_4 [pH 8.0], 300 mM NaCl, 0.4 mM BME, 1 mM PMSF, 100 µg/mL Dnase using a microfluidizer. Lysate was then centrifuged at 16,000 rpm (35,172 x *g*) for 60 minutes in a Beckman JA-17 rotor chilled to 4ºC. Lysate was circulated over 5 mL HiTrap Chelating column (GE Healthcare, Cat# 17-0409-01) charged with 100 mM $CoCl_2$ for 1 hour. Bound protein was then eluted with a linear gradient of imidazole (0-500 mM, 8 CV, 40 mL total, 2 mL/min flow rate). Peak fractions were pooled, combined with SUMO protease (50 µg/mL final concentration), and dialyzed against 4 liters of buffer containing 50 mM Na_2HPO_4 [pH 8.0], 300 mM NaCl, and 0.4 mM BME for 16-18 hours at 4ºC. Dialysate containing SUMO cleaved protein was recirculated for 1 hr over a 5 mL HiTrap Chelating column. Flow-through containing $(Gly)_5$-PLCδ (11-140aa) was then concentrated in a 5 kDa MWCO Vivaspin 20 before being loaded on a Superdex 75 size exclusion column equilibrated in 20 mM Tris [pH 8.0], 200 mM NaCl, 10% glycerol, 1 mM TCEP. Peak fractions containing $(Gly)_5$-PLCδ (11-140aa) were pooled and concentrated to a maximum concentration of 75 µM (1.2 mg/mL) before snap freezing with liquid nitrogen and storage at -80ºC. As previously

described, GGGGG-PLCδ 11-140aa) was labeled with either AF488 or Cy3 using sortase mediated peptide ligation [69,71].

Preparation of small unilamellar vesicles. To make liposomes, 2 μmoles total lipids are combined in a 35 mL glass round bottom flask with 2 mL of chloroform, dried into a film, resuspended in PBS, and then extruded through a 0.05 μm pore size 19 mm polycarbonate membrane (Avanti, Cat# 610002) with filter supports (Avanti, Cat# 610014) on both sides of the polycarbonate membrane as previously described[22,69,71]. Lipid identities used for small unilamellar vesicles (SUVs) were: 1,2-dioleoyl-sn-glycero-3-phosphocholine (18:1 DOPC, Avanti # 850375C), L-α-phosphatidylinositol-4-phosphate (Brain PI(4)P, Avanti Cat# 840045X), L-α-phosphatidylinositol-4,5-bisphosphate (Brain PI(4,5)P_2, Avanti Cat# 840046X).

Preparation of supported lipid bilayers. 25x75 mm coverglass (IBIDI, Cat# 10812) was used to create supported lipid bilayers through previously described methods[71,143]. Briefly, coverglass was cleaned with heated 2% Hellmanex III (Fisher, Cat# 14-385-864), incubated, then thoroughly washed before Pirahna etching on the same day that SLBs were formed. A second thorough rinsing with water washed away any leftover Pirahna residue, then slides were rapidly dried using nitrogen gas. Once dried, glass was adhered to a 6-well sticky-side chamber (IBIDI, Cat# 80608). SLBs were formed by flowing 30 nm SUVs diluted in PBS [pH 7.2] to a total lipid concentration of 0.25 mM and incubated for 30 minutes. IBIDI chambers were then washed with 5 mL of PBS [pH 7.2] before blocking with 1mg/mL syringe-filtered beta casein (ThermoFisher, Cat# 37528) diluted in 1x PBS [pH 7.4]. After blocking SLBs with beta casein, membranes were washed again with 1mL of PBS, followed by 1 mL of kinase buffer before TIRF-M.

Assay for measuring the kinetics of PI(4,5)P_2 production. The kinetics of PI(4)P phosphorylation were measured on SLBs formed in IBIDI chambers and visualized using TIRF microscopy as previously described [69,71]. Imaging reaction buffer contained 20 mM HEPES [pH 7.0], 150 mM NaCl, 1 mM ATP, 5 mM $MgCl_2$, 0.5 mM EGTA, 20 mM glucose, 200 μg/mL beta casein (ThermoScientific, Cat# 37528), 20 mM BME, 320 μg/mL glucose oxidase (Serva, Cat# 22780.01 *Aspergillus niger*), 50 μg/mL catalase (Sigma, Cat# C40-100MG Bovine Liver), and 2 mM Trolox (UV treated as previously described by Hansen et al. 2019). Perishable reagents (i.e. glucose oxidase, catalase, and Trolox) were added 5-10 minutes before image acquisition. For all experiments, we monitored the change in PI(4,5)P_2 membrane density using a solution concentration of 20 nM AF488-GGGGG-PLCδ or Cy3-GGGGG-PLCδ. Density of PIP lipids (lipids/μm^2) was calculated assuming a footprint of 0.72 nm^2 for DOPC lipids [69,121].

Microscope hardware and imaging acquisition. Single molecule imaging experiments were performed on an inverted Nikon Ti2 microscope using a 100x Nikon objective (1.49 NA) oil immersion TIRF objective. The x-axis and y-axis positions were manually controlled using a Nikon motorized stage and joystick. All images were acquired using an iXion Life 897 EMCCD camera (Andor Technology Ltd., UK). Fluorescently labeled proteins were excited with either a 405 nm, 488 nm, 532 nm, 561 nm, or 637 nm diode laser (OBIS laser diode, Coherent Inc. Santa Clara, CA) controlled by a Vortran laser drive with acousto-optic tunable filters (AOTF) control. The power output measured through the objective for single particle imaging was 1-3 mW. Excitation light was passed through the following dichroic filter cubes before illuminating the sample: (1) ZT488/647rpc and (2) ZT561rdc (ET575LP) (Semrock). Fluorescence emission was

detected on an ANDOR EMCCD camera position after a Sutter emission filter wheel housing the following emission filters: ET525/50M, ET600/50M, ET700/75M (Semrock). All in vitro experiments were performed at room temperature (23ºC). Microscope hardware was controlled using Nikon NIS elements.

FRET imaging acquisition. Single molecule FRET imaging experiments were performed on the same microscope as the previous section described. In the case of FRET imaging, fluorescently labeled proteins were excited with either 532 or 561 nm diode laser (OBIS laser diode, Coherent Inc. Santa Clara, CA) controlled by a Vortran laser drive with acousto-optic tunable filters (AOTF) control. The power output measured through the objective for single particle imaging was 1-3 mW. Excitation light was passed through the following dichroic filter cubes before illuminating the sample: (1) ZT488/647rpc and (2) ZT561rdc (ET575LP) (Semrock). Fluorescence emission was detected on an ANDOR EMCCD camera position after passing through a Sutter emission filter wheel loaded with the ET700/75M (Semrock) filter. All in vitro experiments were performed at room temperature (23ºC). Microscope hardware was controlled using Nikon NIS elements.

Single particle tracking. Fluorescent protein detection and tracking was performed using the ImageJ/Fiji TrackMate plugin [117] similarly to methods previously described[22,69,71]. Briefly, data in the form of .nd2 files were loaded in ImageJ. TrackMate was used after brightness was adjusted for easier identification of particles. TrackMate identified molecular tracks in these steps: LoG detector was used to identify particles based on brightness and signal-to-noise ratio. Once identified, particles were tracked for their full lifetime using the LAP tracker. We filtered particle trajectories with these filters: Track Start (removed trajectories that began in first frame), Track

End (removed trajectories present in last frame), Duration (removed trajectories ≤ 2 frames and singular extra-long tracks), Track displacement (removed immobilized particles displacement <0.1), and X - Y location (removed particles near the edge of the images). The TrackMate output files were analyzed using PRISM 9 (GraphPad) to calculate characteristic dwell times and diffusion coefficients.

Step size distribution of single particle trajectories were plotted in Prism as frequency versus step size (μm). For all analysis presented in this manuscript, the bin size for the step size distribution equals 0.01 μm. For curving fitting, the step-size distributions were plotted as probability density versus step size (μm). This was achieved by dividing the frequency distribution (i.e. y-axis values) by the bin size (0.01 μm). The probability density versus step size plots were fit to the following one- or two-species distributions:

Single species model:

$$f(r) = \frac{r}{2D\tau} e^{-\left(\frac{r^2}{4D\tau}\right)}$$

Two species model:

$$f(r) = \alpha \frac{r}{2D_1\tau} e^{-\left(\frac{r^2}{4D_1\tau}\right)} + (1-\alpha) \frac{r}{2D_2\tau} e^{-\left(\frac{r^2}{4D_2\tau}\right)}$$

D1=species 1diffusion coefficient (μm^2/sec), D2= species 2 diffusion coefficient (μm^2/sec), alpha (α_1 = % of species 1, r = step size (μm),α_2 = time interval between steps (sec). Final step size distribution plots were generated in PRISM graphing software and using the following equations: (1 species model): f(x) = x/(2*D1*t)*exp(-(x^2/(4*D1*t))), (2 species model): f(x) = alpha*(x/(2*D1*t)*exp(-(x^2/(4*D1*t))))+(1-alpha)*(x/(2*D2*t)*exp(-(x^2/(4*D2*t)))).

To calculate the single molecule dwell times for, FRET-imaged AF647-PIP5KB (C110S, P163C, C411S), standard single molecule imagining of AF647-PIP5KB (and mutants), and AF647-PIP5KA (and mutants) we generated a cumulative distribution frequency (CDF) plot using the frame interval as the bin size (e.g. 50 ms). The $\log_{10}$(1-CDF) was plotted against the dwell time and fit to either a single or double exponential decay curve.

Single exponential model:

$$f(t) = e^{(-x/\tau)}$$

Two exponential model:

$$f(t) = \alpha * e^{(-x/\tau 1)} + (1 - \alpha) * e^{(-x/\tau 2)}$$

Fitting procedure initiated with a single exponential. In cases of a low-quality single exponential fit, a maximum of two species model was used. For double exponential fit, alpha (α) represents the fraction of fast dissociating population of molecules characterized by the time constant, α_1.

Image analysis, curve fitting, and statistics for single particle dwell time and step size. Image analysis was performed on ImageJ. PRISM 9 (GraphPad) was used for curve fitting. Single molecule dwell time and step size presented in this manuscript represent combined data from 3 technical replicates with 2-3 movies acquired from multiple fields of view for each experimental condition. Dwell time distributions and curve fits were generated with n = 1000-3000 particle trajectories. Step size distribution plots and curve fits represent 10,000-30,000 measured displacements.

Image analysis, curve fitting, and statistics for single molecule FRET (532 laser experiments).

Image analysis was performed on ImageJ. Single particles in FRET were identified using the same methods as the Single Particle Tracking subheading (see above). Once single molecules were determined, we calculated the total number of dimerization events/sec by isolating the total number of tracked events and dividing it by the total time of the video (for example: 2000 events tracked in a 30 second video would yield 66.67 dimerization events per second). Total number of biological replicates used for each plot is given in the figure legend (n=3-10). Statistical analysis between the mean of two populations was conducted via GraphPad using a student's T-test with Welch's correction where variance was unequal.

Image analysis, curve fitting, and statistics for single molecule FRET (561 laser experiments).

Image analysis was performed on ImageJ. Single particles in FRET were identified using the same methods as the Single Particle Tracking subheading (see above). Once single molecules were determined, we isolated the average molecular brightness of each single particle to determine if the particle was designated as in FRET. By comparing the molecular brightness of particles identified in our controls to our experimental FRET condition, we identified particles with a maximum brightness in our FRET condition that far exceeded the brightest particles in our control conditions. We divided the number of molecules brighter than 99% of particles in the donor and acceptor alone controls by the total number of tracked particles (Frequency = #bright molecules/#total molecules) to determine the frequency of particles seen in FRET.

CHAPTER IV

CONCLUDING REMARKS

PIP lipids act as molecular scaffolds, recruiting proteins to their subcellular locations to stimulate a variety of chemical reactions necessary for cellular functions. PI(4,5)P_2 lipids are the most abundant PIP lipid at the inner leaflet of the plasma membrane. So universal is PI(4,5)P_2's presence at the inner leaflet that the standard biosensor to label the plasma membrane in imaging studies is using the PH domain of PLCδ, a PI(4,5)P_2 lipid binding domain. PI(4,5)P_2 lipids regulate a wide variety of cell signaling pathways, including endocytosis, ion channel gating, and cytoskeletal anchoring[15,37,83]. These are processive signaling reactions, needed to happen at a moment's notice and requiring PI(4,5)P_2 lipid pools be readily available. Alternative are the signaling reactions that initiate rapid PI(4,5)P_2 synthesis, quickly increasing the total levels of PI(4,5)P_2 at the inner leaflet to stimulate downstream signaling events. Processes that initiate PI(4,5)P_2 synthesis include the Wnt pathway and phagocytosis[24,138]. Given the overall importance of PI(4,5)P_2 lipids in the cell, understanding how these lipids are synthesized, and studying the mechanisms that control synthesis is critical for both general scientific advancement as well as potentially treating the life-threatening illness that result from misregulation of PI(4,5)P_2 lipid synthesis including prostate and breast cancers, developmental disorders, and muscular dystrophy. This thesis focuses on addressing this question of PI(4,5)P_2 synthesis by focusing on the enzyme PIP5K.

The production of the first crystal structure of PIP5K in 2015 is a turning point for understanding the biochemistry that regulates PIP5K[64]. This study, and the accompanying studies published soon after, solve for the first time the structural motifs that govern PIP5K activity and

regulation[63,64,67]. Much of the biochemical work that followed these studies have used their foundational knowledge to build off and further characterize the protein. Most of these previous studies used assays that lacked high resolution techniques that enabled real-time and concurrent tracking of $PI(4,5)P_2$ production and PIP5K membrane binding. This highlights why these studies, despite their rigor and breakthroughs, were unable to determine that PIP5K was able to bind to its product, $PI(4,5)P_2$ and that the protein existed as a monomer in solution. These findings required the use of TIRF microscopy and single molecule imaging to flesh out, and they highlight the power of using in vitro fluorescence microscopy to study biochemical reactions. Building off the recent work that discovered PIP5K's positive feedback based on product-binding, Chapter II of this dissertation documents the further use of fluorescence-based TIRF techniques and mutagenesis to map the sites of product binding that give rise to positive feedback. For the first time, we present the finding that the specificity loop and PIPBM interacts with $PI(4,5)P_2$ lipids. In particular, the PIPBM binds to $PI(4,5)P_2$ lipids with much higher affinity than with its substrate, PI(4)P, due to the increased electronegative charge on $PI(4,5)P_2$. Additionally, we found that the PIPBM can bind Phosphatidylserine (PS) lipids as well, explaining why PS lipids have previously been shown to activate PIP5K. These findings, taken together, also provide the first mechanistic explanation for why PIP5K prefers to recruit to the inner leaflet over other membrane-bound organelles like the Golgi, which contains a high molar concentration of its substrate PI(4)P. Finally, we showed in this chapter that the PIP5K specificity loop is unique in its ability to bind to $PI(4,5)P_2$ lipids. We show that the related enzyme PIP4K, which also can synthesize $PI(4,5)P_2$ but using the substrate lipid PI(5)P, has a specificity loop that is unable to bind to $PI(4,5)P_2$ lipids. This finding provides a plausible mechanistic explanation for why PIP5K can sense and bind to low concentrations of $PI(4,5)P_2$ lipids, while PIP4K cannot.

Chapter III focuses on following up upon the finding that PIP5K does not exist as a constitutive dimer, as was previously believed by the field. Instead, our recent study showed that PIP5K exists primarily as a monomer in solution but could shift equilibrium to a dimeric conformation after binding to membranes in a density-dependent manner. In Chapter III, we developed a novel FRET biosensor and assay to track PIP5K dimerization in real-time. We used a variety of controls to demonstrate the FRET signal seen in our single molecule TIRF FRET assay is the result of dimerization, and not off target interactions. We used the biosensor to track dimerization lifetime and diffusion, as well as show that PIP5K activity mutants are still able to dimerize with wildtype, providing an explanation for previous findings that catalytically dead PIP5K overexpression in cells leads to increased $PI(4,5)P_2$ levels.

Once we confirmed the efficacy of our FRET sensor, we then used the assay to answer outstanding questions in the field. First, showed that PIP5K enzymes exhibit membrane-mediated heterodimerize, which we hypothesized due to sequence conservation of the dimer interface residues. Using a combination of single molecule tracking and our FRET assay, we showed that heterodimerization was possible. To complement, we created an orthogonal dimer interface mutation PIP5KB (D51R, R254D) that was unable to heterodimerize with either PIP5KB or other PIP5K paralogs. This orthogonal PIP5K is still able to homodimerize and will be a useful mutant for future studies that look to characterize the importance of PIP5K dimerization in vivo.

Finally, we used the recent advances in structure prediction software (Alphafold multimer) to elucidate the mechanism by which PIP4K inhibit PIP5K. Alphafold Multimer predicted that the interaction between PIP4K and PIP5K forms a salt bridge using the dimer interface of PIP5K. While the residue attributed to PIP4K (arginine at site 104) was incorrect, we showed that dimeric PIP5K is not inhibited by PIP4K in our in vitro assays. This suggested to us the mechanism by

which PIP4K inhibits PIP5K is though blocking dimerization, likely through occluding the dimer interface. We used biochemical assays complemented by our FRET biosensor to show with multiple experiments that PIP5K is unable to dimerize in the presence of PIP4K, and that monomeric PIP5K is unable to interact with PIP4K enzymes.

The work presented in Chapter III of this thesis does not, however, determine whether PIP5K dimerization plays any functional role in living cells and organisms. We expect that it does, however no studies to date have thoroughly assessed this question. Future work may seek to focus on using the principles of our in vitro FRET assay and biosensor and applying them to an in vivo context. I would recommend that future work proceeds using the orthogonal mutant established in previous work and in Chapter III of this dissertation.

In conclusion, the work presented in this thesis greatly expands the current understanding of PIP5K regulation. This work also opens new avenues for both the Hansen lab and other labs that seek to understand how PIP5K activity, and thus $PI(4,5)P_2$ synthesis, is regulated. The in vitro nature of this work is optimal for addressing some questions, as our reductionist approach simplifies the questions asked and the answers we must interpret. However, this work only provides plausible explanations and new overarching hypotheses. For example, the work in Chapter II can be interpreted to explain why PIP5K enzymes localize to the inner leaflet. However, they do not act as concrete answers, as those would require the rigorous testing of these new hypotheses in a variety of living cells. These experiments are beyond the scope of this thesis, but it is incumbent upon honest scientists to acknowledge these nuances. Future work will take these in vitro findings and couple them with in vivo experiments to come to a more concrete explanation of these phenomena. The work presented in this thesis is foundational to the future cellular PIP5K studies, just as the crystal structure papers were for this thesis. Ultimately, full understanding of a

scientific question is not possible without the use of a wide array of experimental techniques. Here, we use a reductionist, in vitro fluorescence microscopy approach to unravel these complex biochemical questions. Future work will go far beyond what is presented here, though we must hope, with some personal sense of pride, that the work herein will inspire some future scientist to approach the next question.

APPENDIX A

SUPPLEMENTARY INFORMATION FOR CHAPTER II

Appendix A is the supplemental information for chapter II. It includes data relevant to the content of Chapter II.

Supplemental Figure A1

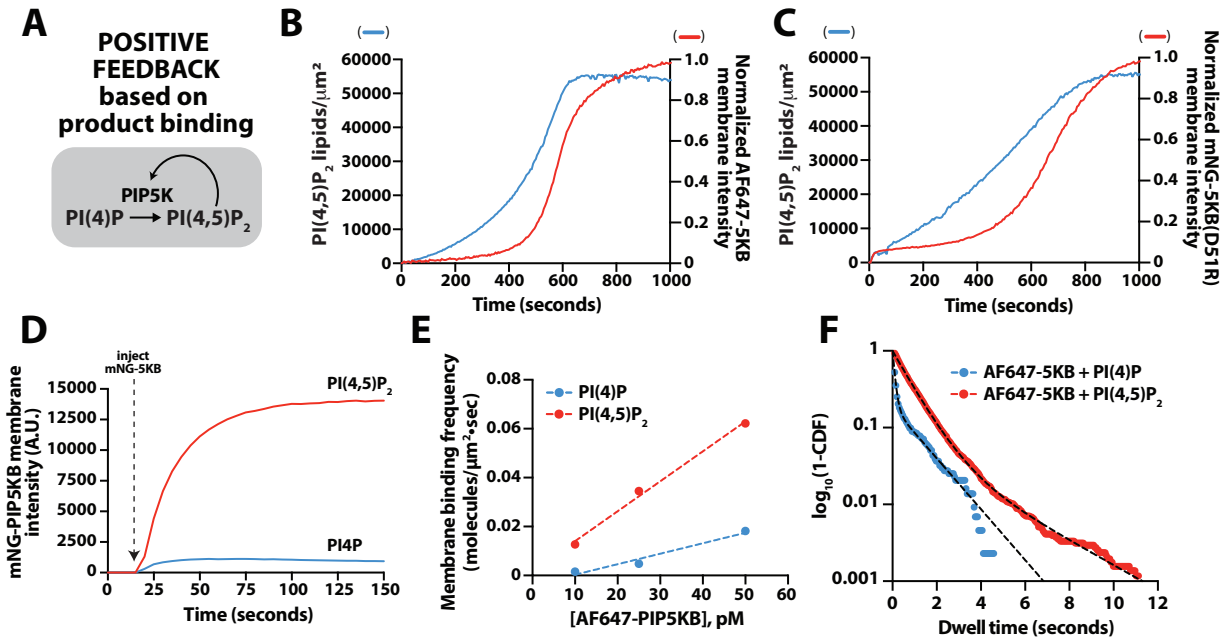

Supplemental Figure A1
PIP5KB displays positive feedback based on PI(4,5)P_2 binding
(A) PIP5K catalyzes the phosphorylation of PI(4)P to generate PI(4,5)P2. Product binding enhances PIP5K membrane localization to drive positive feedback. **(B)** Kinase activity (blue) measures the formation of PI(4,5)P_2 over time by 5 nM AF647-PIP5KB, while simultaneously tracking normalized AF647-PIP5KB membrane localization (red). **(C)** Kinase activity trace (blue) measures the formation of PI(4,5)P_2 over time by 5 nM mNG-PIP5KB (D51R), while simultaneously tracking mNG-PIP5KB (D51R) localization (red). (B-C) Data used to generate plot in Figure 1C. Production of PI(4,5)P_2 was monitored in the presence of 20 nM Cy3-PLCδ. Starting membrane composition: 96% DOPC, 4% PI(4)P. Starting bilayer composition: 96% DOPC, 4% PI(4)P. **(D)** Bulk membrane recruitment of 25 nM mNG-PIP5KB on bilayers containing either 4% PI(4,5)P_2 or 4% PI(4)P. **(E)** Experimental measurement of membrane binding frequency measured in the presence of 10-50 pM mNG-PIP5KB on bilayers containing either 4% PI(4,5)P_2 (k_{ON} = 1.23 nM^{-1}•μm^{-2}•sec^{-1}) or 4% PI(4)P (k_{ON} = 0.43 nM^{-1}•μm^{-2}•sec^{-1}). **(F)** Representative single molecule dwell time distributions measured in the presence of 10 pM AF647-PIP5KB binding to 96% DOPC bilayers

containing either 4% PI(4,5)P_2 (t_1 = 0.82 ± 0.05s, t_2 = 3.1 ± 0.34s, α = 0.95 ± 0.01, n = 14950 molecules) or 100 pM AF647-PIP5KB binding to 4% PI4P (t_1 = 0.13 ± 0.03s, t_2 = 1.64 ± 0.3s, α = 0.88 ± 0.07, n = 3522 molecules). **(D-F)** Imaging buffer contained 1 mM non-hydrolyzable ATPγS to prevent the generation of PI(4,5)P_2 by PIP5KB. Errors equal SD from n = 3 technical replicates.

Supplemental Figure A2

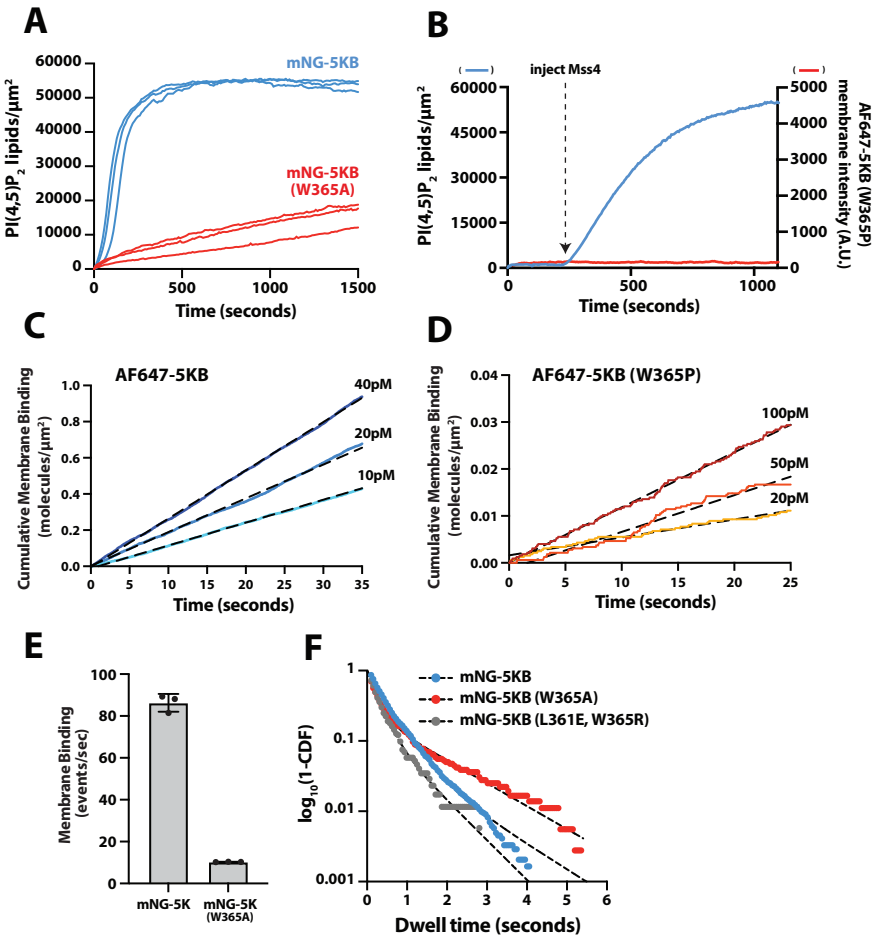

Supplemental Figure A2
PIP5KB specificity loop mutants have reduced kinase activity and PI(4,5)P_2 binding
(A) Lipid kinase activity measured in the presence of 5 nM PIP5KB or 5 nM PIP5KB (W365A). Production of PI(4,5)P_2 was monitored in the presence of 20 nM Cy3-PLCδ. Initial lipid composition: 96% DOPC, 4% PI(4)P. **(B)** Kinase activity trace (blue) measures the formation of PI(4,5)P_2 over time by 5 nM Mss4, while simultaneously visualizing AF647-PIP5KB (W365P) localization (red). Production of PI(4,5)P_2 was monitored in the presence of 20 nM Cy3-PLCδ. Data used to generate plot in Figure 1C. Initial lipid composition: 96% DOPC, 4% PI(4)P. **(C)** Cumulative binding events/time for AF647-PIP5KB WT at concentrations of 10, 20, 40 pM on SLBs containing 96% DOPC and 4% PI(4,5)P_2 lipids. **(D)** Cumulative binding events/time for AF647-PIP5KB (W365P) at concentrations of 20, 50, and 100 pM on SLBs

containing 96% DOPC and 4% PI(4,5)P_2 lipids. **(C-D)** Data link to Figure 1E. **(E)** Membrane binding frequency (events/second) in the presence of 100 pM mNG-PIP5KB (mean = 90.6 ± 3.3 events/sec, $N = 3$ exp) or 100 pM mNG-PIP5KB(W365A) (mean = 10.2 ± 0.03 events/sec, $N = 3$ exp). **(F)** Representative single molecule dwell time distributions measured in the presence of 100 pM mNG-PIP5KB ($t_1 = 0.43 \pm 0.04$ s, $t_2 = 1.07 \pm 0.25$ s, $\alpha = 0.81 \pm 0.09$, n = 1202), 100 pM mNG-PIP5KB(W365A) ($t_1 = 0.21 \pm 0.01$ s, $t_2 = 1.24 \pm 0.01$ s, $\alpha = 0.89 \pm 0.11$, n = 1100), or 100 pM mNG-PIP5KB(L361E, W365R) ($t_1 = 0.21 \pm 0.004$ s, $t_2 = 1.41 \pm 0.63$ s, $\alpha = 0.86 \pm 0.05$, n = 1169). Membrane composition: 98% DOPC, 2% PI(4,5)P_2 lipids. Errors equal SD from n ≥ 3 technical replicates.

Supplemental Figure A3

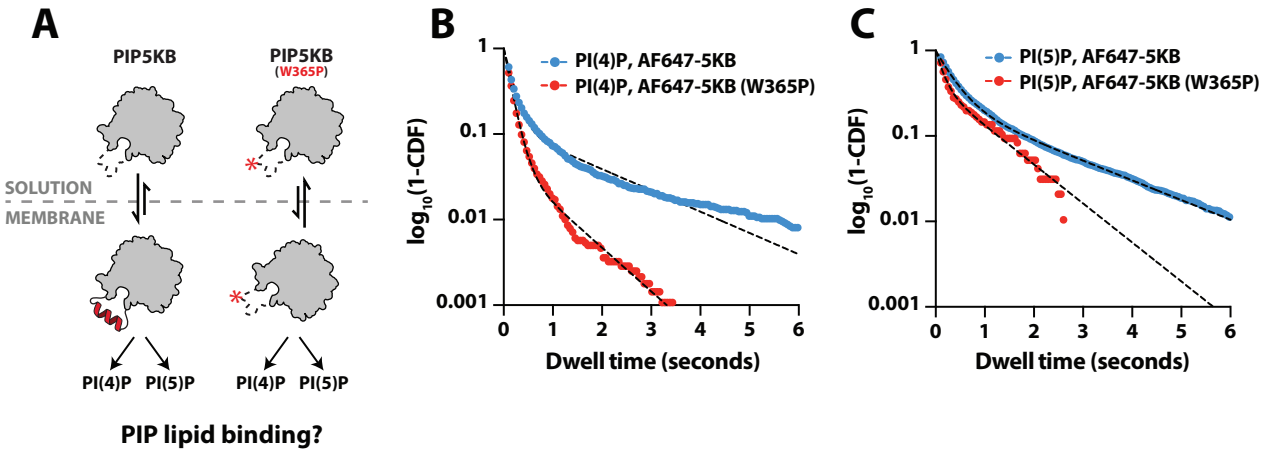

Supplemental Figure A3
PIP5KB exhibits specificity for PI(4)P based on single molecule dwell time analysis
(A) Cartoon illustrating the difference of structural organization of PIP5KB, wild type and W365P, in solution versus bound to a lipid bilayer. **(B)** Single molecule dwell time distributions measured in the presence of either 100 pM AF647-PIP5KB ($t_1 = 0.128 \pm 0.03$ s, $t_2 = 1.64 \pm 0.3$s, $\alpha = 0.88 \pm 0.07$, n = 3522) or 1 nM AF647-PIP5KB(W365P) ($t_1 = 0.159 \pm 0.03$ s, $t_2 = 0.894 \pm 0.06$ s, $\alpha = 0.91 \pm 0.06$, n = 4055) binding to 96% DOPC SLBs containing 4% PI(4)P. **(C)** Single molecule dwell time distributions measured in the presence of either 100 pM AF647-PIP5KB ($t_1 = 0.37 \pm 0.05$ s, $t_2 = 1.72 \pm 0.4$ s, $\alpha = 0.79 \pm 0.07$, n = 7526) or 1 nM AF647-PIP5KB(W365P) ($t_1 = 0.153$ s, $t_2 = 0.954$ s, $\alpha = 0.62$, n = 190) binding to 96% DOPC SLBs containing 4% PI(5)P. Imaging buffer contained 1 mM non-hydrolyzable ATPgS to prevent the generation of PI(4,5)P_2 by PIP5KB. Errors equal SD n = 2-3 technical replicates.

Supplemental Figure A4

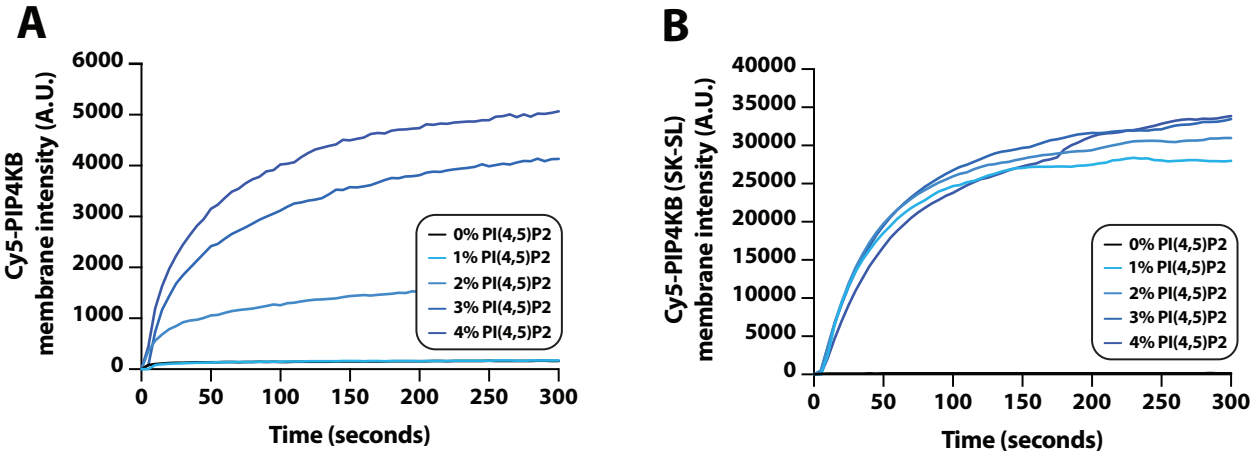

Supplemental Figure A4
Membrane binding traces for Cy5-PIP4K2B and Cy5-PIP4K2B (5K-SL) mutant
(A) Raw membrane localization data of 50 nM Cy5-PIP4K2B WT on SLBs containing 0, 1, 2, 3, and 4% PI(4,5)P_2 lipids. **(B)** Raw membrane localization data of 50 nM Cy5-PIP4K2B (5K-SL) on SLBs containing 0, 1, 2, 3, and 4% PI(4,5)P_2 lipids. (A-B) Graphs correspond to the data plotted in Figure 2F.

APPENDIX B

SUPPLEMENTARY INFORMATION FOR CHAPTER III

Appendix B is the supplemental information for chapter III. It includes data relevant to the content of Chapter III.

Supplemental Figure B1

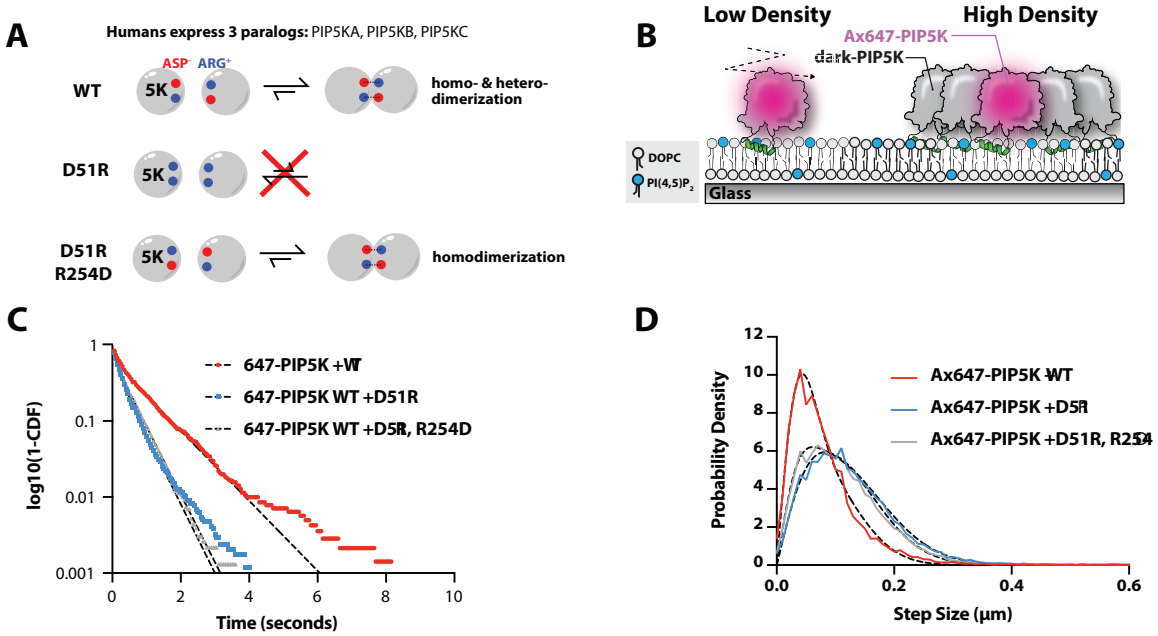

Supplemental Figure B1
Creating a PIP5KB mutant that cannot heterodimerize
(A) Diagram showing the effects of different point mutations on PIP5K dimerization. **(B)** Experimental design for single molecule analysis of Alexa647-PIP5K dimerization **(C)** Representative single molecule dwell times of Alexa647-PIP5K in the presence of high kinase densities (PIP5KB, PIP5KB D51R, or PIP5KB D51R, R254D). **(D)** Step size distributions of Alexa647-PIP5K in the presence of high kinase densities.

Supplemental Figure B2

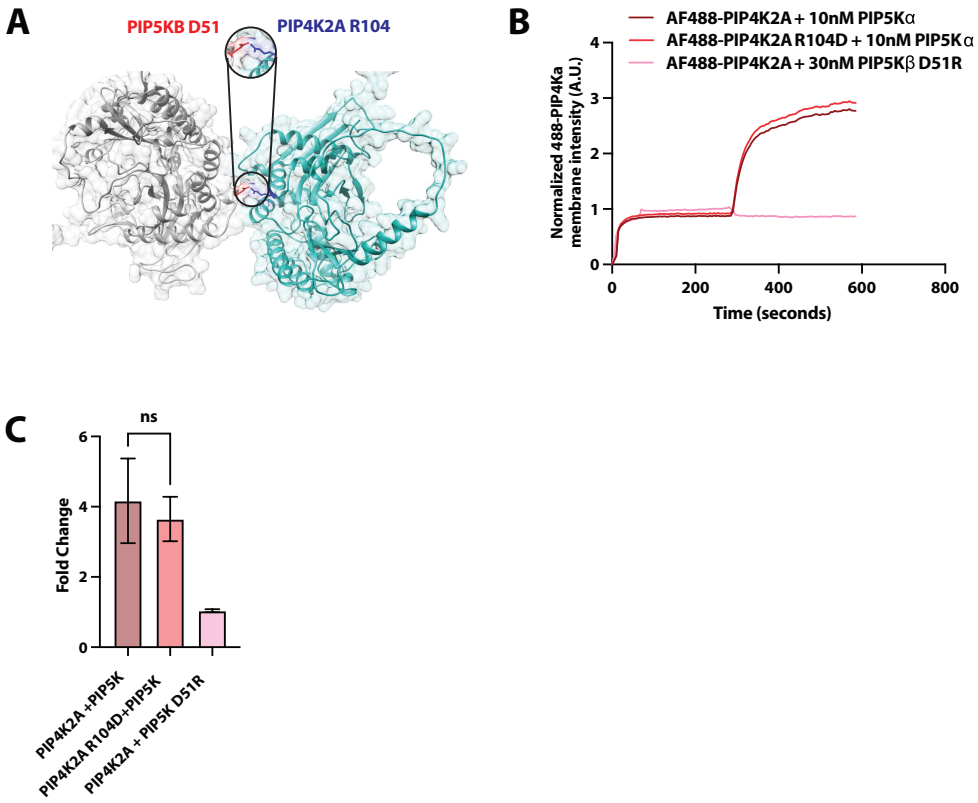

Supplemental Figure B2
Alphafold incorrectly predicts the critical amino acid interaction between PIP5K and PIP4K
(A) Alphafold multimer predicted structure of PIP4K (cyan) and PIP5K (silver) interacting via a salt bridge between PIP4K site R104 and PIP5K site D51. **(B)** Representative fold-change of 50nM AF488-PIP4K2A membrane binding in the presence of 10nM wildtype unlabeled PIP5KA (dark red), in the presence of 10nM monomeric PIP5KB D51R (pink), or 50nM PIP4K R104D in the presence of 10nM wild type unlabeled PIP5KA (red). **(C)** Fold change in membrane binding quantified from (B). Experiments performed on SLBs containing 2% PI(4,5)P_2, 98% DOPC.

REFERENCES CITED

1. Garcia, E. & Ismail, S. Spatiotemporal Regulation of Signaling: Focus on T Cell Activation and the Immunological Synapse. *Int. J. Mol. Sci.* **21**, 3283 (2020).
2. Burke, J. E., Triscott, J., Emerling, B. M. & Hammond, G. R. V. Beyond PI3Ks: targeting phosphoinositide kinases in disease. *Nat. Rev. Drug Discov.* **22**, 357–386 (2023).
3. Mandal, K. Review of PIP2 in Cellular Signaling, Functions and Diseases. *Int. J. Mol. Sci.* **21**, 8342 (2020).
4. Zhivotovsky, B. & Orrenius, S. Cell cycle and cell death in disease: past, present and future. *J. Intern. Med.* **268**, 395–409 (2010).
5. Wheeler, R. J. & Hyman, A. A. Controlling compartmentalization by non-membrane-bound organelles. *Philos. Trans. R. Soc. B Biol. Sci.* **373**, 20170193 (2018).
6. Lu, J. *et al.* Types of nuclear localization signals and mechanisms of protein import into the nucleus. *Cell Commun. Signal.* **19**, 60 (2021).
7. Zerangue, N. *et al.* Analysis of endoplasmic reticulum trafficking signals by combinatorial screening in mammalian cells. *Proc. Natl. Acad. Sci.* **98**, 2431–2436 (2001).
8. Identification of a Golgi-localized peptide reveals a minimal Golgi-targeting motif | Molecular Biology of the Cell. https://www.molbiolcell.org/doi/10.1091/mbc.E22-03-0091.
9. Balla, T. Phosphoinositides: tiny lipids with giant impact on cell regulation. *Physiol. Rev.* **93**, 1019–1137 (2013).
10. Guerin, M. E., Korduláková, J., Alzari, P. M., Brennan, P. J. & Jackson, M. Molecular Basis of Phosphatidyl-myo-inositol Mannoside Biosynthesis and Regulation in Mycobacteria. *J. Biol. Chem.* **285**, 33577–33583 (2010).

11. Goulden, B. D. *et al.* A high-avidity biosensor reveals plasma membrane PI(3,4)P2 is predominantly a class I PI3K signaling product. *J. Cell Biol.* **218**, 1066–1079 (2019).
12. Lemmon, M. A. Pleckstrin Homology (PH) domains and phosphoinositides. *Biochem. Soc. Symp.* 81–93 (2007) doi:10.1042/BSS0740081.
13. Singh, N. *et al.* Redefining the specificity of phosphoinositide-binding by human PH domain-containing proteins. *Nat. Commun.* **12**, 4339 (2021).
14. Dickson, E. J., Jensen, J. B. & Hille, B. Golgi and plasma membrane pools of PI(4)P contribute to plasma membrane PI(4,5)P2 and maintenance of KCNQ2/3 ion channel current. *Proc. Natl. Acad. Sci.* **111**, E2281–E2290 (2014).
15. Effect of hormone-induced plasma membrane phosphatidylinositol 4,5-bisphosphate depletion on receptor endocytosis suggests the importance of local regulation in phosphoinositide signaling | Scientific Reports. https://www.nature.com/articles/s41598-023-50732-x.
16. Miller, T. E. *et al.* Depletion of phosphatidylinositol 4-phosphate at the Golgi translocates K-Ras to mitochondria. *J. Cell Sci.* **132**, jcs231886 (2019).
17. Dong, X. *et al.* PI(3,5)P2 controls membrane trafficking by direct activation of mucolipin Ca2+ release channels in the endolysosome. *Nat. Commun.* **1**, 38 (2010).
18. Burke, J. E. Structural Basis for Regulation of Phosphoinositide Kinases and Their Involvement in Human Disease. *Mol. Cell* **71**, 653–673 (2018).
19. Stephens, L. R., Hughes, K. T. & Irvine, R. F. Pathway of phosphatidylinositol(3,4,5)-trisphosphate synthesis in activated neutrophils. *Nature* **351**, 33–39 (1991).

20. Weixel, K. M., Blumental-Perry, A., Watkins, S. C., Aridor, M. & Weisz, O. A. Distinct Golgi populations of phosphatidylinositol 4-phosphate regulated by phosphatidylinositol 4-kinases. *J. Biol. Chem.* **280**, 10501–10508 (2005).

21. Hammond, G. R. V., Machner, M. P. & Balla, T. A novel probe for phosphatidylinositol 4-phosphate reveals multiple pools beyond the Golgi. *J. Cell Biol.* **205**, 113–126 (2014).

22. Duewell, B. R., Wilson, N. E., Bailey, G. M., Peabody, S. E. & Hansen, S. D. *Molecular Dissection of PI3Kβ Synergistic Activation by Receptor Tyrosine Kinases, GβGγ, and Rho-Family GTPases*. https://elifesciences.org/reviewed-preprints/88991v1 (2023) doi:10.7554/eLife.88991.1.

23. Grinstein, S. Imaging signal transduction during phagocytosis: phospholipids, surface charge, and electrostatic interactions. *Am. J. Physiol.-Cell Physiol.* **299**, C876–C881 (2010).

24. Scott, C. C. *et al.* Phosphatidylinositol-4,5-bisphosphate hydrolysis directs actin remodeling during phagocytosis. *J. Cell Biol.* **169**, 139–149 (2005).

25. Willars, G. B., Nahorski, S. R. & Challiss, R. A. Differential regulation of muscarinic acetylcholine receptor-sensitive polyphosphoinositide pools and consequences for signaling in human neuroblastoma cells. *J. Biol. Chem.* **273**, 5037–5046 (1998).

26. Anderson, K. E. *et al.* Lysophosphatidylinositol-acyltransferase-1 (LPIAT1) is required to maintain physiological levels of PtdIns and PtdInsP(2) in the mouse. *PloS One* **8**, e58425 (2013).

27. Michell, R. H. Inositol phospholipids and cell surface receptor function. *Biochim. Biophys. Acta* **415**, 81–47 (1975).

28. Streb, H., Irvine, R. F., Berridge, M. J. & Schulz, I. Release of Ca2+ from a nonmitochondrial intracellular store in pancreatic acinar cells by inositol-1,4,5-trisphosphate. *Nature* **306**, 67–69 (1983).

29. Zhou, J. *et al.* Phosphatidylinositol-4,5-Bisphosphate Binding to Amphiphysin-II Modulates T-Tubule Remodeling: Implications for Heart Failure. *Front. Physiol.* **12**, 782767 (2021).

30. Chang, C.-L. & Liou, J. Phosphatidylinositol 4,5-Bisphosphate Homeostasis Regulated by Nir2 and Nir3 Proteins at Endoplasmic Reticulum-Plasma Membrane Junctions. *J. Biol. Chem.* **290**, 14289–14301 (2015).

31. Hawkins, P. T., Jackson, T. R. & Stephens, L. R. Platelet-derived growth factor stimulates synthesis of PtdIns(3,4,5)P3 by activating a PtdIns(4,5)P2 3-OH kinase. *Nature* **358**, 157–159 (1992).

32. Fruman, D. A. *et al.* The PI3K Pathway in Human Disease. *Cell* **170**, 605–635 (2017).

33. Prehoda, K. E., Scott, J. A., Mullins, R. D. & Lim, W. A. Integration of multiple signals through cooperative regulation of the N-WASP-Arp2/3 complex. *Science* **290**, 801–806 (2000).

34. Zhao, H., Hakala, M. & Lappalainen, P. ADF/Cofilin Binds Phosphoinositides in a Multivalent Manner to Act as a PIP2-Density Sensor. *Biophys. J.* **98**, 2327–2336 (2010).

35. Hamada, K., Shimizu, T., Matsui, T., Tsukita, S. & Hakoshima, T. Structural basis of the membrane-targeting and unmasking mechanisms of the radixin FERM domain. *EMBO J.* **19**, 4449–4462 (2000).

36. Michie, K. A., Bermeister, A., Robertson, N. O., Goodchild, S. C. & Curmi, P. M. G. Two Sides of the Coin: Ezrin/Radixin/Moesin and Merlin Control Membrane Structure and Contact Inhibition. *Int. J. Mol. Sci.* **20**, 1996 (2019).

37. Suh, B.-C. & Hille, B. PIP2 is a necessary cofactor for ion channel function: How and why? *Annu. Rev. Biophys.* **37**, 175–195 (2008).

38. Pritchard, H. a. T., Leblanc, N., Albert, A. P. & Greenwood, I. A. Inhibitory role of phosphatidylinositol 4,5-bisphosphate on TMEM16A-encoded calcium-activated chloride channels in rat pulmonary artery. *Br. J. Pharmacol.* **171**, 4311–4321 (2014).

39. Saleh, S. N., Albert, A. P. & Large, W. A. Activation of native TRPC1/C5/C6 channels by endothelin-1 is mediated by both PIP3 and PIP2 in rabbit coronary artery myocytes. *J. Physiol.* **587**, 5361–5375 (2009).

40. Huang, C. L., Feng, S. & Hilgemann, D. W. Direct activation of inward rectifier potassium channels by PIP2 and its stabilization by Gbetagamma. *Nature* **391**, 803–806 (1998).

41. Suh, B.-C. & Hille, B. Recovery from muscarinic modulation of M current channels requires phosphatidylinositol 4,5-bisphosphate synthesis. *Neuron* **35**, 507–520 (2002).

42. Logan, M. R. & Mandato, C. A. Regulation of the actin cytoskeleton by PIP2 in cytokinesis. *Biol. Cell* **98**, 377–388 (2006).

43. Jung, S.-R. *et al.* β-arrestin-dependent PI(4,5)P2 synthesis boosts GPCR endocytosis. *Proc. Natl. Acad. Sci. U. S. A.* **118**, e2011023118 (2021).

44. Loew, L. M. Where does all the PIP2 come from? *J. Physiol.* **582**, 945–951 (2007).

45. Pan, W. *et al.* Wnt3a-Mediated Formation of Phosphatidylinositol 4,5-Bisphosphate Regulates LRP6 Phosphorylation. *Science* **321**, 1350–1353 (2008).

46. Botelho, R. J. *et al.* Localized biphasic changes in phosphatidylinositol-4,5-bisphosphate at sites of phagocytosis. *J. Cell Biol.* **151**, 1353–1368 (2000).

47. Chalhoub, N. & Baker, S. J. PTEN and the PI3-Kinase Pathway in Cancer. *Annu. Rev. Pathol.* **4**, 127–150 (2009).

48. Malek, M. *et al.* PTEN Regulates PI(3,4)P2 Signaling Downstream of Class I PI3K. *Mol. Cell* **68**, 566-580.e10 (2017).

49. Vieira, O. V. *et al.* Distinct roles of class I and class III phosphatidylinositol 3-kinases in phagosome formation and maturation. *J. Cell Biol.* **155**, 19–25 (2001).

50. Boronenkov, I. V. & Anderson, R. A. The sequence of phosphatidylinositol-4-phosphate 5-kinase defines a novel family of lipid kinases. *J. Biol. Chem.* **270**, 2881–2884 (1995).

51. Gupta, A. *et al.* Phosphatidylinositol 5-phosphate 4-kinase (PIP4K) regulates TOR signaling and cell growth during Drosophila development. *Proc. Natl. Acad. Sci. U. S. A.* **110**, 5963–5968 (2013).

52. Mathre, S. *et al.* Functional analysis of the biochemical activity of mammalian phosphatidylinositol 5 phosphate 4-kinase enzymes. *Biosci. Rep.* **39**, BSR20182210 (2019).

53. Sharma, S., Mathre, S., Ramya, V., Shinde, D. & Raghu, P. Phosphatidylinositol 5 Phosphate 4-Kinase Regulates Plasma-Membrane PIP3 Turnover and Insulin Signaling. *Cell Rep.* **27**, 1979-1990.e7 (2019).

54. Wang, D. G. *et al.* PIP4Ks Suppress Insulin Signaling through a Catalytic-Independent Mechanism. *Cell Rep.* **27**, 1991-2001.e5 (2019).

55. Poli, A. *et al.* Phosphatidylinositol 5 Phosphate (PI5P): From Behind the Scenes to the Front (Nuclear) Stage. *Int. J. Mol. Sci.* **20**, 2080 (2019).

56. Szentpetery, Z., Várnai, P. & Balla, T. Acute manipulation of Golgi phosphoinositides to assess their importance in cellular trafficking and signaling. *Proc. Natl. Acad. Sci. U. S. A.* **107**, 8225–8230 (2010).

57. Paolo, G. D. *et al.* Impaired PtdIns(4,5)P2 synthesis in nerve terminals produces defects in synaptic vesicle trafficking. *Nature* **431**, 415–422 (2004).

58. Cristobal, C. D. *et al.* Daam2 couples translocation and clustering of Wnt receptor signalosomes through Rac1. *J. Cell Sci.* **134**, jcs251140 (2021).

59. Yudin, Y., Liu, L., Nagwekar, J. & Rohacs, T. Methods to study phosphoinositide regulation of ion channels. *Methods Enzymol.* **652**, 49–79 (2021).

60. Mao, Y. S. *et al.* Essential and unique roles of PIP5K-γ and -α in Fcγ receptor-mediated phagocytosis. *J. Cell Biol.* **184**, 281–296 (2009).

61. van den Bout, I. & Divecha, N. PIP5K-driven PtdIns(4,5)P2 synthesis: regulation and cellular functions. *J. Cell Sci.* **122**, 3837–3850 (2009).

62. Uhlén, M. *et al.* Proteomics. Tissue-based map of the human proteome. *Science* **347**, 1260419 (2015).

63. Muftuoglu, Y., Xue, Y., Gao, X., Wu, D. & Ha, Y. Mechanism of substrate specificity of phosphatidylinositol phosphate kinases. *Proc. Natl. Acad. Sci.* **113**, 8711–8716 (2016).

64. Hu, J. *et al.* Resolution of structure of PIP5K1A reveals molecular mechanism for its regulation by dimerization and dishevelled. *Nat. Commun.* **6**, 8205 (2015).

65. Kunz, J. *et al.* The Activation Loop of Phosphatidylinositol Phosphate Kinases Determines Signaling Specificity. *Mol. Cell* **5**, 1–11 (2000).

66. Kunz, J., Fuelling, A., Kolbe, L. & Anderson, R. A. Stereo-specific Substrate Recognition by Phosphatidylinositol Phosphate Kinases Is Swapped by Changing a Single Amino Acid Residue. *J. Biol. Chem.* **277**, 5611–5619 (2002).

67. Liu, A., Sui, D., Wu, D. & Hu, J. The activation loop of PIP5K functions as a membrane sensor essential for lipid substrate processing. *Sci. Adv.* **2**, e1600925 (2016).

68. Fairn, G. D. *et al.* An electrostatic switch displaces phosphatidylinositol phosphate kinases from the membrane during phagocytosis. *J. Cell Biol.* **187**, 701–714 (2009).

69. Hansen, S. D. *et al.* Stochastic geometry sensing and polarization in a lipid kinase–phosphatase competitive reaction. *Proc. Natl. Acad. Sci.* **116**, 15013–15022 (2019).

70. Amos, S.-B. T. A., Kalli, A. C., Shi, J. & Sansom, M. S. P. Membrane Recognition and Binding by the Phosphatidylinositol Phosphate Kinase PIP5K1A: A Multiscale Simulation Study. *Structure* **27**, 1336-1346.e2 (2019).

71. Hansen, S. D., Lee, A. A., Duewell, B. R. & Groves, J. T. Membrane-mediated dimerization potentiates PIP5K lipid kinase activity. *eLife* **11**, e73747 (2022).

72. Funakoshi, Y., Hasegawa, H. & Kanaho, Y. Activation mechanisms of PIP5K isozymes by the small GTPase ARF6. *Adv. Enzyme Regul.* **50**, 72–80 (2010).

73. Marquer, C. *et al.* Arf6 controls retromer traffic and intracellular cholesterol distribution via a phosphoinositide-based mechanism. *Nat. Commun.* **7**, 11919 (2016).

74. Weernink, P. A. O. *et al.* Activation of type I phosphatidylinositol 4-phosphate 5-kinase isoforms by the Rho GTPases, RhoA, Rac1, and Cdc42. *J. Biol. Chem.* **279**, 7840–7849 (2004).

75. Adhikari, H. & Counter, C. M. Interrogating the protein interactomes of RAS isoforms identifies PIP5K1A as a KRAS-specific vulnerability. *Nat. Commun.* **9**, 3646 (2018).

76. Wills, R. C. *et al.* A novel homeostatic mechanism tunes PI(4,5)P2-dependent signaling at the plasma membrane. *J. Cell Sci.* **136**, jcs261494 (2023).

77. Di Paolo, G. & De Camilli, P. Phosphoinositides in cell regulation and membrane dynamics. *Nature* **443**, 651–657 (2006).

78. Hammond, G. R. V. & Burke, J. E. Novel roles of phosphoinositides in signaling, lipid transport, and disease. *Curr. Opin. Cell Biol.* **63**, 57–67 (2020).

79. Mitchell, K. T., Ferrell, J. E. & Huestis, W. H. Separation of phosphoinositides and other phospholipids by two-dimensional thin-layer chromatography. *Anal. Biochem.* **158**, 447–453 (1986).

80. Nasuhoglu, C. *et al.* Nonradioactive analysis of phosphatidylinositides and other anionic phospholipids by anion-exchange high-performance liquid chromatography with suppressed conductivity detection. *Anal. Biochem.* **301**, 243–254 (2002).

81. Wenk, M. R. *et al.* Phosphoinositide profiling in complex lipid mixtures using electrospray ionization mass spectrometry. *Nat. Biotechnol.* **21**, 813–817 (2003).

82. Janmey, P. A., Bucki, R. & Radhakrishnan, R. Regulation of actin assembly by PI(4,5)P2 and other inositol phospholipids: an update on possible mechanisms. *Biochem. Biophys. Res. Commun.* **506**, 307–314 (2018).

83. Rozelle, A. L. *et al.* Phosphatidylinositol 4,5-bisphosphate induces actin-based movement of raft-enriched vesicles through WASP-Arp2/3. *Curr. Biol.* **10**, 311–320 (2000).

84. Hansen, S. B. Lipid agonism: The PIP2 paradigm of ligand-gated ion channels. *Biochim. Biophys. Acta* **1851**, 620–628 (2015).

85. Antonescu, C. N., Aguet, F., Danuser, G. & Schmid, S. L. Phosphatidylinositol-(4,5)-bisphosphate regulates clathrin-coated pit initiation, stabilization, and size. *Mol. Biol. Cell* **22**, 2588–2600 (2011).

86. Mandal, K. Review of PIP2 in Cellular Signaling, Functions and Diseases. *Int. J. Mol. Sci.* **21**, 8342 (2020).

87. Wills, R. C. & Hammond, G. R. V. PI(4,5)P2: signaling the plasma membrane. *Biochem. J.* **479**, 2311–2325 (2022).

88. Honda, A. *et al.* Phosphatidylinositol 4-Phosphate 5-Kinase is a Downstream Effector of the Small G Protein ARF6 in Membrane Ruffle Formation. *Cell* 12 (1999).

89. Jenkins, G. H., Fisette, P. L. & Anderson, R. A. Type I phosphatidylinositol 4-phosphate 5-kinase isoforms are specifically stimulated by phosphatidic acid. *J. Biol. Chem.* **269**, 11547–11554 (1994).

90. Tolias, K. F. *et al.* Type I Phosphatidylinositol-4-phosphate 5-Kinases Synthesize the Novel Lipids Phosphatidylinositol 3,5-Bisphosphate and Phosphatidylinositol 5-Phosphate. *J. Biol. Chem.* **273**, 18040–18046 (1998).

91. Zhang, X. *et al.* Phosphatidylinositol-4-phosphate 5-Kinase Isozymes Catalyze the Synthesis of 3-Phosphate-containing Phosphatidylinositol Signaling Molecules. *J. Biol. Chem.* **272**, 17756–17761 (1997).

92. Ishihara, H. *et al.* Cloning of cDNAs Encoding Two Isoforms of 68-kDa Type I Phosphatidylinositol4-phosphate 5-Kinase. *J. Biol. Chem.* **271**, 23611–23614 (1996).

93. Ishihara, H. *et al.* Type I Phosphatidylinositol-4-phosphate 5-Kinases: CLONING OF THE THIRD ISOFORM AND DELETION/SUBSTITUTION ANALYSIS OF MEMBERS OF THIS NOVEL LIPID KINASE FAMILY. *J. Biol. Chem.* **273**, 8741–8748 (1998).

94. Loijens, J. C. & Anderson, R. A. Type I Phosphatidylinositol-4-phosphate 5-Kinases Are Distinct Members of This Novel Lipid Kinase Family. *J. Biol. Chem.* **271**, 32937–32943 (1996).

95. Coppolino, M. G. *et al.* Inhibition of Phosphatidylinositol-4-phosphate 5-Kinase Iα Impairs Localized Actin Remodeling and Suppresses Phagocytosis. *J. Biol. Chem.* **277**, 43849–43857 (2002).

96. Di Paolo, G. *et al.* Recruitment and regulation of phosphatidylinositol phosphate kinase type 1 gamma by the FERM domain of talin. *Nature* **420**, 85–89 (2002).

97. Ling, K., Doughman, R. L., Firestone, A. J., Bunce, M. W. & Anderson, R. A. Type I gamma phosphatidylinositol phosphate kinase targets and regulates focal adhesions. *Nature* **420**, 89–93 (2002).

98. Semenas, J. *et al.* The role of PI3K/AKT-related PIP5K1α and the discovery of its selective inhibitor for treatment of advanced prostate cancer. *Proc. Natl. Acad. Sci. U. S. A.* **111**, E3689-3698 (2014).

99. Amos, S.-B. T. A., Kalli, A. C., Shi, J. & Sansom, M. S. P. Membrane Recognition and Binding by the Phosphatidylinositol Phosphate Kinase PIP5K1A: A Multiscale Simulation Study. *Structure* **27**, 1336-1346.e2 (2019).

100. Arioka, M., Nakashima, S., Shibasaki, Y. & Kitamoto, K. Dibasic amino acid residues at the carboxy-terminal end of kinase homology domain participate in the plasma membrane

localization and function of phosphatidylinositol 5-kinase γ. *Biochem. Biophys. Res. Commun.* **319**, 456–463 (2004).

101. Li, L., Fierer, J. O., Rapoport, T. A. & Howarth, M. Structural Analysis and Optimization of the Covalent Association between SpyCatcher and a Peptide Tag. *J. Mol. Biol.* **426**, 309–317 (2014).
102. Zakeri, B. *et al.* Peptide tag forming a rapid covalent bond to a protein, through engineering a bacterial adhesin. *Proc. Natl. Acad. Sci.* **109**, (2012).
103. Nishimura, T. *et al.* Osh Proteins Control Nanoscale Lipid Organization Necessary for PI(4,5)P2 Synthesis. *Mol. Cell* **75**, 1043-1057.e8 (2019).
104. Hernández-Deviez, D. J., Roth, M. G., Casanova, J. E. & Wilson, J. M. ARNO and ARF6 regulate axonal elongation and branching through downstream activation of phosphatidylinositol 4-phosphate 5-kinase alpha. *Mol. Biol. Cell* **15**, 111–120 (2004).
105. Shulga, Y. V., Anderson, R. A., Topham, M. K. & Epand, R. M. Phosphatidylinositol-4-phosphate 5-Kinase Isoforms Exhibit Acyl Chain Selectivity for Both Substrate and Lipid Activator. *J. Biol. Chem.* **287**, 35953–35963 (2012).
106. Yamazaki, M. *et al.* Phosphatidylinositol 4-phosphate 5-kinase is essential for ROCK-mediated neurite remodeling. *J. Biol. Chem.* **277**, 17226–17230 (2002).
107. Gawden-Bone, C. M. *et al.* PIP5 Kinases Regulate Membrane Phosphoinositide and Actin Composition for Targeted Granule Secretion by Cytotoxic Lymphocytes. *Immunity* **49**, 427-437.e4 (2018).
108. Ikenouchi, J., Hirata, M., Yonemura, S. & Umeda, M. Sphingomyelin clustering is essential for the formation of microvilli. *J. Cell Sci.* **126**, 3585–3592 (2013).

109. Kumari, A., Ghosh, A., Kolay, S. & Raghu, P. Septins tune lipid kinase activity and PI(4,5)P2 turnover during G-protein-coupled PLC signalling in vivo. *Life Sci. Alliance* **5**, e202101293 (2022).

110. Schill, N. J., Hedman, A. C., Choi, S. & Anderson, R. A. Isoform 5 of PIPKIγ regulates the endosomal trafficking and degradation of E-cadherin. *J. Cell Sci.* **127**, 2189–2203 (2014).

111. Unoki, T. *et al.* NMDA receptor-mediated PIP5K activation to produce PI(4,5)P_2 is essential for AMPA receptor endocytosis during LTD. *Neuron* **73**, 135–148 (2012).

112. Vasudevan, L. *et al.* The beta- and gamma-isoforms of type I PIP5K regulate distinct stages of Ca2+ signaling in mast cells. *J. Cell Sci.* **122**, 2567–2574 (2009).

113. Maib, H. & Murray, D. H. A mechanism for exocyst-mediated tethering via Arf6 and PIP5K1C-driven phosphoinositide conversion. *Curr. Biol.* **32**, 2821-2833.e6 (2022).

114. Blagoveshchenskaya, A. *et al.* Integration of Golgi trafficking and growth factor signaling by the lipid phosphatase SAC1. *J. Cell Biol.* **180**, 803–812 (2008).

115. Stefan, C. J., Audhya, A. & Emr, S. D. The yeast synaptojanin-like proteins control the cellular distribution of phosphatidylinositol (4,5)-bisphosphate. *Mol. Biol. Cell* **13**, 542–557 (2002).

116. Várnai, P. & Balla, T. Live cell imaging of phosphoinositides with expressed inositide binding protein domains. *Methods San Diego Calif* **46**, 167–176 (2008).

117. Devaux, P. F. Static and dynamic lipid asymmetry in cell membranes. *Biochemistry* **30**, 1163–1173 (1991).

118. Zhang, M. *et al.* Rational design of true monomeric and bright photoactivatable fluorescent proteins. *Nat. Methods* **9**, 727–729 (2012).

119. Gibson, D. G. *et al.* Enzymatic assembly of DNA molecules up to several hundred kilobases. *Nat. Methods* **6**, 343–345 (2009).

120. Guimaraes, C. P. *et al.* Site-specific C-terminal and internal loop labeling of proteins using sortase-mediated reactions. *Nat. Protoc.* **8**, 1787–1799 (2013).

121. Vacklin, H. P., Tiberg, F. & Thomas, R. K. Formation of supported phospholipid bilayers via co-adsorption with beta-D-dodecyl maltoside. *Biochim. Biophys. Acta* **1668**, 17–24 (2005).

122. Jaqaman, K. *et al.* Robust single-particle tracking in live-cell time-lapse sequences. *Nat. Methods* **5**, 695–702 (2008).

123. Balla, T. Phosphoinositides: Tiny Lipids With Giant Impact on Cell Regulation. *Physiol. Rev.* **93**, 1019–1137 (2013).

124. Fairn, G. D. *et al.* An electrostatic switch displaces phosphatidylinositol phosphate kinases from the membrane during phagocytosis. *J. Cell Biol.* **187**, 701–714 (2009).

125. Harraz, O. F., Hill-Eubanks, D. & Nelson, M. T. PIP2: A critical regulator of vascular ion channels hiding in plain sight. *Proc. Natl. Acad. Sci. U. S. A.* **117**, 20378–20389 (2020).

126. Hilgemann, D. W. & Ball, R. Regulation of Cardiac Na+,Ca2+ Exchange and KATP Potassium Channels by PIP2. *Science* **273**, 956–959 (1996).

127. Voelker, T. L. *et al.* Acute phosphatidylinositol 4,5 bisphosphate depletion destabilizes sarcolemmal expression of cardiac L-type Ca^{2+} channel $Ca_V1.2$. *Proc. Natl. Acad. Sci.* **120**, e2221242120 (2023).

128. Phosphatidylinositol 4,5-Bisphosphate Functions as a Second Messenger that Regulates Cytoskeleton–Plasma Membrane Adhesion - ScienceDirect. https://www.sciencedirect.com/science/article/pii/S0092867400815603.

129. Manna, P. & Jain, S. K. Phosphatidylinositol-3,4,5-Triphosphate and Cellular Signaling: Implications for Obesity and Diabetes. *Cell. Physiol. Biochem. Int. J. Exp. Cell. Physiol. Biochem. Pharmacol.* **35**, 1253–1275 (2015).

130. Ménager, C., Arimura, N., Fukata, Y. & Kaibuchi, K. PIP3 is involved in neuronal polarization and axon formation. *J. Neurochem.* **89**, 109–118 (2004).

131. Yu, J. S. L. & Cui, W. Proliferation, survival and metabolism: the role of PI3K/AKT/mTOR signalling in pluripotency and cell fate determination. *Dev. Camb. Engl.* **143**, 3050–3060 (2016).

132. PIP5KIγ is required for cardiovascular and neuronal development | PNAS. https://www.pnas.org/doi/abs/10.1073/pnas.0700019104.

133. Loi, M. Lowe syndrome. *Orphanet J. Rare Dis.* **1**, 16 (2006).

134. Narkis, G. *et al.* Lethal Contractural Syndrome Type 3 (LCCS3) Is Caused by a Mutation in PIP5K1C, Which Encodes PIPKIγ of the Phophatidylinsitol Pathway. *Am. J. Hum. Genet.* **81**, 530–539 (2007).

135. Traynor-Kaplan, A. *et al.* Fatty-acyl chain profiles of cellular phosphoinositides. *Biochim. Biophys. Acta Mol. Cell Biol. Lipids* **1862**, 513–522 (2017).

136. Griffiths, G., Back, R. & Marsh, M. A quantitative analysis of the endocytic pathway in baby hamster kidney cells. *J. Cell Biol.* **109**, 2703–2720 (1989).

137. Hammond, G. R. V. & Burke, J. E. Novel roles of phosphoinositides in signaling, lipid transport, and disease. *Curr. Opin. Cell Biol.* **63**, 57–67 (2020).

138. Pan, W. *et al.* Wnt3a-mediated formation of phosphatidylinositol 4,5-bisphosphate regulates LRP6 phosphorylation. *Science* **321**, 1350–1353 (2008).

139. Einspahr, K. J., Peeler, T. C. & Thompson, G. A. Rapid changes in polyphosphoinositide metabolism associated with the response of Dunaliella salina to hypoosmotic shock. *J. Biol. Chem.* **263**, 5775–5779 (1988).

140. Rapid Turnover of Phosphatidylinositol-4,5-Bisphosphate in Insulin-Secreting Cells Mediated by Ca2+ and the ATP-to-ADP Ratio | Diabetes | American Diabetes Association. https://diabetesjournals.org/diabetes/article/56/3/818/15166/Rapid-Turnover-of-Phosphatidylinositol-4-5.

141. Link, T. M. *et al.* TRPV2 plays a pivotal role in macrophage particle binding and phagocytosis. *Nat. Immunol.* **11**, 232–239 (2010).

142. Chen, Y.-J., Chang, C.-L., Lee, W.-R. & Liou, J. RASSF4 controls SOCE and ER-PM junctions through regulation of PI(4,5)P2. *J. Cell Biol.* **216**, 2011–2025 (2017).

143. Benjamin R. Duewell, Katie A. Faris, & Scott D Hansen. Molecular basis of product recognition during PIP5K-mediated production of PI(4,5)P2 with positive feedback. *bioRxiv* 2023.09.04.556152 (2023) doi:10.1101/2023.09.04.556152.

144. Honda, A. *et al.* Phosphatidylinositol 4-phosphate 5-kinase alpha is a downstream effector of the small G protein ARF6 in membrane ruffle formation. *Cell* **99**, 521–532 (1999).

145. Rameh, L. E., Tolias, K. F., Duckworth, B. C. & Cantley, L. C. A new pathway for synthesis of phosphatidylinositol-4,5-bisphosphate. *Nature* **390**, 192–196 (1997).

146. Doughman, R. L., Firestone, A. J. & Anderson, R. A. Phosphatidylinositol phosphate kinases put PI4,5P(2) in its place. *J. Membr. Biol.* **194**, 77–89 (2003).

147. Loijens, J. C., Boronenkov, I. V., Parker, G. J. & Anderson, R. A. The phosphatidylinositol 4-phosphate 5-kinase family. *Adv. Enzyme Regul.* **36**, 115–140 (1996).

148. Mao, Y. S. *et al.* Essential and unique roles of PIP5K-gamma and -alpha in Fcgamma receptor-mediated phagocytosis. *J. Cell Biol.* **184**, 281–296 (2009).

149. Sasaki, J. *et al.* Regulation of anaphylactic responses by phosphatidylinositol phosphate kinase type I α. *J. Exp. Med.* **201**, 859–870 (2005).

150. Wang, D. G. *et al.* PIP4Ks Suppress Insulin Signaling through a Catalytic-Independent Mechanism. *Cell Rep.* **27**, 1991-2001.e5 (2019).

151. Wills, R. C. *et al.* A novel homeostatic mechanism tunes PI(4,5)P2-dependent signaling at the plasma membrane. *J. Cell Sci.* **136**, jcs261494 (2023).

152. Brown, F. D., Rozelle, A. L., Yin, H. L., Balla, T. & Donaldson, J. G. Phosphatidylinositol 4,5-bisphosphate and Arf6-regulated membrane traffic. *J. Cell Biol.* **154**, 1007–1017 (2001).

153. Chatah, N. E. & Abrams, C. S. G-protein-coupled receptor activation induces the membrane translocation and activation of phosphatidylinositol-4-phosphate 5-kinase I alpha by a Rac- and Rho-dependent pathway. *J. Biol. Chem.* **276**, 34059–34065 (2001).

154. Sun, Y., Dandekar, R. D., Mao, Y. S., Yin, H. L. & Wülfing, C. Phosphatidylinositol (4,5) Bisphosphate Controls T Cell Activation by Regulating T Cell Rigidity and Organization. *PLoS ONE* **6**, e27227 (2011).

155. Antonescu, C. N., Aguet, F., Danuser, G. & Schmid, S. L. Phosphatidylinositol-(4,5)-bisphosphate regulates clathrin-coated pit initiation, stabilization, and size. *Mol. Biol. Cell* **22**, 2588–2600 (2011).

156. Hansen, S. D. *et al.* Stochastic geometry sensing and polarization in a lipid kinase–phosphatase competitive reaction. *Proc. Natl. Acad. Sci.* **116**, 15013–15022 (2019).

157. Hansen, S. D., Lee, A. A., Duewell, B. R. & Groves, J. T. Membrane-mediated dimerization potentiates PIP5K lipid kinase activity. *eLife* **11**, e73747 (2022).

158. Verma, A. K., Noumani, A., Yadav, A. K. & Solanki, P. R. FRET Based Biosensor: Principle Applications Recent Advances and Challenges. *Diagnostics* **13**, 1375 (2023).

159. Wang, S., Vafabakhsh, R., Borschel, W. F., Ha, T. & Nichols, C. G. Structural dynamics of potassium-channel gating revealed by single-molecule FRET. *Nat. Struct. Mol. Biol.* **23**, 31–36 (2016).

160. Xu, L., Gao, Y., Kuang, H., Liz-Marzán, L. M. & Xu, C. MicroRNA-Directed Intracellular Self-Assembly of Chiral Nanorod Dimers. *Angew. Chem. Int. Ed.* **57**, 10544–10548 (2018).

161. Hu, J. *et al.* Resolution of structure of PIP5K1A reveals molecular mechanism for its regulation by dimerization and dishevelled. *Nat. Commun.* **6**, 8205 (2015).

162. Ershov, D. *et al.* TrackMate 7: integrating state-of-the-art segmentation algorithms into tracking pipelines. *Nat. Methods* **19**, 829–832 (2022).

163. Villalobos, C., Foehring, R. C., Lee, J. C. & Andrade, R. Essential Role for Phosphatidylinositol 4,5-Bisphosphate in the Expression, Regulation, and Gating of the Slow Afterhyperpolarization Current in the Cerebral Cortex. *J. Neurosci.* **31**, 18303–18312 (2011).

164. Kruse, M. & Whitten, R. J. Control of Neuronal Excitability by Cell Surface Receptor Density and Phosphoinositide Metabolism. *Front. Pharmacol.* **12**, 663840 (2021).

165. Khrongyut, S. *et al.* Localization of phosphatidylinositol 4-phosphate 5-kinase (PIP5K) α, β, γ in the three major salivary glands in situ of mice and their response to β-adrenoceptor stimulation. *J. Anat.* **234**, 502–514 (2019).

166. Lacalle, R. A. *et al.* Type I phosphatidylinositol 4-phosphate 5-kinase homo- and heterodimerization determines its membrane localization and activity. *FASEB J. Off. Publ. Fed. Am. Soc. Exp. Biol.* **29**, 2371–2385 (2015).

167. Broussard, J. A. & Green, K. J. Research Techniques Made Simple: Methodology and Applications of Förster Resonance Energy Transfer (FRET) Microscopy. *J. Invest. Dermatol.* **137**, e185–e191 (2017).

168. Protein complex prediction with AlphaFold-Multimer | bioRxiv. https://www.biorxiv.org/content/10.1101/2021.10.04.463034v2.

169. Wang, T. *et al.* PIP5K1α is Required for Promoting Tumor Progression in Castration-Resistant Prostate Cancer. *Front. Cell Dev. Biol.* **10**, 798590 (2022).

170. Exploiting the PI3K/AKT Pathway for Cancer Drug Discovery | Nature Reviews Drug Discovery. https://www.nature.com/articles/nrd1902.

171. Vanhaesebroeck, B., Guillermet-Guibert, J., Graupera, M. & Bilanges, B. The emerging mechanisms of isoform-specific PI3K signalling. *Nat. Rev. Mol. Cell Biol.* **11**, 329–341 (2010).

172. Lawrence, M. S. *et al.* Discovery and saturation analysis of cancer genes across 21 tumour types. *Nature* **505**, 495–501 (2014).

173. De novo design of protein structure and function with RFdiffusion | Nature. https://www.nature.com/articles/s41586-023-06415-8.

174. A Human Interactome in Three Quantitative Dimensions Organized by Stoichiometries and Abundances | Elsevier Enhanced Reader. https://reader.elsevier.com/reader/sd/pii/S0092867415012702?token=B514F25E254DF23

953D1DC5F50A95F8A2421912094C1903251D726B3985B02BD27E4D3B2B53D890CCCFCD

0286B18B773&originRegion=us-east-1&originCreation=20220831002415

doi:10.1016/j.cell.2015.09.053.